Enhanced Delaware Air Toxics Assessment Study

E-DATAS

Project Report
September, 2006

Enhanced Delaware Air Toxics Study (E-DATAS)

Final Report

Prepared for:

U.S. EPA Region 3
Philadelphia, PA

September 19, 2006

Acknowledgements

Special thanks to Dr. Murray Johnston, Department of Chemistry, University of Delaware and his research team for their support in collecting, analyzing and interpreting over 500,000 particles in Wilmington, DE:

Melissa Reinard
Matthew Dreyfus
Michael Tolocka

Also special thanks to Dr. Andrey Khlystov, Civil and Environmental Engineering, Duke University and his research team for their support in collecting, analyzing, and interpreting over 130,000 data points collected during the mobile monitoring intensives:

Lastly, a special thanks to Dr. Vlad Isakov and Dr. Jason Ching, U.S. EPA-NERL, for their technical guidance and assistance during this study

Department of Natural Resources & Environmental Control
Division of Air & Waste Management

Main Office
89 Kings Highway
Dover, DE 19901
302-739-9402

New Castle Office
715 Grantham Lane
New Castle, DE 19720
302-323-4542

TABLE OF CONTENTS

FIGURES

TABLES

E.0 Executive Summary

The Delaware Air Quality Management Section (AQMS) has had the fortunate opportunity to have been awarded funding through the National Air Toxics Monitoring Program Community Assessments, to perform an additional ambient monitoring field study in Wilmington, Delaware.

Since AQMS recently completed a state-wide toxics monitoring effort in 2003 per the Delaware Air Toxics Assessment Study [*DATAS, Aug 2005*], AQMS strived to develop an enhanced study that would provide a dataset to further the understanding of the pollutants sources that impact air quality in Wilmington. Through collaborative partnerships with University of Delaware (U of D) and Duke University (Duke) research teams, an ambient air monitoring study, defined as the Enhanced Delaware Air Toxics Study (E-DATAS) was conducted at the Martin Luther King Monitoring Site (MLK). The study began in April 2005 and continued through February 2006.

As described in the Scope-of-Work for this project [*E-DATAS, June 2004*], the partnership chose the MLK monitoring site because:

- The site is located in an urban setting
- The location provides a mix of pollutant sources
- The sampling results from the DATAS [*DATAS, Aug 2005*], indicated slightly elevated ambient measurements for select toxins in comparison to the other four monitoring sites
- The site contained many of the necessary infrastructures to perform E-DATAS.

The E-DATAS Study

In developing E-DATAS, AQMS, in partnership with the U of D and Duke, established the following project goals:

- Characterize the seasonal ambient variability of ambient aerosols of aerodynamic diameters of 50, 110, 220, 440, and 770 nm at the MLK site. Real-time measurements were performed during four, one-month intensive efforts using the Rapid Single-particle Mass Spectrometer, version 3 (RSMS-3).
- Implement an approach in which selected industry within a 10-km radius of the MLK site could be characterized according to their ambient aerosol contribution. Data obtained during this effort was vital to better identifying a source's contribution to the ambient air composition at the MLK site.
- Study the spatial and seasonal variability of target ambient compounds (formaldehyde, chromium species, particulate matter, and ozone) using both

research-specific and commercially available technology to perform mobile, real-time ambient measurements within the Wilmington area. These measurements were performed during four, one-week intensive efforts that were coordinated with the aerosol measurements.

- Utilize and integrate into E-DATAS many of the federal- and state-run ambient measurements being performed at the MLK site. For this study, particulate, carbon monoxide, nitric oxide, and wind measurements were incorporated into E-DATAS.
- Develop efficient, effective, and long-term partnerships with the research community, in efforts to continue to provide value-added data to enhance AQMS' and the public's understanding of the state of Delaware's air quality. E-DATAS clearly signifies the importance of developing these partnerships, as this field application would not have been performed otherwise.

The project was organized into two separate components: (1) spatial characterization of select compounds through implementation of mobile measurements in the Wilmington area, with the MLK site being the starting location for measurements and (2) aerosol characterization at the MLK site (fixed location).

Each project component entailed unique work plans, sampling equipment, and research expertise. Specific Quality Assurance Project Plans and Operating Procedures are identified in Appendix A and Appendix B. All data collected during this study is presented in Appendices C through E.

The commonality between the two components were (1) they were both performed as short-term intensive monitoring efforts that provided ample data to characterize seasonal variability of their target measurements, emphasizing the MLK site, (2) both components measured total particle counts.

The MLK aerosol intensives were performed during the following periods:

- May – June 2005
- July – August 2005
- November 2005
- January – February 2006.

During each aerosol intensive at the MLK site, a one-week mobile monitoring effort was performed to document spatial variability of target compounds.

A description of the spatial and MLK site aerosol characterization is presented in the following subsections.

Mobile Characterization of Selected Compounds

Duke performed the mobile characterization for E-DATAS using a mobile laboratory mini-van that was equipped with a battery pack and a true-sine inverter that allows for autonomous operation of research equipment without external power sources. Several high-time resolution instruments were deployed during this study to measure the spatial distribution of the following species:

- Water-soluble hexavalent and trivalent chromium in the $PM_{2.5}$ size range
- Formaldehyde
- Ozone (only during the summer 2005 campaign)
- Particulate matter (aerosol) size distribution and concentration (in the size range 12 m – 270 nm in diameter).

The instruments for chromium and formaldehyde measurements were specifically developed for this study. Total particulate measurements were performed using a commercially available scanning mobility particle sizer (SMPS).

The driving route was predetermined by the partnership members and consisted of mostly quiet residential streets, avoiding busier roadways where possible. The same route was traversed several times in order to obtain a reliable statistical characterization of the variability of each point.

Aerosol Characterization at the MLK site

The U of D performed the fixed-site aerosol characterization at the MLK site. The Real-Time Single Particle Mass Spectrometer (RSMS-3) was used at the MLK site to perform these real-time measurements. The instrument has been developed by the U of D and has been used at several locations in the United States (Atlanta, Houston, Pittsburgh, and Baltimore).

The instrument samples ambient aerosols through a PM_{10} inlet containing a 3.8 cm o.d. duct extending 1 meter above the trailer and approximately 5 meters above ground at the MLK site. Air is drawn from the duct into the RSMS-3 through a ¼ inch o.d. copper tube. After drying, the particles entered into the mass spectrometer through one of five flow limiting orifices, 50, 110, 220, 440, and 770 nm. Total particle measurements were performed using a commercially available Scanning Mobility Particle Sizer (SMPS).

Sample Results and Conclusions

At the conclusion of the E-DATAS field monitoring efforts an enormous dataset was established for ambient aerosol characterization at the MLK site with over 500,000

ambient aerosol particles being analyzed with the RSMS-3. Additionally over 61,000 aerosol size distributions were collected via the mobile monitoring effort with 42,426 data points being collected for formaldehyde, and 26,843 data points collected for chromium.

The project conclusions that are summarized below are organized by monitoring activity, (mobile monitoring vs. fixed-site aerosol monitoring).

Mobile Monitoring

Through implementation of the Duke University Mobile Laboratory, over 130,000 data points were measured during the E-DATAS to characterize the spatial, temporal and seasonal variability of water-soluble hexavalent and trivalent chromium, formaldehyde, ozone, and particulate matter.

The analyses of this data indicate the following significant conclusions:

- Aerosol number concentration, chromium VI, and $PM_{0.27}$ varied significantly by location.
- The variability in formaldehyde and ozone concentrations during the summer 2005 campaign was lower in comparison to the aerosol concentration. Since both formaldehyde and ozone are either partially or fully produced by photochemistry, this result is expected.
- Only formaldehyde showed a seasonal trend with concentrations being highest during the spring and summer, while the winter campaign had the lowest concentration.
- $PM_{0.27}$ shows a seasonal trend similar to that of formaldehyde, but the trend is largely obscured by the strong variability in the data.
- Comparison of the mobile data to the federal- / state-run network indicates:
    - Comparisons with CO and NOx concentrations measured at the central site do not correlate well with the mobile results for formaldehyde, $PM_{0.27}$, or chromium VI.
    - Both formaldehyde and $PM_{0.27}$ correlate well with the PM_{10} and $PM_{2.5}$ measured at the central site. This suggests that $PM_{0.27}$ and formaldehyde are influenced by long-range sources.
    - Formaldehyde and $PM_{0.27}$ show a positive correlation with temperature, suggesting photochemical activity.

Fixed-Site Aerosol Monitoring

With over 500,000 ambient aerosol particles, data had to be analyzed in clusters of 40,000 particles. Data collected from each of the four monitoring intensives was kept separate from other intensives. For the MLK site, data were separated into 16 chemical composition classes: OCANS (organic carbon, ammonium nitrate, and ammonium sulfate containing particles), ammonium nitrate, potassium, EOC (elemental and organic carbon), amine, sodium, potassium with sodium, iron, iron with cerium/lanthanum, lead, zinc, zinc with lead, tin/antimony, lithium, vanadium, and other metals.

From the analysis of this dataset, AQMS has the following understanding of the source contributions at the MLK site.

- Air quality at the MLK site has both local and regional characteristics.
- The MLK site is impacted by wood and biomass burning. There is a slight bias toward wind directions for the northwest where the greatest nearby residential population exits. There is also a slight bias toward the nighttime, consistent with residential wood burning.
- The MLK site is impacted by diesel vehicle exhaust, as indicated by the EOC measurements. The slight enhancement of EOC when the wind is from the east may indicate a contribution from industrial combustion sources. Also, diesel emissions from the nearby DART depot impact the MLK site.
- The MLK site measurements have signatures from stack emissions where aliphatic amines have been added during the scrubbing process used to remove SO2 from the effluent.
- Multiple local industrial combustion processes to the east and southwest contribute to the MLK site signature.
- Particle composition signatures associated with emissions from the Delaware City Refinery, CitiSteel, and the Delmarva Edgemoor Power Plant were detected in the ambient air sampled at the MLK site. Bag sampling at the CitiSteel site confirmed this source signature and association.
- Emissions from local industrial combustion impact the MLK site. Particle classes associated with local industrial emissions all have characteristic increases in concentration in the early morning, late evening or both.
- Signatures from particles thought to be emitted from large ships were measured at the MLK site. Wind dependence (110°) indicates that the Port of Wilmington is a possible source for the MLK site ambient measurements.
- In broad estimates, the Wilmington aerosol is characterized as follows:
    - Secondary aerosol of regional origin constitutes about 38% of PM_1.
    - Secondary aerosol of local origin constitutes about 27% of PM_1.
    - Biomass burning contributes about 14% of PM_1.

- Primary particulate emissions from vehicular traffic contribute about 8% of $PM_{1.}$
- Primary particulate emissions from local industrial sources contribute about 13% of $PM_{1.}$

1.0 Introduction

In 2003, the Delaware Air Quality Management Section (AQMS), with the support of the Environmental Protection Agency, began a state-wide Delaware Air Toxics Assessment Study (DATAS) with the intent to gain a better understanding of ambient air toxics concentrations throughout Delaware and the potential health risks associated with exposure to those toxics. Delaware's goal has been to develop an improved air toxics monitoring network and emissions inventories to support the quantitative evaluation, characterization, and tracking of ambient air toxic concentrations.

Consistent with the goals and objectives of the Urban Air Toxics Strategy, DATAS was designed to assist with the following activities:

- Assessment of potential risk due to air toxics in communities throughout the state,
- Development of a prototype study of air dispersion modeling,
- Development of a statewide air toxics risk management plan,
- Improvement of emission inventories for air toxics. .

The DATAS involved the development of a five-station monitoring network for 2003 and a speciated 2003 air toxics emission inventory. Along with meteorological data, the data are currently being integrated into an ambient air quality model with the objective of creating a meaningful resource that can be used to more accurately characterize potential risk, both regionally and locally. This is Phase II of the two phase DATAS project, which is expected to be completed in 2007.

Although Phase I of the DATAS project is complete, the results led to additional areas of interest, such as episodes of elevated aerosols and metals, and specific source attribution. The AQMS recognized the need for improved temporal and spatial resolution monitoring, as well as additional information on air particle size distribution and composition, in order to build on the results from Phase I of DATAS.

Through a funding opportunity provided by the National Air Toxics Monitoring Program-Community Assessments, AQMS was able to implement an enhanced Delaware Air Toxics Study (E-DATAS). The E-DATAS was designed to provide AQMS with: (1) improved spatial and time resolved data, (2) an opportunity to utilize state of the art particle size distribution and composition technology through partnerships with top tier research facilities, and (3) an enhanced understanding of the pollutant sources that impact air quality in Wilmington.

1.1. E-DATAS Study

Of the five monitoring sites used for the DATAS project, the Wilmington site was chosen for the E-DATAS based on results from the first phase of the project. This urban site is impacted by a mix of pollutant sources. The DATAS results generally showed higher

pollutant concentrations compared to the other sites, and therefore this site was chosen for the E-DATAS. The monitoring station is located on Martin Luther King Boulevard (MLK).

To provide the highest level of research for this project AQMS collaborated with experts from the University of Delaware, Duke University, and U.S. EPA National Exposure Research Laboratory (NERL) to provide state of the art equipment and top technical advice. The University if Delaware Department of Chemistry and Biochemistry utilized a Real-time Single-particle Mass Spectrometer, version-3 (RSMS-3) to measure particle number size distribution and composition, and a fixed Scanning Mobility Particle Sizer (SMPS) to perform particle-size measurements. The RSMS-3 technology was used to determine particle size distribution and composition of continuously monitored air during four one-month intensive monitoring efforts, one for each climatological season, and for source sampling (i.e., bag sampling) of air at suspected emission sites in the Wilmington area.

The Duke University Civil and Environmental Engineering Department performed mobile measurements for this project. Personnel from Duke University employed aerosol and gas collectors which continuously measured formaldehyde (HCHO), chromium species (Cr^{+3} and Cr^{+6}), and ozone (O_3) while moving along mapped routes surrounding the monitoring site. Additionally, the mobile monitoring unit was equipped with a mobile SMPS which measured particle size distribution in route.

Mobile monitoring was performed during four one week intensives, which was coordinated with the University of Delaware sampling effort. During each intensive, the mobile unit performed daily six-hour measurements (11:00 AM to 5:00 PM).

Fixed monitoring followed a month-long monitoring intensive during which ambient air was continuously monitored at the MLK site. Additionally, source sampling at suspected emission source points was conducted using sample bags which were analyzed using RSMS-3 equipment. Mobile and fixed monitoring intensive periods were conducted between April 2005 and February 2006.

1.2. E-DATAS Enhancements

1.2.1. Mobile monitoring

Mobile monitoring supplies information on two counts. First, it provides spatial information from mobile transits, e.g., along and normal to traffic pattern, along the crosswind paths of point sources used to characterize the monitored data. Secondly, mobile monitoring provides spatial variability information at fine scales which can be used to validate the modeled concentration distribution function of the variability for the grid cell in which the monitor is located. This will be useful to evaluating the National Exposure Research Laboratory's (NERL) so-called "Neighborhood-scale" air quality

modeling paradigm described as follows: Since exposure estimates depend on concentration and dosage, both the grid model prediction of concentration, as well as the magnitude of the range of the within-grid variability becomes an important measure of risk. The U.S. EPA Neighborhood scale modeling project is designed to provide model outputs of both gridded concentrations from its Community Multi-scale Air Quality (CMAQ) modeling system for air toxics, as well as model outputs of the concentration distribution functions that describe the with-in grid variability. This paradigm for air toxics assumes that when significant within-grid concentration variability is known to exist, additional information on the characteristics of such distributions will be supplied to complement the grid resolved simulations from the CMAQ modeling system as inputs to risk-based population exposure models and assessments. The contribution to this variability is a result of source dispersion within grid as well as from the photochemistry from within grid transport and turbulence. Currently, a formal collaboration is in place between the AQMS, U.S. EPA Region III, and U.S. EPA – NERL towards implementing the neighborhood-scale modeling approach for the State of Delaware and Philadelphia. The mobile monitoring component of this project will be invaluable toward evaluation of the spatial variability distribution predictions.

1.2.2. Scanning mobility particle sizer (SMPS)

Number weighted size distributions of air particles can be determined in situ using SMPS technology. The SMPS technique combines electrical aerosol analyzer with condensation particle counters (CPC) to determine particle sizes in the 5 – 800 nm range [*Brouwer et al., 2004*]. The SMPS relies on bringing aerosols to charge equilibrium and a differential mobility analyzer selects particles of uniform sizes according to electrical mobility. The CPC then counts the particles to determine concentrations for each size range.

1.2.3. Rapid single-particle mass spectrometry

The E-DATAS used single-particle mass spectrometry technology, RSMS-3 in this case, to provide additional data necessary in identifying chemical markers for source apportionment. This information can be used to aid in the development of control strategies for reducing hazardous air pollutant (HAP) impacts at the communities of interest. Single particle mass spectrometers are ideally suited to count ambient particles as a function of size and composition.[*Johnston*, 2000; *Johnston and Wexler*, 1995; *Noble and Prather*, 2000].

Because of the sheer volume of data being collected, typically tens to hundreds of thousands of particle spectra, statistical or neural network chemo metric treatments have been employed to classify particles into a relatively small number of groups having similar spectra. These groups can then be correlated with particle size, meteorological variables, time-of-day, and known emission sources to characterize the ambient aerosol. The ionization method used in single particle mass spectrometry, laser ablation, is

applicable to a wide range of particle compositions – organic and inorganic, semi-volatile and refractory. Metals are particularly well suited for detection. [*Rhoads et al, 2003; Pharses et at, 2003; Lake et al, 2003*]

1.3. Scope

The design and implementation of E-DATAS involved combining the efforts of the AQMS, University of Delaware, and Duke University along with technical advice from the U.S. EPA-NERL to enhance Delaware's current air toxics monitoring program.

Scanning mobility particle sizers (SMPS) were used by the University of Delaware and Duke University to determine particle size distributions in outdoor ambient air near the MLK monitoring site. Real-time single-particle mass spectrometry was used by the University of Delaware to further determine particle size and composition of air particles at the MLK site and from suspected emission sources. Mobile monitoring was used by Duke University to characterize the spatial distribution within Wilmington of gas-phase formaldehyde, water soluble chromium species, and ozone. The overall goal of this partnership was to gain a better understanding of ambient concentrations of hazardous air pollutants (HAPs) in urban Wilmington.

The following report describes, in depth, the results from each sampling method (mobile monitoring, RSMS fixed and source, and SMPS) applied by the research groups during the E-DATAS study. Further, study results have been interpreted and compared (i.e., mobile versus fixed sites), and potential applications of these results in future projects have been recommended.

2.0 Methods

2.1. Mobile Tracks Sampling Approach

The mobile measurements of formaldehyde and water-soluble chromium species as well as number size distribution of the aerosol have been carried out in Wilmington, DE, providing information on spatial distribution of these components on a scale of a hundred meters. High time resolution instruments for on-line measurements of the target components were installed on the Duke University mini-van mobile laboratory equipped with a Global Positioning System (GPS). The instruments employed in the study are described in separate sections of this document. The measurements were performed while driving and the concentrations were recorded as a function of time and location.

2.1.1. The mobile laboratory

The Duke University mobile laboratory (Figure 2-1) is a mini-van equipped with a battery pack and a true-sine inverter that allows autonomous operation of research equipment without external power sources. An on-board GPS (Garmin GPSmap 76CS) provides the location of the vehicle as a function of time, which is logged every second. The clocks of the GPS and the on-board computers and instruments are synchronized prior to each run. After accounting for the delays in instrument response, the location and concentration data are matched providing concentration fields as a function of space and time.

Figure 2-1. Duke University mobile laboratory

The sampling inlet was placed on the extendable mast, which is built into the van (Figure 2-1). The mast is on the left side of the vehicle, 1 m from the rear end. During the mobile

measurements the inlet was placed at 3 m height. The instruments were sampling through a 2-meter long Teflon manifold (½" o.d.).

Mobile measurements place a number of constraints on the instrumentation. First of all, they require a high time resolution. To have spatial resolution of 150 m at the driving speed of 20 miles per hour (32 km/h) the instrument should have a time resolution of about 15 seconds. The instruments need to be sensitive enough to distinguish elevated concentrations above the background. The instruments also need to be stable at the conditions of the driving, i.e. have minimum interference from the vibrations and acceleration/deceleration induced by the moving vehicle.

Several high-time resolution instruments were deployed during the E-DATAS, measuring spatial distribution of the following species:

- Water-soluble hexavalent and trivalent chromium in $PM_{2.5}$ size range
- Formaldehyde
- Ozone (only during the summer 2005 campaign)
- Particulate matter (aerosol) size distribution and concentration (in the size range12 nm – 270 nm in diameter)

The instruments for chromium and formaldehyde measurements were specifically developed for this study. Each of the instruments is described in separate sections below.

2.1.2. The route

The driving route was selected in collaboration with the E-DATAS science team such that it passes near the MLK central monitoring station and then extends to other areas of the city (Figure 2-2). The driving route used mostly quiet residential streets, while avoiding, where possible, busier roadways. This was done to avoid the dominating effect of the on-road emissions on the measurement results. By driving through quiet streets with little or no traffic, a more accurate assessment of the off-road concentrations can be obtained. The effect of the traffic on the concentration field can be assessed by inspecting concentrations at intersections with busier streets.

Because the concentration field varies not only with place but also with time, the same route was traversed several times (minimum 3) in order to obtain a reliable statistical characterization of the variability at each point and compare the mean values between different locations.

The sampling design for the mobile sampling was established with the goal to capture the concentration field variability in both space and time. To satisfy this requirement, a fixed sampling route was laid out; it included transects through various areas in Wilmington and allowed repeated traverses to achieve improved and reliable characterization of these variabilities. The route and the driving schedule were adjusted after the first

measurement campaign (Spring 2006) based on the measurement results and the input from the science team. It was found that the transect of the city should be performed within one hour, such that the atmospheric composition does not change significantly during that time. For a similar reason the originally planned schedule of sampling 3 times a day for 2 hours (7 am – 9 am, 11 am – 1 pm, 3 pm – 5 pm) was abolished, because the concentrations were changing too rapidly in the morning (because of the mixing of the atmosphere and the increasing photochemical activity), obscuring the spatial variability within the city. Instead, one sampling run from 11 am until 5 pm was adapted for the following campaigns. It was also decided that instead of concentrating on individual neighborhoods, one after the other, it is more beneficial for model evaluations to perform transects through several neighborhoods of the city during one run covering an area approximately corresponding to a 4 km grid, which is used in the air quality models.

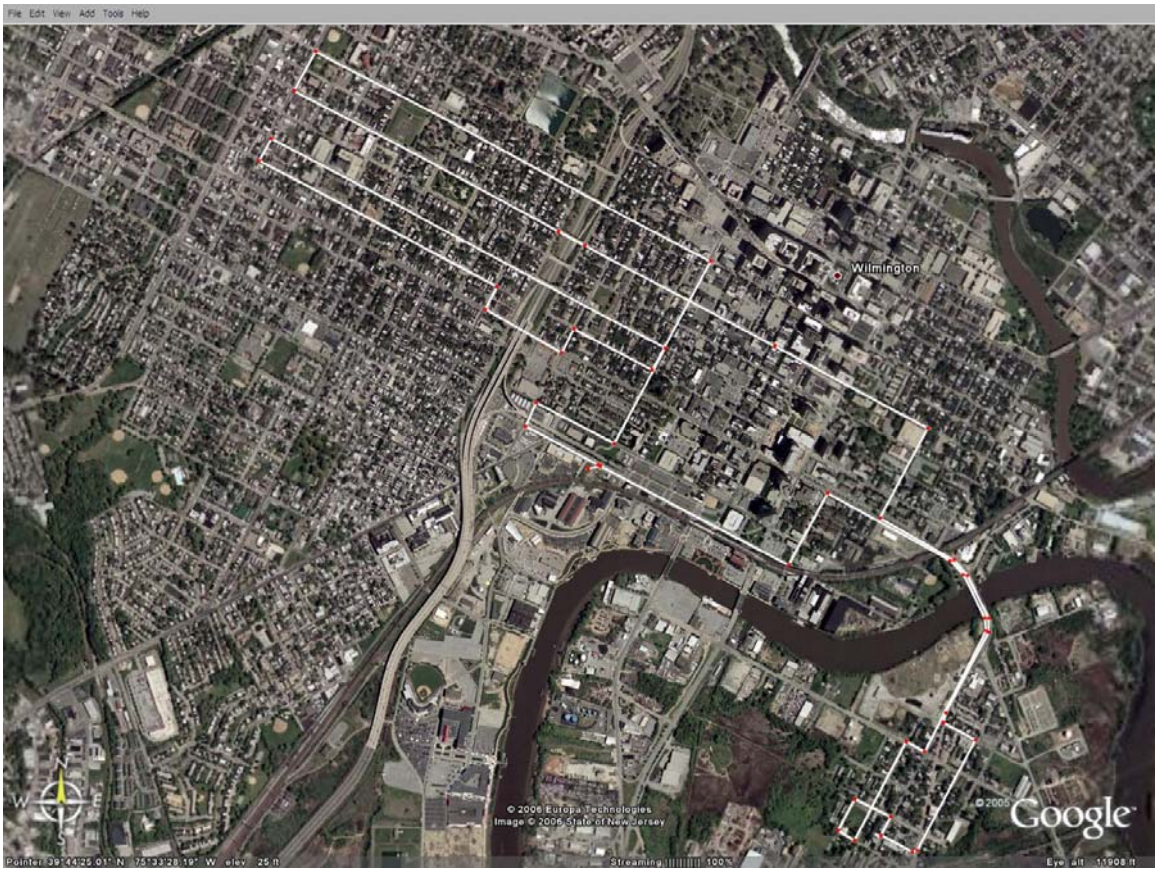

Figure 2-2. Satellite picture of Wilmington, DE showing the driving route.

2.1.3. Schedule

Mobile measurements were performed during four campaigns, one each season (winter, spring, summer and fall), allowing characterization of seasonal variability of different local sources, as well as the spatial distribution of the aerosol. The campaigns were held during the following periods:

Spring 2005:	04/25 – 5/1
Summer 2005:	7/31 – 8/6
Fall 2005:	11/10 – 11/14
Winter 2006:	2/23 – 2/26

2.1.4. Quality Assurance

All of the measurements were performed according to the approved Quality Assurance Project Plan (QAPP). The instruments were calibrated in the laboratory prior to each campaign. The blanks, flow rates and other critical operational parameters were checked on a regular basis during the measurements.

2.2. Real-Time Single Particle Mass Spectrometer (RSMS-*3*)

RSMS-3 is a dual-polarity laser ablation time-of-flight mass spectrometer that was deployed to the MLK site for single particle measurements. A detailed description of the instrument is given by *Lake et al., 2003*. Ambient aerosol was sampled through a PM_{10} inlet containing a 3.8 cm o.d. duct extending 1 meter above the trailer and approximately 5 meters above ground. Air was drawn from the duct into RSMS-3 through a ¼ in. o.d. copper tube. Moisture content of the air was reduced by passing the aerosol through a Nafion dryer (Permapure, Inc., Toms River, NJ). After drying, the particles entered the mass spectrometer through one of five flow limiting orifices. Particle sizes selected by the flow limiting orifices had median aerodynamic diameters of 50, 110, 220, 440, and 770 nm. Data collected within this size range was used to give an estimate of PM_1.

The size selected particle beam is drawn through four differential pumping stages into the mass spectrometer, where particles are ablated with a collinear, counter-propagating 193-nm laser beam (GAM Laser, Orlando, FL). A laser ablated single particle produced positive and negative fragments, which were mass analyzed with dual drift tubes. The source region for the ions was 1 cm wide and was surrounded by two stainless steel mesh grids held at ± 1080 V. A second set of grids, held 1 cm from the source grids, were held at ± 8790 V. The field free drift regions were 63.5 cm long and were also held at ± 8790 V. Once the ions exited the drift tube, they were accelerated with multichannel plate detectors (Burle Electrooptics, Inc., Sturbridge, MA). Each detector was connected to two 500 MHz digitizer channels (Acquiris, Monroe, NY) which had overlapping detection sensitivities. The effective dynamic range was approximately 300 after accounting for baseline offset, background noise, and detector saturation.

Particle transmission into the mass spectrometer is dependent upon the Stokes number for aerosol flow through a critical orifice located downstream from the flow-limiting orifice. The median (aerodynamic) diameter transmitted is dependent upon the pressure of the critical orifice, which is determined by the flow-limiting orifice selected. A range of particle sizes are actually transmitted into the mass spectrometer, with a determined σ_g

(standard deviation) of 1.2 [*Phares et al., 2002*]. Because the particles analyzed by this instrument are too small to be efficiently detected by light scattering, the excimer laser is simply free-fired at a constant rate (50 Hz) during the sampling period. Particles are detected by monitoring the ion signal from both positive and negative ion detectors.

A particle is considered "detected" and its mass spectra are saved whenever the signal intensity from either the positive or the negative ion detector exceeds an experimentally determined threshold level above background. The raw spectra are converted from the time domain to m/z (signal to noise) domain, integrated, summed into 1 m/z unit increments ± 0.5 about each integer, and normalized. The processed spectra are separated into composition classes with the fast adaptive resonance algorithm, ART2-a [*Phares et al., 2001*].

The operating schedule for RSMS during E-DATAS is given in section 3.1.1. Most single particle measurements were performed during one-month long intensive measurement periods. Four intensives were completed, one each in winter, spring, summer and fall to check for seasonal variations. Other single particle measurements were performed in the periods between intensives in an effort to characterize several key sources within a 10 km grid around the MLK site. These source sampling experiments are described in greater detail in sections 2.3 and 3.1.5.

A particle concentrator, m-VACES (mini-versatile aerosol concentration enhancement system) [*Geller et al., 2005*], was installed with RSMS-3 for the summer, fall, and winter intensives. The particle concentrator enhanced the number of particles entering the mass spectrometer thereby increasing the overall hit rate. A drawback to the m-VACES system was that it needed constant adjustments to keep the aerosol concentration optimized. Thus, the amount of time which RSMS-3 could collect data each day was often limited as the system could not be left unsupervised for long periods of time.

2.3. Source Sampling

Several particulate matter (PM) emitting sites were identified by AQMS to be sampled directly with RSMS-3. Source sampling was accomplished by pulling air at 30 Lpm directly into a 0.5 m^3 Tedlar coated bag with an oil-free pump. After it was filled, the bag was sealed and transported back to the measurement site for analysis. While the source sample was being collected, RSMS-3 simultaneously measured aerosol at the MLK site. Ambient aerosol at the MLK site was assumed to be a background control sample when compared to the source sample. Source samples were either taken directly from emission stacks or indirectly from an area downwind from the emission stack.

Because of unquantifiable wall losses during aerosol sampling and transport of the bags, the bag and MLK aerosols were analyzed only at one aerodynamic size setting of RSMS-3 (220 nm), which typically corresponds to the maximum of particle emission from a combustion source. (See discussion in Section 3.1.1.) The distribution of particle classes from the bag and MLK samples were compared to determine if a particle class showed an

enhanced concentration in the bag sample. Once a particle class was identified as a possible fingerprint for a local source, the entire single particle dataset was reevaluated to examine the properties of the particle class.

2.4. Measurements of Cr(III), Cr(VI)

The Steam-Jet Aerosol Collector - Long Pathlength Absorbance Spectroscopy (SJAC-LPAS), a high time resolution, automated instrument for mobile measurements of spatial distribution of hexavalent and water-soluble trivalent chromium in ambient aerosols, has been developed for this study. Because of the novelty of this instrument, it is described here in more detail.

2.4.1. Aerosol Sampling and Collection

The schematic of SJAC-LPAS system is shown in Figure 2-3. Ambient aerosol is collected with the Steam-Jet Aerosol Collector (SJAC) [*Khlystov, et al.*, 1995]. The air is sampled into the SJAC at a rate of 16.7 liters per minute through a Teflon-coated $PM_{2.5}$ cyclone (URG, Inc.). The SJAC operates by injecting steam into the sampled air stream, which causes water vapor to condense on the sampled aerosol particles. Particles grow due to water condensation to a size of at least 1μm in diameter and are collected by a cyclone. The SJAC collects quantitatively particles down to a few nanonmeters in diameter (collection efficiency 99%) [*Khlystov, et al.*, 1995]. The collected liquid containing dissolved aerosol species is continuously pumped out with an 8-channel Dynamax RP-1 (Rainin Instrument Co., Emeryville, CA) peristaltic pump and is directed to the Long Pathlength Absorption Spectroscopy - Continuous Flow Analysis system (LPAS-CFA), where the concentration of hexavalent chromium is determined.

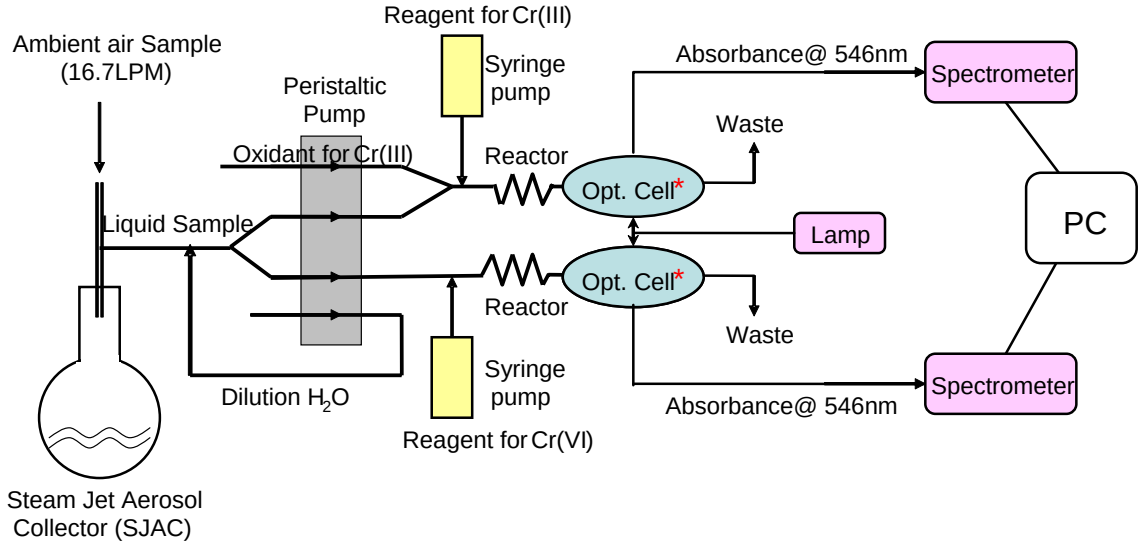

Figure 2-3. General schematic of SJAC-LPAS system for measurements of hexavalent and trivalent chromium in ambient aerosol.

2.4.2. LPAS-CFA system

The LPAS-CFA system uses the well established diphenycarbazide (DPC) colorimetric method [*Allen*, 1958]. Application of this method for environmental chromate analysis has been limited by its relatively poor sensitivity. Liquid Core Waveguide (LCW) optical cells have been used to increase the sensitivity of colorimetric methods [*Lei, et al.*, 1983] and have been successfully applied to Cr(VI) determination with the DPC method [*Li, et al.*, 2003; *Yao and Byrne*, 1999]. A LCW provides long optical pathlength by constraining light propagation within a liquid medium which has a higher refractive index (R.I.) than the surrounding solid tubing [*Lei, et al.*, 1983]. Teflon AF-2400 (DuPont), has an R.I. of 1.29 and many of the desirable chemical properties of Teflon [*Altkorn, et al.*, 1997].

Before entering the LPAS-CFA system, the collected sample is diluted with a constant flow of double-deionized water to ensure sufficient flow for Cr(VI) and Cr(III) analysis. The diluted sample then passes a debubbler. The bubble formation in the system is further prevented by using an exit restriction to increase backpressure. The flow after the debubbler is divided equally for the Cr(VI) and Cr(III) analysis. A computer-controlled syringe pump (Versa 6, Kloehn Ltd., Las Vegas, NV) is used to deliver the reagent. Super-serpentine mixer (1/16”OD, 0.030”ID, 2m long, GlobalFIA Inc., Fox island, WA) is used for mixing and reacting the sample with the DPC reagent. The serpentine mixer has a minimal axial dispersion, which is an important factor for a fast instrument response.

The sample is then directed to the LCW optical cell. The design of the LCW cell follows that described elsewhere [*Yao and Byrne*, 1999]. A 5m long Teflon AF-2400 tubing (0.031” OD and 0.008” ID, Random Technologies, San Francisco, CA) is used as the

LCW. Two optical fibers (200μm and 600μm) are used to connect the cell to a LS-1 Tungsten Halogen Light Source and a USB2000 Miniature Fiber Optic spectrometer (all from Ocean Optics, Dunedin, FL). Absorbances at the detection wavelength of 546 nm and the non-absorbing wavelength of 700 nm are used to calculate chromium concentration, with the non-absorbing wavelength serving to compensate for any eventual drifts in the signal.

The setup for the Cr(III) analysis is similar to that for Cr(VI) analysis except that the liquid sample is oxidized by adding a solution of hydrogen peroxide and directing the flow through a one-meter long super-serpentine mixer before mixing it with the DPC reagent. Cr(III) concentration is then determined as the difference between the two lines.

2.4.3. Reagents and Standards

All solutions were prepared with double deionized water and using analytical grade reagents. 1,5-diphenylcarbazide (Alfa Aesar, Ward Hill, MA), acetone (Fisher), NaOH (Fisher), H_2O_2 (Acros Organics), $K_2Cr_2O_7$ (Fisher), $CrK(SO_4)_2$ (Fisher) were obtained as indicated. Trace-metal grade sulfuric acid was obtained from EM Science (Darmstadt, Germany). The following reagent compositions were used. 1,5-diphenylcarbazide (DPC) solution was prepared by dissolving 0.167g of the reagent in 100 ml of acetone and then mixed with 1.67% H_2SO_4 solution in 1:1 volume ratio. 0.1% H_2O_2 solution was prepared by diluting 0.143 ml of H_2O_2 with 0.1 M NaOH solution to 100 ml.

2.4.4. Calibration and Limit of Detection

The analytical part of the system was calibrated using Cr(VI) and Cr(III) standard solutions. The absorbance signals for both Cr(VI) and Cr(III) have linear relationship with chromium concentration (Fig. 4), but the signal response for Cr(III) is less sensitive than that for Cr(VI). The Limit of Detection (LOD) for the Cr(VI) and Cr(III) aerosol measurements, defined as three times the standard deviation of the blank (reagents + deionized water) measured in laboratory conditions, is 0.19 ng/m^3 for Cr(VI) and 1.9 ng/m^3 for Cr(III). When the system is running on a moving vehicle, the vibrations and frequent acceleration/deceleration caused by the driving affect the system stability. Data obtained from a moving vehicle showed a larger standard deviation, and thus a higher LOD of 0.48 ng/m^3 for hexavalent chromium. If only hexavalent chromium (no Cr(III)) is measured, the LOD under driving conditions is lowered to 0.24 ng/m^3, because no dilution is required to provide a sufficient flow to the detector.

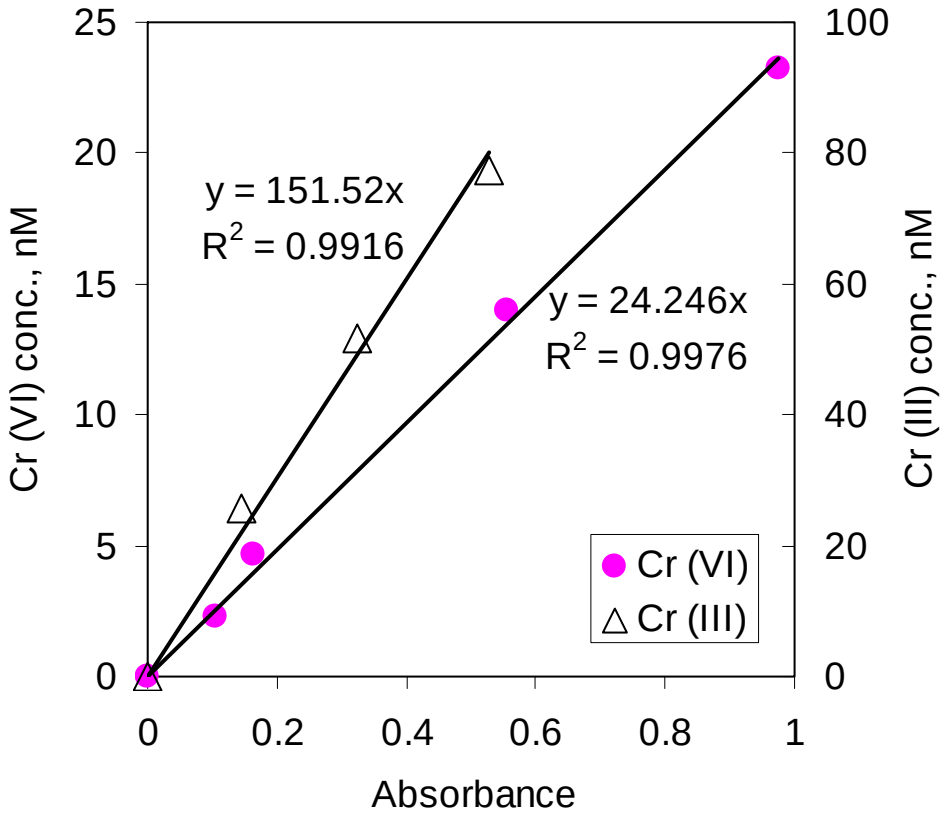

Figure 2-4 Calibration curves of Cr(VI) and Cr(III) standard solutions.

2.4.5. Response Time

The time resolution of the instrument was tested by observing the signal change in response to a step change in chromium concentration. Due to the time needed to transfer the sample from the point of collection to the optical cell, there is a considerable delay before a change in signal is detected. The delay times (as defined by the time difference between the input concentration change and the 50% change of the signal) are 8'30" for the Cr(VI) line and 9'57" for the Cr(III) line, reproducible to within 3 seconds. Due to the mixing processes in the system, a step change in the input concentration appears as an S-shaped curve. The system response function, which is the system response to an infinitely sharp pulse input (δ-signal) can be found by differentiating the S-shaped response curve with respect to time. The time resolution of the instrument was assessed by convoluting the response function with a rectangular pulse function of different duration representing a plume. Our objective was to be able to observe plumes having a concentration at least two times higher than the background. System responses to plumes of different duration are shown in Figure 2-5. Due to the mixing processes in the instrument, the plume signals are smeared out. When the plume duration is 15 seconds or longer, the signal due to the plume can be distinguished from the noise of the background (the instrument noise is 10%). Time resolution of 15 sec corresponds to a spatial resolution of about 150 m, if measurements are made at a driving speed of 30 km per hour.

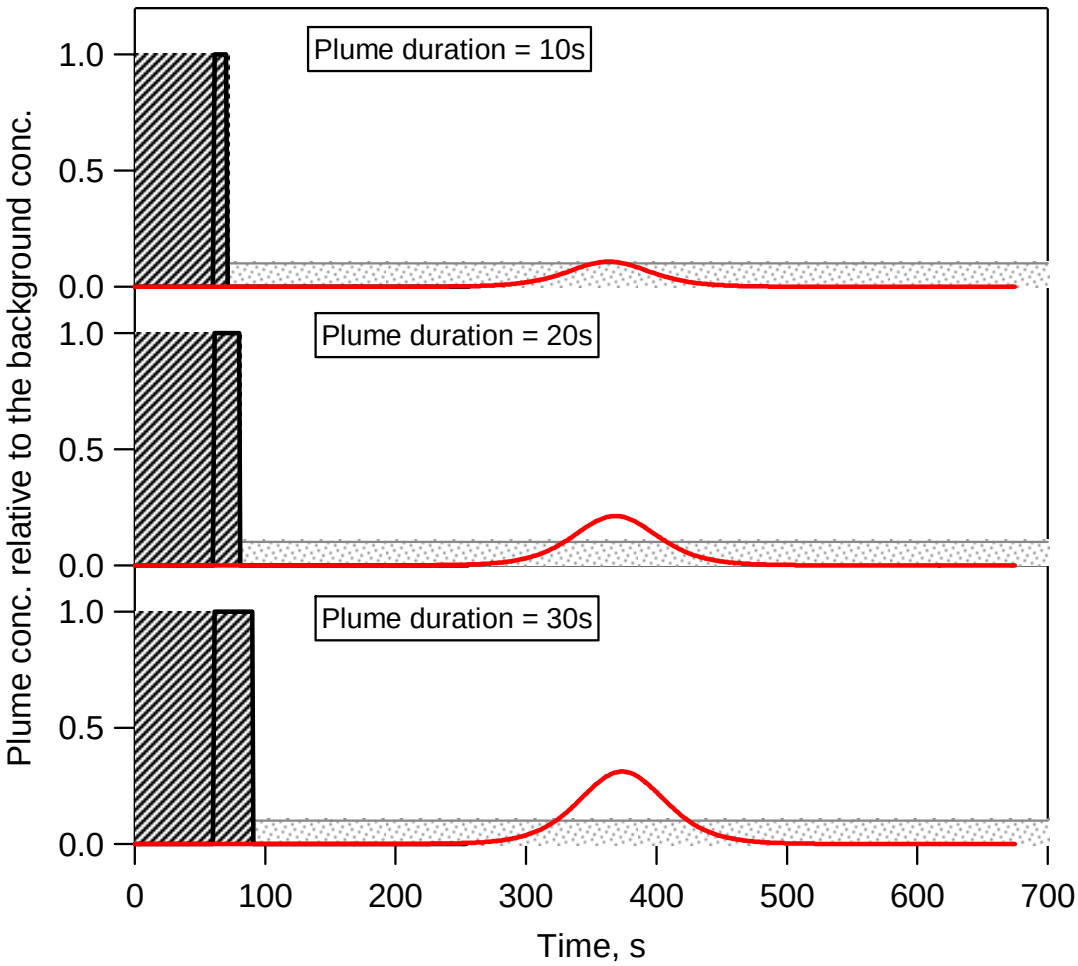

Figure 2-5 Modeled system response to plumes of different duration. The grey area represents the noise level.

2.4.6. Field deployment

Although the ambient Cr(VI) concentration was within the measurable range, the concentration of water-soluble Cr(III) was found to be usually below the LOD. Therefore, the instrument was mostly run measuring Cr(VI) only (the Cr(III) line was switched off) to decrease the detection limit for Cr(VI).

2.5. Measurements of HCHO

2.5.1. General description of the instrument

The instrument for formaldehyde measurements was based on the instrument described by Fan and Dasgupta, 1994, with several modifications. A general schematic of the

instrument is shown in 2-6. Formaldehyde is collected using continuous-flow wet-walled denuder [*Simon, et al.*, 1991]. The air sample flow rate is 5.2 LPM. The air stream passes through a gap between two parallel plates which are covered with a film of flowing water. Formaldehyde dissolves in the liquid which is continuously pumped out for analysis.

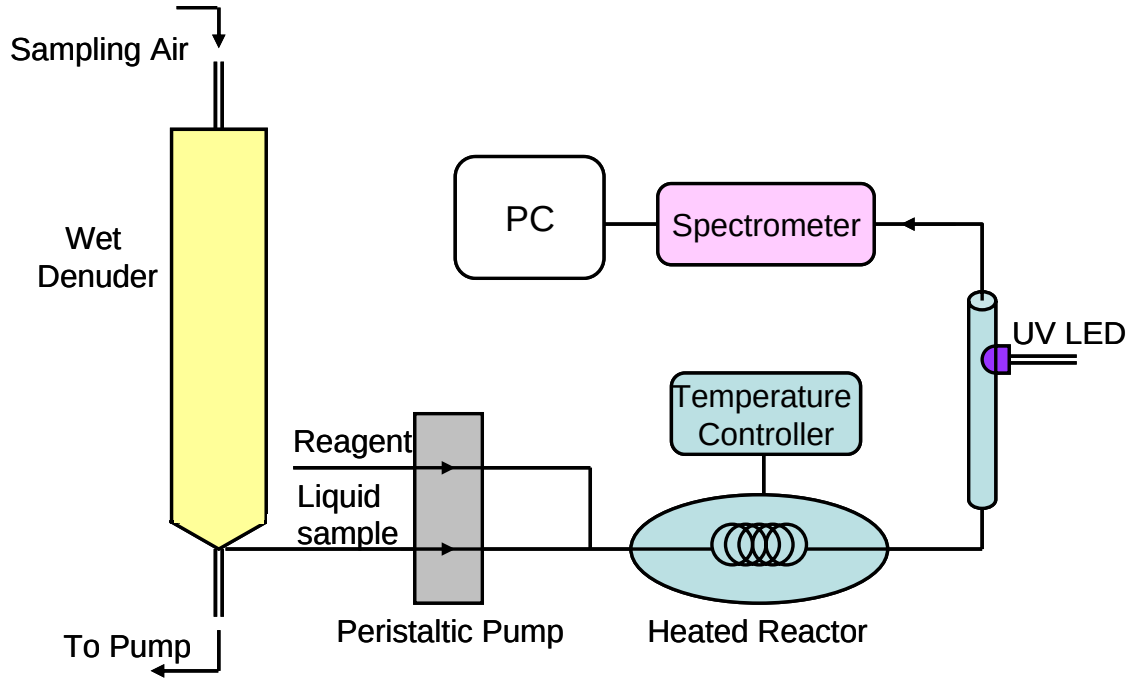

Figure 2-6. A general schematic of the instrument for formaldehyde measurements.

The formaldehyde collected in the denuder liquid is debubbled and transported to the heated reactor to react with 1,3-cyclohexandione (CHD) and the fluorescence is detected using a USB2000 Miniature Fiber Optic spectrometer (Ocean Optics, Dunedin, FL) with a GaN-based UV-LED as the excitation source. The excitation wavelength is 375 nm, and the fluorescence emission is measured at 465 nm. Instead of the Flow Injection Analysis that is used in the Fan and Dasgupta system, we used a continuous flow analysis (CFA) system to increase the time resolution of the instrument. The other modification is the use of a fluorescence detection cell based on the Liquid Core Waveguide made of Teflon AF (Dupont). The design of the cell follows that of Li, et al., 2003.

2.5.2. Calibration and Response Time

The instrument was calibrated using a gas-permeation standard, showing a linear response. The detection limit of the instrument is 0.026 μmol/m^3 (0.78 μg/m^3 or 0.64 ppbv). The response time was determined similarly to the procedure described for the chromium instrument. The instrument was subject to a step change in concentration of formaldehyde in air by switching between zero air and formaldehyde standards. The time

resolution of the formaldehyde instrument is 20 s, similar to that of the chromium instrument.

2.6. Measurements of ozone

During the Summer 2005 campaign a 2B Technologies Model 202 ozone monitor (Golden, Colorado) was installed on the mobile laboratory. The instrument was provided by the Air Pollution Prevention and Control Division of the U.S. EPA's NERL. The ozone monitor has a measurement range from 1.5 ppbv to 100,000 ppbv. The precision and accuracy are the greater of 1.5 ppbv or 2%. It determines ozone concentration based on the well established technique of absorption of UV light at 254 nm. The monitor is light-weight (4.7 lb., 2.1 kg.) and has a low power consumption (4 W). The time resolution of the instrument is 10 s. The instrument was calibrated prior to the campaign by the personnel of the U.S. NERL.

2.7. Scanning Mobility Particle Sizer

2.7.1. Mobile Measurements

Vehicular traffic is one of the main sources of the $PM_{2.5}$ in urban areas. Most of the particles emitted by traffic are small and are found in the ultra-fine size range (100 nm in diameter or smaller), while the PM transported from distant sources is larger, with sizes around 0.3-0.5 micrometers [*Seinfeld and Pandis*, 1998]. The PM from long-range sources varies slowly, with time scales ranging from hours to days. The vehicular sources, on the other hand, show a strong diurnal and spatial variability. Therefore, in the absence of other direct PM sources, the traffic is expected to be the dominant source of spatial and temporal variability of $PM_{2.5}$ mass within a city. By monitoring the aerosol size range where the traffic particulates are emitted, i.e. the ultra-fine size range (smaller than 100 nm in diameter), it is possible to catch most of the variability of the $PM_{2.5}$ aerosol mass within the city.

Particle size distribution measurements were performed using the Scanning Mobility Particle Sizer (SMPS) [*Wang and Flagan*, 1989]. The SMPS sizes particles from 12 nm to 300 nm using electrical mobility technique by selecting particles in a narrow mobility range, which depends on the voltage setting of the instrument. The selected particles are counted with a Condensation Particle Counter (CPC). By performing an exponential ramping of the SMPS voltage, particles of different sizes are selected and counted, providing the number concentration as a function of size (i.e. the number size distribution).

The SMPS was built using standard parts from TSI Inc (TSI 3071 Differential Mobility Analyzer and TSI 3010 Condensation Particle Counter). The SMPS performed one-minute measurements of the aerosol number and size distribution in the size range 12 nm

– 270 nm, thus covering the ultra-fine size range, as well as about half of the mass distribution of the long-range transported particles [*Seinfeld and Pandis*, 1998].

The size distribution measured with the SMPS can be used to calculate the volume concentration of the aerosol. The volume concentration is a proxy for aerosol mass concentration. It appears that the volume concentration in urban air can be used to calculate the mass concentration within 20% accuracy using the particle density of 1.5 g/cm^3 [*Khlystov, et al.*, 2004]. Thus, by observing the volume concentration of PM in the ultra-fine size range one can characterize the spatial variability of the $PM_{2.5}$ mass.

2.7.2. Fixed site measurements

A scanning mobility particle sizer (SMPS; TSI Inc., Model 3081) system was operated continuously during RSMS-3 measurements. Aerosol was drawn into the instrument through the PM_{10} inlet described in Section 2.3. The SMPS was connected to the inlet with ¼" o.d. copper tubing. Every three minutes, the SMPS measured the particle size distribution from 20 – 453 nm. Unfortunately, the system required maintenance during the summer intensive and was not operational.

3.0 Results and Discussion

3.1. RSMS-3 Analyses

3.1.1. Particle Composition Classes in Wilmington

Over 482,000 particles were analyzed with RSMS-3 at the MLK field site during the study. Table 3.1 shows the dates of each of the intensive sampling periods, as well as the number of particles analyzed in each. An additional 40,000 particles were analyzed during the source sampling that was conducted between the intensive periods.

Table 3-1. Dates and number of particles analyzed during intensive periods in the Wilmington study.

	Spring	Summer	Fall	Winter
Dates	05MAY05-02JUN05	13JUL05-25AUG06	17NOV05-23NOV05	26JAN06-26FEB06
Number of Particles	19,984	81,669	166,527	214,458

The particles were first classified using an unsupervised clustering artificial neural network, ART2-a (adaptive resonance theory), to sort the particles. ART2-a compares the dot product of two particle mass spectra vectors to an experimentally determined vigilance parameter. If the dot product is larger than the vigilance parameter, the particles are considered the same and are grouped together. If the dot product is less than the vigilance parameter, the particles are considered different and are classified separately. Each time a new particle is added to a class, the overall weighted class vector shifts toward the vector of the added spectrum by a factor known as the learning parameter. More detail on ART2-a can be found in *Phares et al., 2001*.

Due to the massive quantity of data produced by RSMS-3 during E-DATAS, the mass spectra had to be analyzed by ART2-a in groups of 40,000 (data from each intensive was kept separate from the other intensives). Small variations in signal intensities of the various particle types caused each run of the clustering algorithm to produce approximately 300 ART2-a classes. ART2-a classes having the same dominant m/z values but slightly different relative intensities were considered to be the same particle type and were manually combined into a single class. Two classes were subdivided based on the presence of minor chemical components. The original potassium class was split into two classes: potassium and potassium with sodium. The original lead class was split into two classes: lead and lead with zinc classes. As will be seen, subdividing these classes is useful as minor differences in particle composition can often be attributed to different particle sources.

After automated (ART2-a) and manual processing of the Wilmington data, 16 unique chemical composition classes were identified. These classes are: OCANS (organic carbon, ammonium nitrate, and ammonium sulfate containing particles), ammonium nitrate, potassium, EOC (elemental and organic carbon), amine, sodium, potassium with sodium, iron, iron with cerium/lanthanum, lead, zinc, zinc with lead, tin/antimony, lithium, vanadium, and other metals. These classes are discussed individually below. For each particle class, a figure is presented with the averaged mass spectra of all particles grouped into the class, fraction of particles vs. time of day, fraction of particles vs. wind direction, and fraction of particles vs. aerodynamic diameter (Figures 3-1 through 3-16). The percentages given in this section are the fraction of total particles in the E-DATAS data set.

RSMS-3 has been previously deployed at U.S. EPA Particulate Matter Supersites in Baltimore [*Tolocka et al., 2005*] and Pittsburgh [*Bein et al., 2005*], and earlier versions of the instrument were deployed at Particulate Matter Supersites in Atlanta [*Rhodes et al., 2003*] and Houston [*Phares et al., 2003*]. The particle composition classes identified in Wilmington are similar to those identified in other locations. Table 3.2 shows a comparison of the fraction of particles detected for each class in Wilmington, Baltimore, Pittsburgh, Houston and Atlanta.

Table 3-2. Comparison of major particle composition types in Atlanta, Houston, Baltimore and Wilmington[a]

Particle Classes	Wilmington	Baltimore	Pittsburgh	Houston	Atlanta
OCANS[b]	36%	51%	11%	--	74%
Ammonium Nitrate	23%	11%	54%	--	1.7%
Elemental/Organic Carbon	9.9%	20%	9.8%	16%	1.4%
Amine	3.5%	--[c]	3.3%	2.7%	--
Potassium	18%	7.8%	--	31%	7.8%
Potassium, Sodium	2.7%	--	5.8%	7.6%	1.3%
Sodium	2.4%				
Iron	1.3%	1.9%	2.3%	6.1%	3.0%
Iron, Cerium/Lanthanum	0.28%	--	0.3%	--	--

Particle Classes	Wilmington	Baltimore	Pittsburgh	Houston	Atlanta
Lead	0.88%	3.8%	2.9%	0.44%	0.4%
Lead, Zinc	0.11%				
Zinc	0.38%	1.6%	--	1.7%	--
Vanadium	0.26%	1.5%	--	0.64%	--
Tin/Antimony	0.54%	--	0.8%	--	0.3%
Lithium	0.13%	--	2.3%	--	--
Other Metals	0.11%	--	1.4%	1.7%	2.0%
Silicon dioxide	--	--	--	30%	0.4%

[a]Values given for each city are the percentages of particles in the data set. The Atlanta, Houston, and Pittsburgh composition classes have been modified to fit the composition designations used in the Baltimore and Wilmington studies. Totals may not add up to 100% due to rounding errors (>10% rounded to the nearest 1%, <10% rounded to the nearest 0.1%) and because some particle classes could not be fit into the designated categories.

[b]OCANS = organic carbon, ammonium nitrate, ammonium sulfate.

[c]Aliphatic amines are observed in Baltimore single particle spectra, but the Art2-a approach used caused them to be grouped into different composition types.

3.1.1.1. OCANS (Organic Carbon, Ammonium Nitrate, Ammonium Sulfate) (36%)

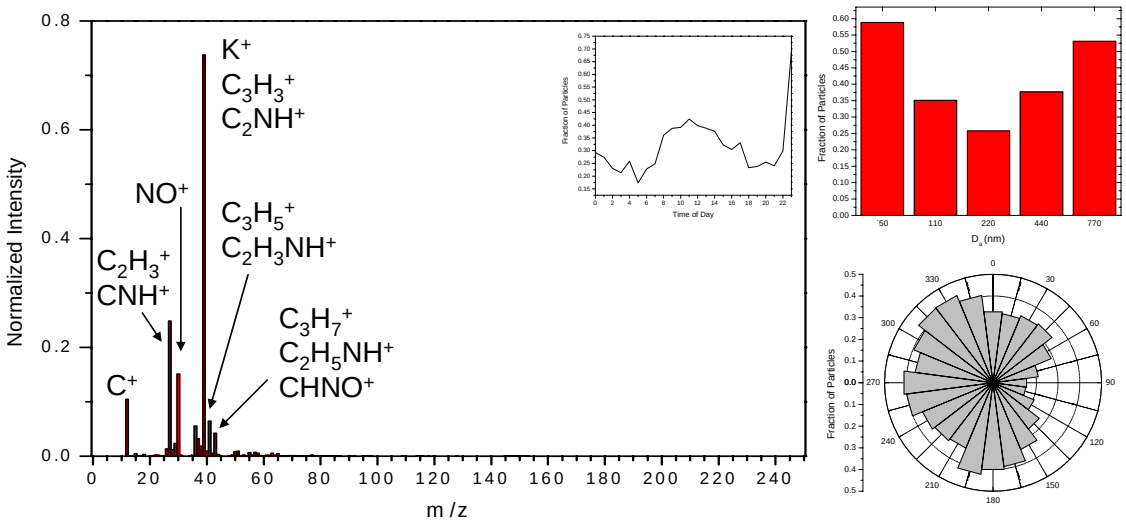

Figure 3-1. Summary statistics for the OCANS (organic carbon, ammonium nitrate, ammonium sulfate particle) class, 36% of the total particles analyzed.

OCANS particles are "internally" mixed particles consisting mainly of secondary components: sulfate, nitrate and secondary organic species. Since particles are ionized by laser ablation in RSMS-3, most organic compounds are extensively fragmented and molecular information is lost. Therefore, primary and secondary organic carbon cannot be distinguished and both are possible components of these particles. The OCANS particle class is indicated by low m/z hydrocarbon fragment ions and NO^+ (m/z 30) in the positive ion mass spectrum (Figure 3-1). Large OCANS particles (> ca. 200 nm) are thought to be regional in origin: particles that have grown considerably by condensation of secondary components as they are transported over a significant distance to the measurement site [*Ondov and Wexler, 1998*]. Besides a small decrease from the east (90°), the windflower plot in Figure 3-1 shows roughly equal probability for these particles from all wind directions, which is a characteristic of regional aerosol. Small OCANS particles (< ca. 200 nm) are thought to be of local origin with a long enough residence time in the atmosphere for growth by secondary components, but not long enough to grow completely. The majority of these particles are observed during the daytime hours when photochemical processing of secondary aerosol precursors is greatest. Together, large and small OCANS particles make up the largest fraction of the aerosol in Wilmington. As discussed later, OCANS and ammonium nitrate class particles allow estimation of 1) the total burden of secondary aerosol components and 2) the regional contribution to ambient aerosol.

3.1.1.2. Ammonium Nitrate (23%)

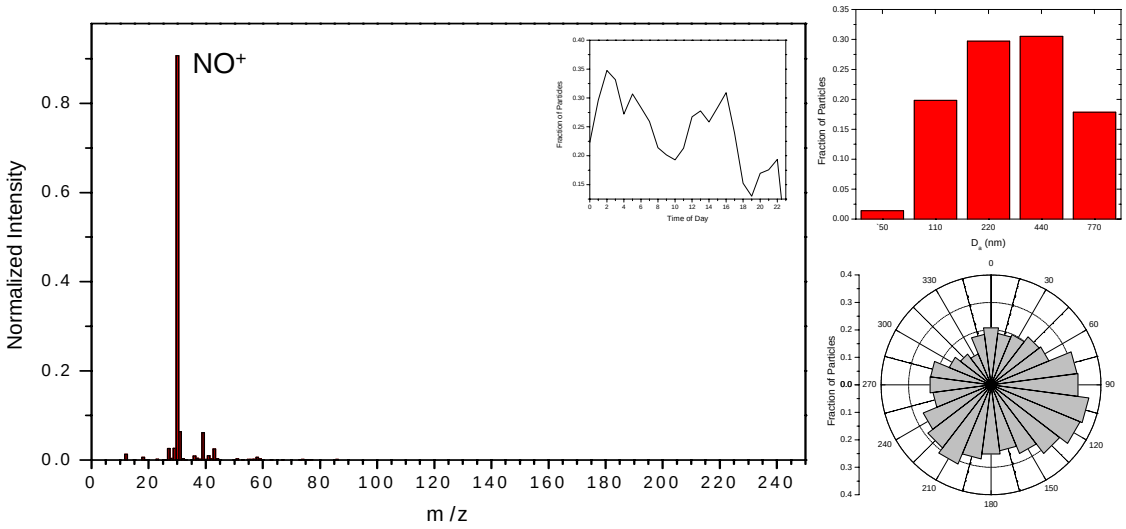

Figure 3-2. Summary statistics for the ammonitum nitrate particle class, 23% of the total particles analyzed

Ammonium nitrate particles are indicated by a dominant signal at m/z 30, a marker ion for nitrate (Figure 3-2). Other ions characteristic of OCANS particles may be observed, but the dominance of the nitrate signal indicates that of the three main secondary components (nitrate, sulfate, organic carbon), nitrate is largest. What was said above for OCANS particles is also generally true for nitrate particles, with the caveat that nitrate particles are more likely to be detected under conditions where formation of particulate nitrate is enhanced. For example, relative to OCANS particles, nitrate particles are more likely to be detected in the nighttime and early morning when the temperature is low and the relative humidity is high, as these conditions promote condensation of ammonium nitrate onto the particle phase (Figure 3-2). Nitrate particles are also preferentially observed in the late afternoon hours when gas phase production of HNO_3 from NO_x emissions is generally greatest. There is no significant directionality associated with the detection of these particles (Figure 3-2), which is consistent with a secondary origin.

The laser ablation method used in RSMS-3 has a strong bias toward the detection of nitrate. A recent study by *Tolocka et al. (2006)* shows that RSMS-3 data are best reconciled with measurements with a continuous nitrate monitor when the number of nitrate particles detected by RSMS-3 is divided by 2. In effect, the bias toward nitrate detection causes ambient particles containing large amounts of ammonium nitrate to be more efficiently detected than particles containing little or no ammonium nitrate. This conclusion is supported by laboratory studies of particle detection by RSMS-3 [*Kane and Johnston, 2000*]. Accordingly, the number fraction, number concentration and mass

concentration of particles in the nitrate class of the E-DATAS dataset have been determined by dividing the number of particles detected by a factor of two.

3.1.1.3. Potassium (18%)

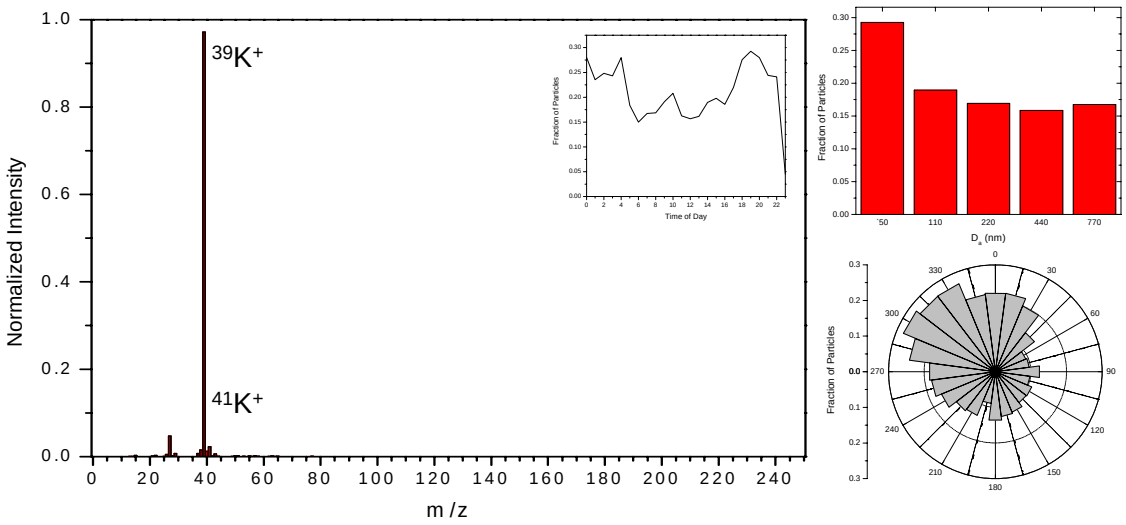

Figure 3-3. Summary statistics for the potassium particle class, 18% of the total particles analyzed.

The potassium class (Figure 3-3) is indicated by large signals at m/z 39 and 41 in the proper isotopic ratio. These particles are thought to be produced by biomass burning, which produces a KCl core on which partially decomposed/oxidized organics condense. Since potassium is much more sensitively detected by laser ablation than organic matter, K^+ dominates the mass spectrum. These particles are most abundant in the smallest size bins, which is consistent with wood burning. There is a slight bias toward wind directions from the northwest where the greatest nearby residential population exists. There is also a slight bias toward the nighttime, again consistent with residential wood burning. It is also possible that particles of this type are emitted from food processing activities, although a detailed study to confirm such a correspondence has not been performed.

Tolocka et al. (2006) also showed that the detection efficiency of potassium particles is approximately 1.5 times greater than the average detection efficiency for all particles. To account for this, the number fraction, number concentration and mass concentration of particles in the potassium class of the E-DATAS dataset have been determined by dividing the number of particles detected by 1.5.

3.1.1.4. EOC (Elemental and Organic Carbon) (9.9%)

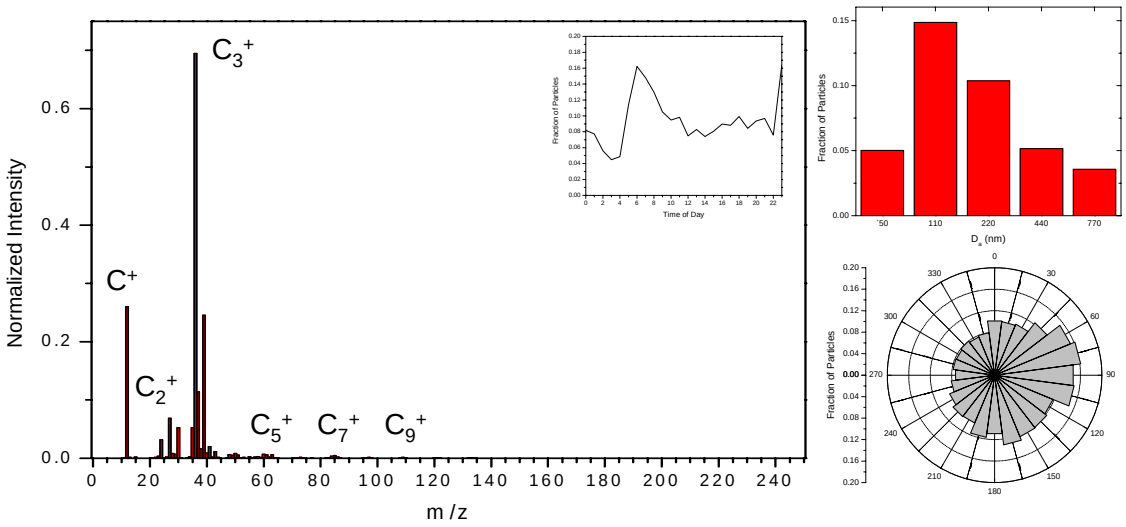

Figure 3-4. Summary statistics for the elemental carbon particle class, 9.9% of the total particles analyzed.

Elemental and organic carbon (EOC) particles (Figure 3-4) are indicated by a series of carbon peaks ranging from C_1^+ to C_3^+ (m/z 12, 24, 36), with some spectra containing clusters up to C_{10}^+ and higher. While the main component of these particles is thought to be elemental carbon, we cannot rule out that a significant amount of organic carbon also exists in these particles. EOC particles are characteristic of diesel vehicle exhaust, and in Baltimore, 99% of the particles emitted by metropolitan buses were of this type [*Tolocka et al., 2005*]. It should be noted, however, that particles of this type may also originate from stack emissions. There is little directionality associated with these particles, which is consistent with diffuse (non-point) sources. The size distribution (peak at 110 nm) suggests a combustion source. The slight enhancement when the wind is from the east may indicate a contribution from industrial combustion facilities. A major increase in the number of these particles is observed in the morning rush hour period, when buses from the nearby DART depot are leaving for the daily run and vehicular traffic is greatest. An afternoon increase coinciding with the evening rush hour is not observed. This is consistent with gas phase CO measurements in several cities where no increase in the CO concentration was observed during the evening rush hour. The lack of an afternoon signature has been attributed to a higher mixing height than in the morning.

3.1.1.5. Aliphatic Amines (3.5%)

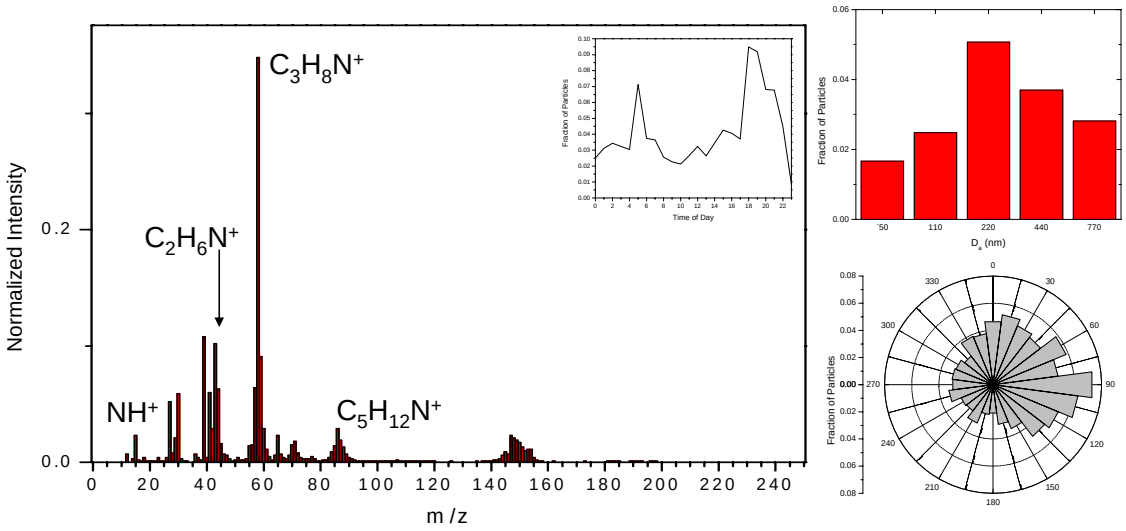

Figure 3-5. Summary statistics for the amine particle claws, 3.5% of the total particles analyzed.

The amine class (Figure 3-5), like the OCANS class, is indicated by several low m/z hydrocarbon ions. However, these particles also show ions corresponding specifically to aliphatic amines (m/z 58, 72 and 86). Other ions (m/z 66 and 149) are also often observed. These particles have a slight directional dependence to the east and tend to be detected in the early morning and late evening hours. Furthermore, these particles are most abundant in the 200 nm size range, which is typical of large scale combustion sources that use current technology to reduce particulate emissions [*McElroy et al., 1982*]. As will be seen with other classes below, the early morning and/or late evening time frames and a bias toward an aerodynamic diameter on the order of 100-200 nm are common for particles emitted from local industrial combustion processes. It is likely that these particles arise from stack emissions where aliphatic amines have been added during the scrubbing process used to remove SO_2 from the effluent. The amines probably condense on the particles as the effluent from the stack expands into ambient air and cools.

3.1.1.6. Sodium (2.4%)

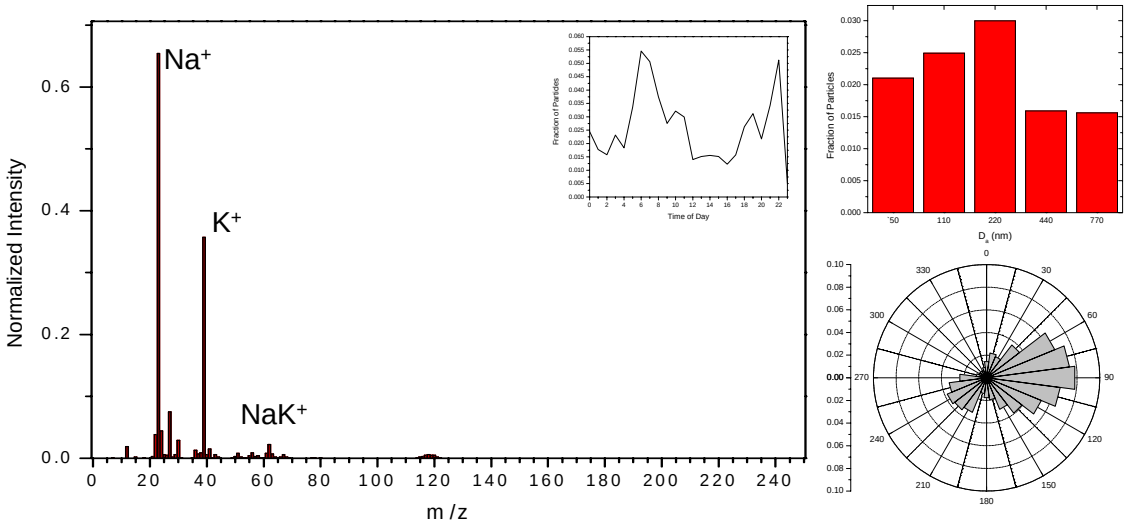

Figure 3-6. Summary statistics for the sodium particle class, 2.4% of the total particles analyzed.

Particles within the sodium class are indicated by intense peaks for sodium and potassium with the sodium peak being somewhat larger (Figure 3-6). The size distribution reaches a maximum at 220 nm and the time of day dependence shows that these particles are detected preferentially in the early morning and late evening. These characteristics are typical of local industrial combustion processes. The windflower plot shows enhancements to the east and southwest suggesting multiple sources. It is possible that some of these particles correspond to sea salt aerosol. However, the strong time of day and directionality dependencies suggest that most are from local sources.

3.1.1.7. Potassium with Sodium (2.7%)

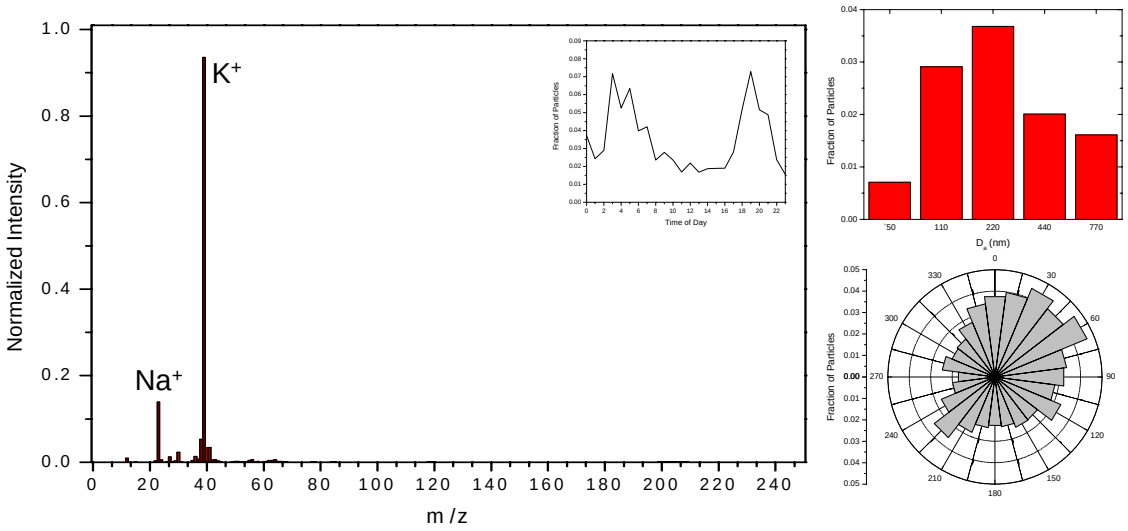

Figure 3-7. Summary statistics for the potassium with sodium particle class, 2.7% of the total particles analyzed.

The potassium with sodium class is similar to the sodium class above but exhibits a much more intense potassium peak (Figure 3-7). The time of day dependence and size distribution of this class are quite similar to those of the sodium class, although the directionality is much less pronounced. The similarities with the sodium class suggest that many of the potassium with sodium particles share a common source with the sodium class particles. However, the lack of a strong directionality suggests that many of the particles in this class share a common source with particles in the potassium class (Section 3.1.1.4), i.e. biomass burning. Indeed, the potassium with sodium class was identified by searching for particles in the potassium class that exhibited a significant Na^+ signal intensity. The potassium with sodium particles cannot correspond to sea salt aerosol because the potassium signal (and corresponding concentration in the particles) is too large for sea salt.

3.1.1.8. Iron (1.3%)

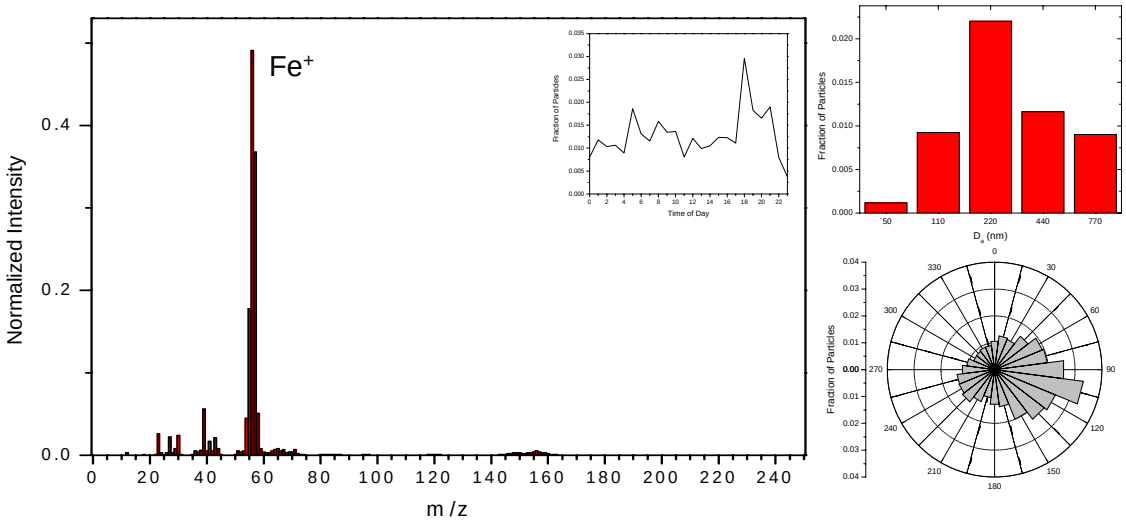

Figure 3-8. Summary statistics for the iron particle class, 1.3% of the total particles analyzed.

The iron particle class (Figure 3-8) is characterized by an intense peak at m/z 56. The spectra for particles within this class also often contain some signal intensity corresponding to small amounts of sodium and potassium. The number of particles in this class rise sharply in the early morning and late evening, and the size distribution reaches a maximum at 220 nm. These characteristics are typical of particles emitted from local industrial combustion processes. These particles are slightly more prevalent from the southeast, but the rather weak wind direction dependence suggests that these particles are emitted from several sources.

3.1.1.9. Iron with Cerium/Lanthanum (0.28%)

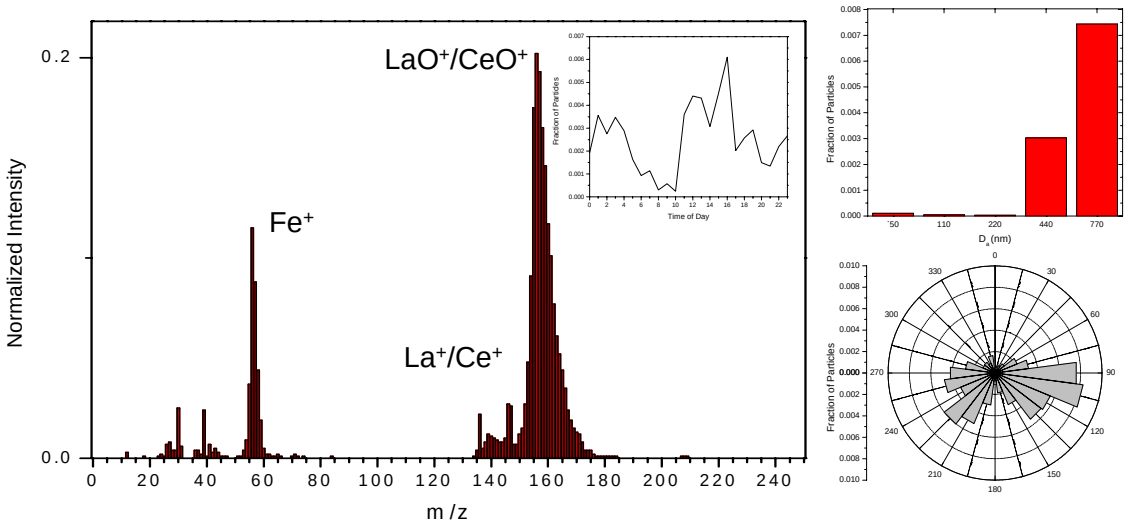

Figure 3-9. Summary statistics for the iron with cerium/lanthanum particle class, 0.28% of the total particles analyzed.

The iron cerium/lanthanum class is characterized by strong signals at m/z 56, 140 and 156 corresponding to Fe^+, Ce^+/La^+ and CeO^+/LaO^+ (Figure 3-9). Although we expect that these particles are primarily composed of cerium, the limited mass resolution associated with the mass spectra of these particles does not allow the presence of lanthanum to be ruled out. Cerium is known to be used in the catalytic cracking of petroleum and is often added to metal alloys. These particles are found primarily in the largest aerodynamic diameter size bins, and it may be that RSMS-3 is detecting the small diameter end of a coarse mode distribution. However, it is important to note that because of the large density of these particles (assuming a mixture of elemental carbon and metal oxides) the volume equivalent diameter is roughly 200 nm for an aerodynamic diameter of 770 nm. Particles in this class were detected with slightly greater frequency in the late afternoon. The windflower plot shows two strong directionalities, one from 210-220°, which corresponds to the refinery in Delaware City, DE, and another from 90-100°, which corresponds to Delmarva Edgemoor, a coal-fired power generation facility. Bag sampling from the Delmarva Edgemoor stack (Section 3.1.5) confirmed that these particles were emitted from that site.

It is possible that these types of particles transform as they are transported from the stack to the MLK site, accounting for the low fraction of particles of this type in the dataset. One possibility is that these particles transform by condensation of aliphatic amines (see Section 3.1.1.3) and are classified as a part of that group. Note that other particle classes were also detected in the bag sample (Section 3.1.5).

3.1.1.10. Lead (0.88%)

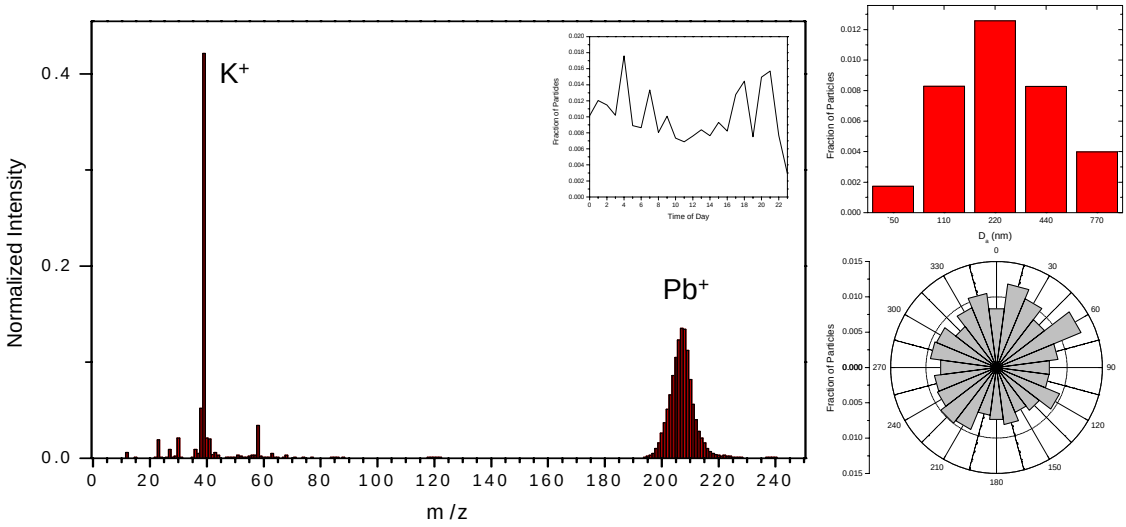

Figure 3-10. Summary statistics for the lead particle class, 0.88% of the total particles analyzed.

Particles in the lead class are indicated by a broad, isotopically unresolved peak around m/z 208 along with an intense K^+ peak at m/z 39 (Figure 3-10). The peak of the size distribution is at an aerodynamic diameter of 220 nm, and particles are preferentially detected in the early morning and late evening hours. These characteristics are typical of particles emitted from local industrial combustion processes. The lack of a significant directionality in the windflower plot suggests multiple sources. These particles are thought to be composed of elemental carbon and lead and potassium oxides. Because of the high particle density, an aerodynamic diameter of 220 nm corresponds to a volume equivalent diameter of approximately 58 nm.

3.1.1.11. Zinc (0.38%)

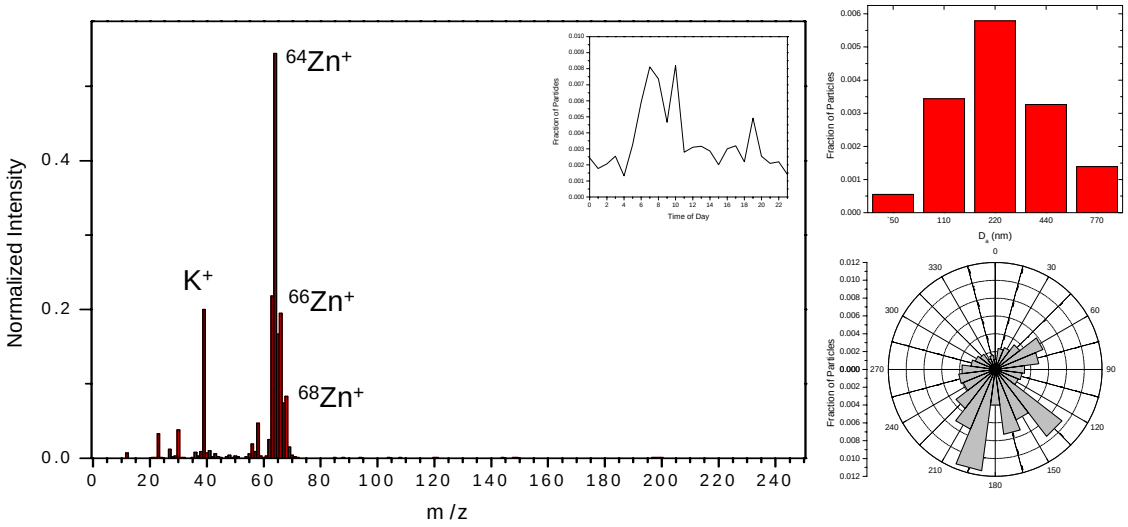

Figure 3-11. Summary statistics for the zinc particle class, 0.38% of the total particles analyzed.

The zinc particle class is indicated by a group of ions corresponding to the isotopic distribution of Zn^+ at m/z 64, 66 and 68 (Figure 3-11). Often, smaller signals from Na^+ and K^+ are observed in the spectra. The size distribution is centered at an aerodynamic diameter of 220 nm and these particles are most likely to be detected in the early morning hours with an additional slight enhancement in the evening – consistent with a local industrial combustion source. As with other metal classes discussed previously, the large density of these particles (assuming a mixture of elemental carbon and metal oxides) cause a 220 nm aerodynamic diameter to correspond to a volume equivalent diameter of 58 nm. The windflower plot shows that most particles come from the northeast, southeast, and southwest and multiple sources are suggested.

3.1.1.12. Zinc with Lead (0.11%)

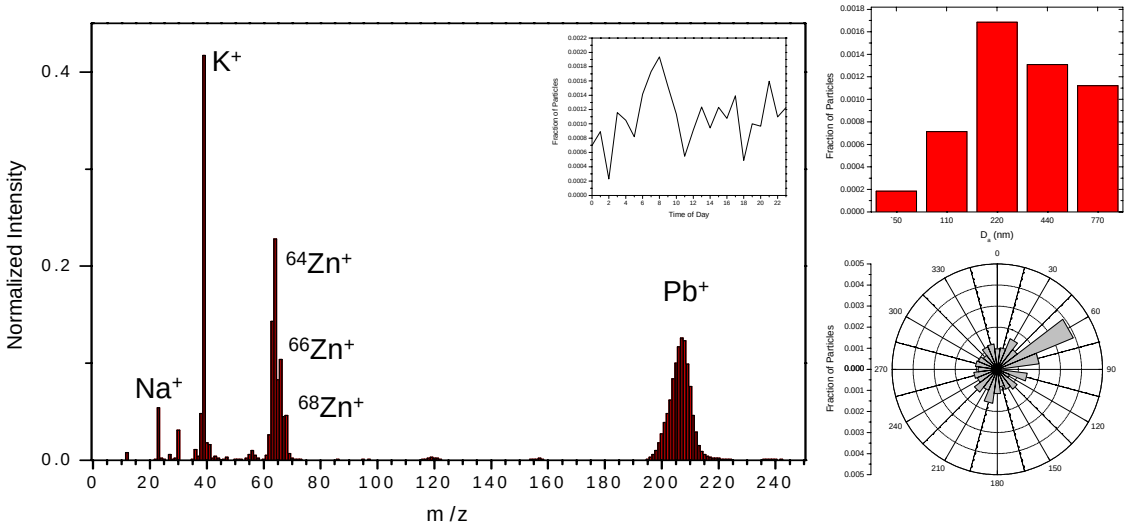

Figure 3-12. Summary statistics for the zinc with lead particle class, 0.11% of the total particles analzyed.

The zinc with lead class is different from the zinc class above in that a strong signal is observed for Pb^+ centered at m/z 208 (Figure 3-12). The size distribution reaches a maximum at 220 nm and the time of day dependence shows a slight enhancement in the early morning – both are indicators of a local industrial combustion source. The windflower plot shows that particles in this class are preferentially detected from the northeast (60^o), which is in the direction of CitiSteel, a steel manufacturing facility. Bag sampling at the CitiSteel site (see Section 3.1.5) confirms that particles of this composition are emitted from that facility. As with other metal classes, the high density of these particles (assuming a mixture of elemental carbon and metal oxides) causes an aerodynamic diameter of 220 nm to correspond to a volume equivalent diameter of about 48 nm.

3.1.1.13. Tin/Antimony (0.54%)

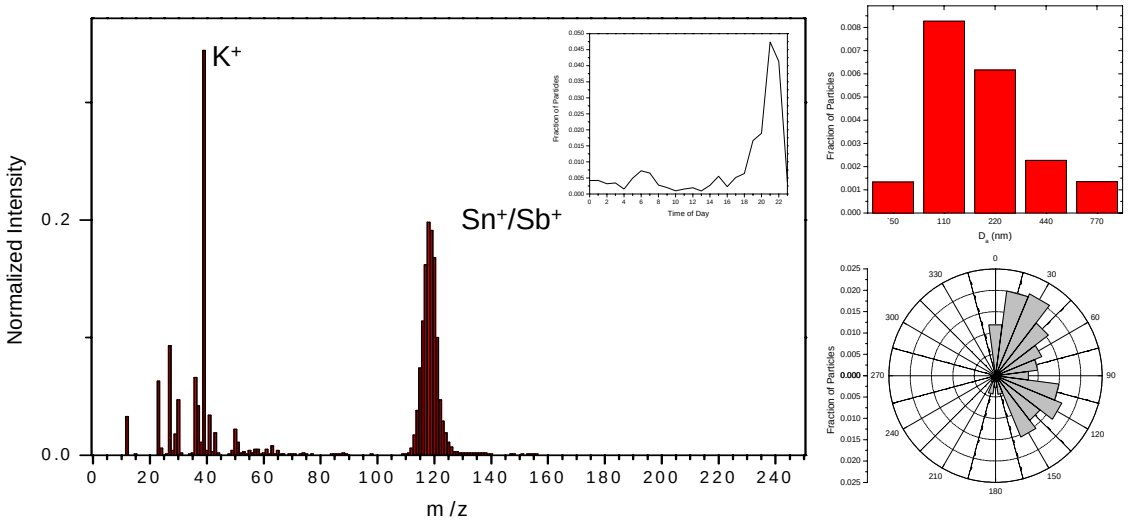

Figure 3-13. Summary statistics for the tin/antimony particle class, 0.54% of the total particles analyzed.

The tin/antimony class (Figure 3-13) is indicated by broad signals in the 115-120 m/z region along with a relatively intense potassium signal. Because of the limited mass resolution of these spectra, it cannot be determined whether tin, antimony or both are present in these particles. The size distribution reaches a maximum in the 110-220 nm region and the time of day dependence shows a strong preference for detection in the evening hours. Both are indicators of local industrial combustion sources. The windflower plot shows a strong directionality from the northeast and southeast, suggesting that multiple sources exist. As with other metal classes, the large density of these particles (assuming a mixture of elemental carbon and metal oxides) cause an aerodynamic diameter of 110 nm to correspond to a volume equivalent diameter of about 27 nm.

3.1.1.14. Lithium (0.13%)

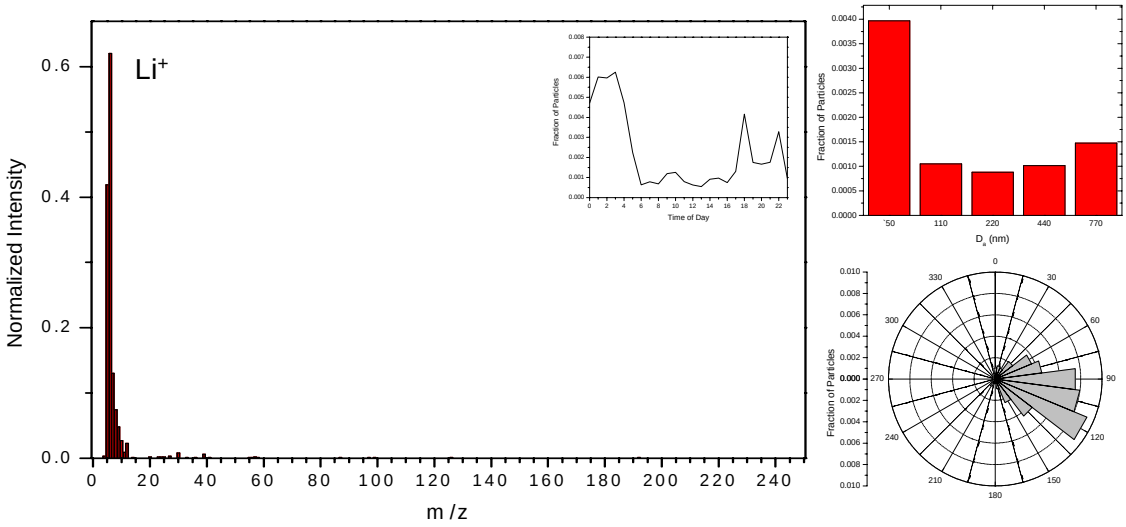

Figure 3-14. Summary statistics for the lithium particle class, 0.13% of the total particles analyzed.

A small fraction of the particles collected and analyzed at the MLK site were composed of lithium (Figure 3-14). These particles were almost exclusively detected in the early morning hours, and were found primarily in the smallest particle size bin. The small size of these particles suggests that they were formed in a high temperature process. It should be noted that the lower density of these particles relative to other metal particles causes the aerodynamic diameter to be smaller for the same volume equivalent diameter. For a mixture of elemental carbon and lithium oxide, an aerodynamic diameter of 50 nm corresponds to a volume equivalent diameter of about 25 nm. As seen in the windflower plot, these particles have a strong directional dependence to the east. Lithium particles were detected in Pittsburgh, and were attributed to steel manufacturing processes. Lithium particles are also known to originate from coal combustion, and these particles could originate in part from the Delmarva Edgemoor power generation facility located to the east (90°) of the MLK site. However, they were not detected in the bag sampling experiment at Delmarva.

3.1.1.15. Vanadium (0.26%)

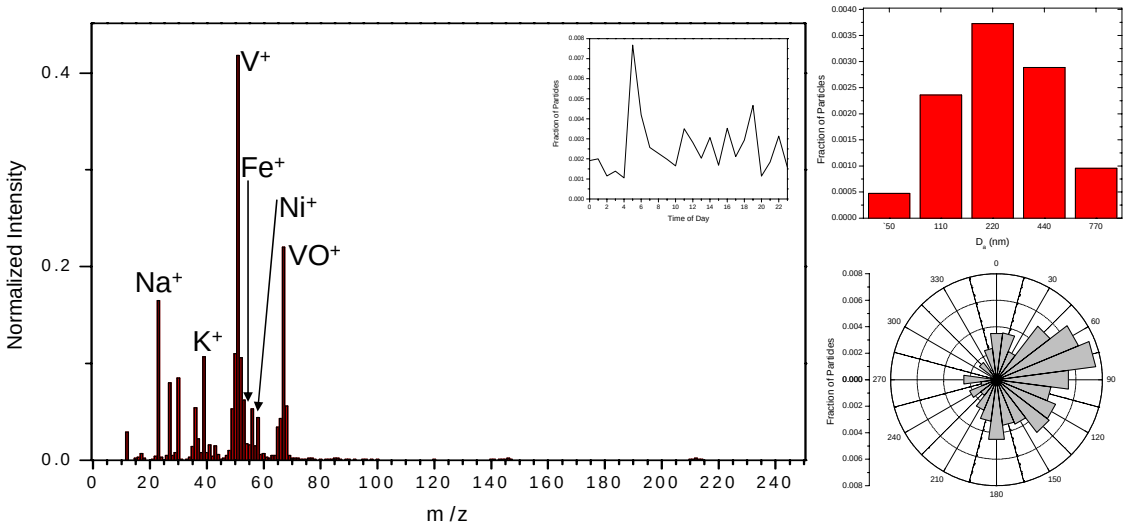

Figure 3-15. Summary statistics for the vanadium particle class, 0.26% of the total particles analyzed.

Vanadium particles are indicated by their intense peaks at m/z 51 and m/z 67, which correspond to V^+ and VO^+ (Figure 3-15). Sodium, potassium, and nickel are also often associated with these particles. Vanadium is found in petroleum and usually related to residential and industrial oil burning, as well as petroleum refinement. The size distribution reaches a maximum at 220 nm (the corresponding volume equivalent diameter is about 71 nm assuming a mixture of elemental carbon and metal oxides) and the time of day dependence shows a strong preference for detection in the early morning hours, consistent with the firing of oil powered boilers at the start of the day. These particles have a bias toward the east, with slight increases in detection frequency to the northeast, southeast and south.

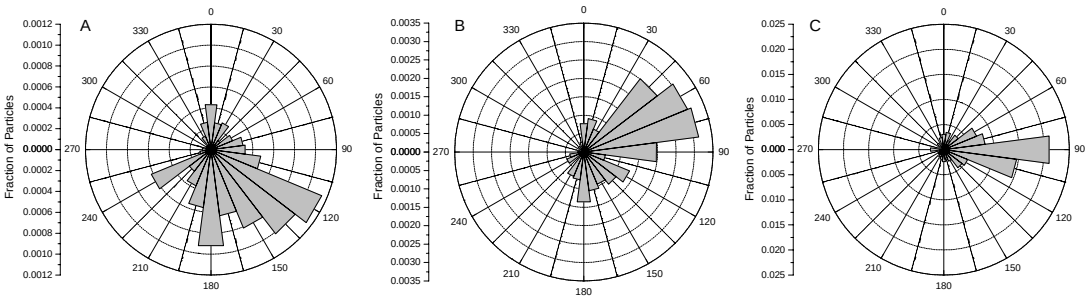

Figure 3-16. Subdivision of the vanadium particle class: A) vanadium with nickel, B) vanadium with iron, and C) all other vanadium

The vanadium class was examined in more detail by searching for particles that also contained nickel or iron (Figure 3-16). Particles containing nickel in addition to vanadium also often had signal intensity corresponding to iron in the particles, and had a strong southeastern dependency (Panel A of Figure 3-16). These types of particles are thought to be emitted from large ships and could originate from the Port of Wilmington area (approximately 110° from the MLK site). Vanadium particles containing iron (Panel B of Figure 3-16) were seen mostly from the northeast direction (general direction of CitiSteel), while vanadium particles without iron or nickel (Panel C of Figure 3-6) came from the east (Delmarva Power; DuPont Edgemoor). However, vanadium particles were not detected in the bag experiments from these sites.

3.1.1.16. Other Metals (0.11%)

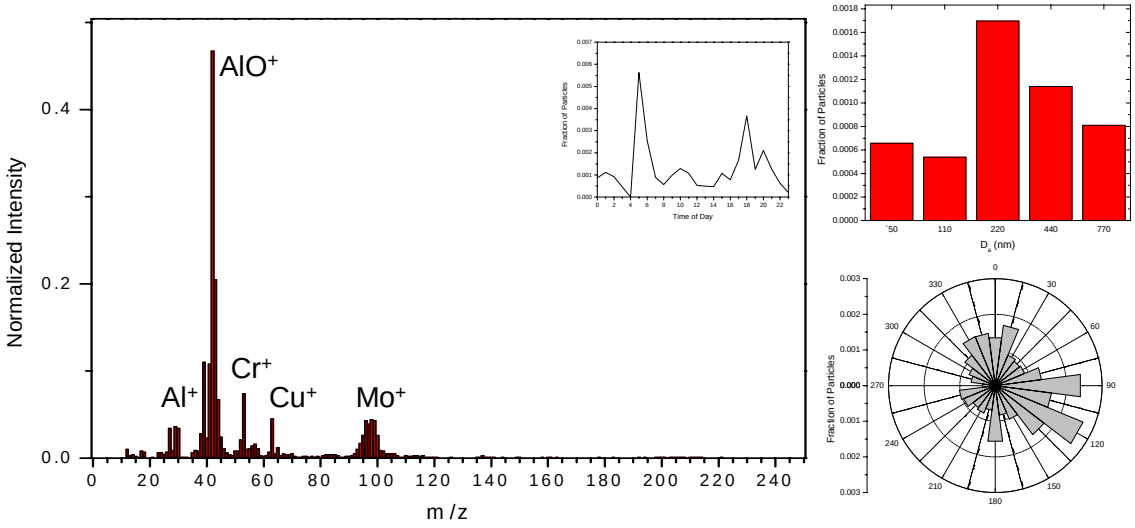

Figure 3-17. Summary statistics for the combination of other metal particle classes, 0.11% of the total particles analyzed.

A few other metals were detected at the MLK site, but the total number of particles in each class was small and not statistically significant. Therefore, these particles were combined into one "class" (Figure 3-17). Within this class can be seen particles containing aluminum and aluminum oxide, chromium, copper, silver, and molybdenum. These particles are detected preferentially in the early morning and late evening hours and the size distribution reached a maximum at 220 nm. These characteristics are typical of industrial combustion sources. Although the windflower plot shows a strong bias for detection from the east, southeast, and south (90°, 120°, and 180°), there is no significant correlation of these directions to any individual metal or combinations of metals.

3.1.1.17. Unclassified Particles

An additional 6,236 particles were detected at the MLK site, but were unable to be grouped into any particular particle class. These particles typically had low intensity peaks that could not be correlated to any known element or compound, and could not be grouped together in any significant numbers. The particles could be due to noise in the raw data, miscalibration of the raw data, or small amounts of real particles that were not expected. These particles made up 1.3% of the overall dataset and were not included in any calculation (fraction of particles in the dataset, fraction of total particles, fraction of total mass, etc.).

3.1.2. Size Dependence

Several particle classes show similar size distributions. Particles in the metal classes generally exhibited a maximum in the size distribution at either 110 or 220 nm. It is important to note that RSMS-3 measures aerodynamic diameter, and the corresponding volume equivalent diameters are in the 20-50 nm range. This size range is consistent with particles that are formed during high temperature industrial processes. Particles in the amine class showed a similar maximum in the size distribution, although the corresponding volume equivalent diameter is much larger. While amine particles are also thought to be produced from industrial sources, the particle formation mechanism may be different – condensation beyond the stack exit rather than formation inside the stack.

EOC and potassium particles tended to be detected preferentially in the smaller size bins. However, it should be noted that the densities of these particles are much lower than those of the metal particle classes, making the volume equivalent diameters similar to the metal oxide particles. EOC particles are known to originate from mechanical engine exhaust, such as from diesel vehicles while potassium particles are thought to be due to biomass burning – both are examples of "small scale" combustion from non-point sources.

The largest particle sizes consisted mostly of secondary aerosol components, e.g. the OCANS and nitrate classes. The one exception is the iron cerium/lanthanum class where it seems that the low size end of a coarse mode was detected. Secondary aerosol particles at the high end of the RSMS-3 size range are thought to have been transported over a longer distance from their primary source, thus giving them time to grow. Secondary aerosol particles at the small end of the RSMS-3 size range are thought to be the result of atmospheric processing in the local airshed.

3.1.2.18. Calculation of Number and Mass concentrations

When coupled with SMPS readings, the number of particles detected and analyzed with RSMS-3 over a designated time period can be converted to number and mass concentrations. RSMS-3 collects particles in 5 size bins, corresponding to median aerodynamic diameters, d_{va}, of 50, 110, 220, 440, and 770 nm. The SMPS analyzes aerosol with electrical mobility diameters, d_m, of 20 – 453 nm. Reconciling the two requires calculation of the volume equivalent diameter. Particles are assumed spherical and thus, d_m is equal to the volume equivalent diameter, d_{ve}. (This assumption is expected to be valid for secondary component particles – OCANS and nitrate – which constitute a majority of the particles analyzed. Particles produced directly from combustion are more likely to have a fractal geometry. However, there was no independent measure of particle shape in this experiment.) Since d_{ve} is related to d_{va} through particle density, the d_m range analyzed by the SMPS can be converted to d_{va} [see Equation 1, below]. Assuming an average particle density of 1.7 g/cm^3 [*Pitz et al., 2003*], the SMPS size range measured as d_m was converted to a d_{va} size range of 34 – 770.1 nm. Figure 3-18 shows the average number concentration versus aerodynamic diameter

collected by the SMPS for the spring, fall, and winter intensives. Shadowed in red is the particle size range that is effectively transported into RSMS-3, that is, ±1 σ_g about each aerodynamic diameter size bin selected by RSMS-3.

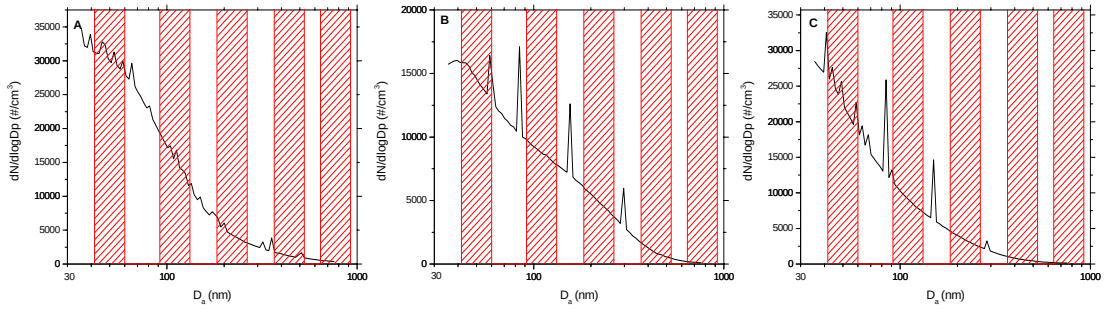

Figure 3-18. Average number concentration measured with the SMPS for A) the spring intensive, B) the fall intensive, and C) the winter intensive.

For each season, the average number concentration of particles for each RSMS-3 size bin ±1 σ_g was calculated from the averaged SMPS data. This average is representative of the average number concentration of particles during the intensive. The number of particles of each composition type collected by RSMS-3 during each intensive period were tabulated and sorted by size bin. Then, the fraction of particles in each size bin for each particle composition over the entire intensive was calculated. Calculating the overall fraction that each particle size and type makes up in the dataset acts as an average particle type number distribution for that intensive. By comparing the average number concentration of a certain size bin to the fraction of particle types which make up that number concentration, the number concentration of each class can then be calculated.

Once the number concentration distribution is calculated for each class, it can be converted to mass concentration. Since RSMS-3 analyzes particles based on aerodynamic diameter, d_{va}, the particles must be converted to their volume equivalent diameter, d_{ve}, before converting to mass. This is done by comparing the density of the particle, ρ_p, to the standard density of a particle, ρ_o = 1 g/cm^3, and considering the shape factor, χ_v [*DeCarlo, et al. 2004* and *Slowik, et al. 2004*]. For these calculations particles are assumed spherical (χ_v = 1), and the particle density for non metals was assumed to be the bulk density of the detected chemical components. The densities of metal particles were calculated by averaging the density of the bulk metal oxides, then finding the value between that average and the density for elemental carbon. This method for estimating the density of metal containing particles is consistent with the experimentally determined density for a metal oxide particle class in Pittsburgh, where *Bein, et al.* (2006) reconciled RSMS measurements with MOUDI data.

The density values assumed for each particle class are listed in Table 3.3. It should be realized that the true densities, particularly for the metal particle classes, may be different.

Once a density value for a particle class is assigned, d_{ve} can be calculated (Equation 1):

$$d_{va} = \frac{\rho_p}{\rho_o} \frac{d_{ve}}{\chi_\upsilon} \quad [1]$$

Assuming no there are no voids within the particle, the mass, m_p, of a known type of particle can be calculated (Equation 2):

$$m_p = \frac{\pi}{6} \rho_p d_{ve}^3 \quad [2]$$

By multiplying the mass of a single particle by the total number of particles determined to be that type, the overall amount of mass due to the particle class can be estimated.

Table 3-3. Comparison of particle class to fraction of number concentration, assumed density, fraction of mass concentration (PM_1), fraction of fine particles (220-770 nm), and fraction of ultrafine particles (50-110 nm).

Particle Class	Fraction of Number Concentration	Assumed Density (g/cm^3)	Fraction of Mass Concentration (PM_1)	Fraction of Fine Particle Mass (220-770 nm)	Fraction of Ultrafine Particle Mass (50-110 nm)
OCANS	43%	1.8	38%	38%	37%
Ammonium Nitrate	8.8%	1.8	29%	30%	12%
Potassium	18%	1.8	13%	12%	20%
EOC	13%	1.7	6.9%	6.1%	18%
Amines	4.4%	1.5	5.6%	5.6%	5.2%
Sodium	3.7%	2.2	3.2%	3.2%	3.2%
Potassium, Sodium	3.3%	2.0	2.0%	1.9%	3.3%
Iron	1.0%	3.6	0.68%	0.71%	0.28%
Iron, Cerium/Lanthanum	0.16%	3.9	0.08%	0.08%	0.02%
Lead, Potassium	1.3%	3.8	0.46%	0.43%	0.88%
Zinc	0.29%	3.8	0.08%	0.08%	0.08%
Lead, Zinc	0.10%	4.5	0.04%	0.04%	0.03%
Tin/Antimony	0.88%	4.1	0.07%	0.06%	0.16%
Lithium	0.88%	2.0	0.17%	0.15%	0.37%
Vanadium	0.50%	4.2	1.2%	1.2%	0.18%
Other Metals	0.18%	3.7	0.04%	0.04%	0.03%

3.1.2.19. Implications of Number and Mass Concentrations

Table 3-3 shows how the overall number concentration and mass concentration are distributed among the classes of particles detected by RSMS-3. It is important to note that the summer data is left out of these calculations because of the lack of SMPS data. Number concentrations are dominated by the OCANS, potassium, and EOC classes. Ammonium nitrate, amines, sodium, and potassium with sodium make up a lesser fraction of the number concentration. Since mass is dependent on d^3 of the particle, it is expected that classes which have larger numbers of large particles will contribute more to the overall mass. To illustrate this idea, compare the fraction of ammonium nitrate particles to the number and mass concentrations. The plot of the fraction of particles in the dataset of ammonium nitrate, Figure 3-2, shows a bias toward larger size particles. Ammonium nitrate makes up 14% of all detected particles, but since most of these particles are in the larger size bins, and there are fewer numbers of larger particles overall, the ammonium nitrate class only makes up 8.8% of the total number concentration. Since larger particles contribute more to the total mass concentration, ammonium nitrate particles constitute 29% of the overall particle mass concentration in the E-DATAS dataset. In contrast, potassium particles are mostly found in the smaller particle size bins (Figure 3-3) and account for 15% of the total number of particles analyzed. Thus, these particles correspond to 18% of the particle number concentration, and only 13% of the particle mass concentration.

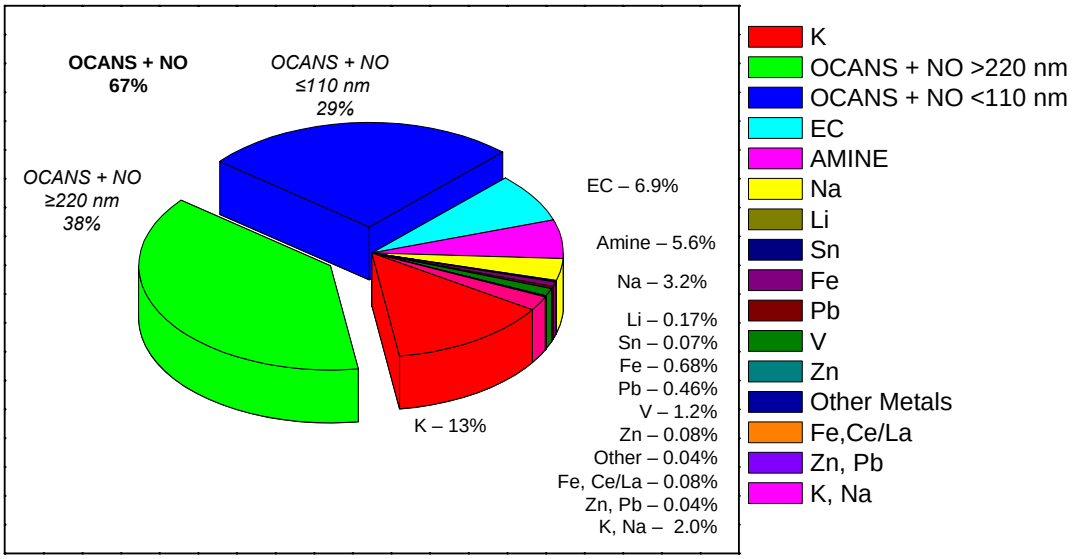

Figure 3-19. Fraction of total mass concentration (PM_1) that each class represents in the Wilmington aerosol. The nitrate and OCANS classes are combined and then divided into the fraction of mass concentration the class makes up in the fine (≥220 nm) and ultrafine (≤110 nm) size range.

Figure 3-19 is a representation of the PM_1 data in Table 3-3 where the masses of the OCANS and ammonium nitrate classes are combined and subdivided into fine (≥220 nm) and ultrafine (≤110 nm) mass concentrations. Together, these classes represent 67% of the total mass concentration in the E-DATAS dataset. Large OCANS and ammonium nitrate particles (≥220 nm) are attributed to regional sources, and are characteristic of particles that have grown by condensation of secondary components are they are transported over a large distance to the field site [*Ondov and Wexler, 1998*]. Small OCANS and ammonium nitrate particles (≤110 nm), on the other hand, are more likely due to atmospheric processing in the local airshed. These particles exist long enough in the atmosphere to grow large enough to be detected, but do not grow completely. Thus, it can be seen that regional secondary aerosol (OCANS and ammonium nitrate mass due to particles ≥220 nm) contributes approximately 38% of the total mass concentration, while local secondary aerosol (OCANS and ammonium nitrate mass due to particles ≤110 nm) contributes approximately 29% of the total mass concentration.

Class distributions of the total particle mass in the fine (≥220 nm) and ultrafine (≤110 nm) size ranges are also displayed in Table 3-3. EOC and potassium, which are thought to be due to primary emissions from vehicle exhaust and biomass burning, respectively, make up a large portion of the ultrafine mass concentration, while secondary aerosol makes up the majority of the fine mass concentration. This is not surprising as primary aerosol is generally smaller in size while secondary aerosol is generally larger.

3.1.3. Wind Direction Dependence

The MLK site is situated within 10 km of many PM emitters. To aid in source determination, particles analyzed by RSMS-3 were tagged with wind direction data that was collected and logged at the measurement site every minute. Knowing the wind direction when a particular particle composition type was analyzed can help identify particle sources. Particles with a strong wind dependence are typically from dominant local sources, while particles from multiple local sources have less directionality. Particles from regional or diffuse local sources have little, if any directional dependence.

The metal particle classes generally exhibit a strong wind dependence, as they correspond to primary emissions from specific sources. The zinc with lead particle class, Figure 3-12, is one such example. The large fraction of particles coming from the north east (60°) was correlated to CitiSteel, a steel processing facility, during source sampling (Section 3.1.5). Several other classes also have a strong correlation with wind direction. Iron and cerium/lanthanum particles (Figure 3- 9) have a strong directional dependence to the southwest, which corresponds to an oil refining facility in Delaware City, DE and to the east, which corresponds to a Delmarva Edgemoor, coal-fired power generation plant. The correlations of zinc with lead and iron with cerium/lanthanum particles were confirmed with bag sampling at the source sites (Section 3.1.5). Lithium particles (Figure 3-14) are also often seen originating from coal fired facilities, and the easterly dependence of these particles may also be due to the Delmarva Edgemoor plant, although none of these particle types were detected in the source sampling. The zinc class (Figure 3-11) is

correlated with the zinc with lead class in the northeast direction. The correlation of wind direction between two particle classes often suggests similar, but separate sources. The zinc class also has two other apparent sources in the southeast and southwest directions. The sodium class (Figure 3-6) shows two distinct sources, one from the east and another from the southwest. Tin/antimony particles (Figure 3-13) are biased toward the north east and the southwest. Vanadium (Figure 3-15) is another particle class which shows directionality. This class was further subdivided through correlations with other metals: vanadium with nickel (and sometimes iron), vanadium with iron (but no nickel), and all other vanadium particles (generally having no other metals). These subclasses showed different wind directionalities (Section 3.1.1.15). Specific sources that could correspond to these emissions include ship emissions at the Port of Wilmington, CitiSteel, and Delmarva Edgemoor and/or DuPont Edgemoor respectively. Other metal particle classes have less wind directionality associated with them, suggesting multiple sources. These include the amine (Figure 3-5), sodium (Figure 3-6), potassium with sodium (Figure 3-7), iron (Figure 3-8), and lead (Figure 3-10) classes.

The OCANS (Figure 3-1) and nitrate (Figure 3-2) classes contain secondary aerosol components and, as expected, exhibit hardly any wind directionality. Local emissions from diffuse non-point sources also exhibit little wind directionality. These include the potassium class associated with biomass burning (Figure 3-3) and EOC class associated with vehicular traffic (Figure 3-4). An afternoon rush hour peak is not observed, as is often the case with other traffic signatures (e.g. CO).

3.1.4. Time of Day Dependence

Trends based on time of day are also often important for distinguishing sources. The EOC class, for example, is typically assigned as a particle that comes from vehicle exhaust. This is supported in the time of day distribution by a large peak seen during the morning rush hour period, 5-9 am (Figure 3-4).

Time trends can also coincide with naturally occurring events, such as an increase in daily temperature, relative humidity, or an increase or decrease in the overall atmospheric mixing layer. OCANS particles tend to increase in concentration during the day as photochemical processing of secondary aerosol precursors builds up (Figure 3-1). Ammonium nitrate, and to a lesser extent, amines tend to have higher fractions of particles detected in the early morning and late evening. This makes sense since ammonium nitrate is a semi-volatile compound and it is more likely to exist in the particle phase during periods of low temperature and/or high relative humidity. While it is expected that daytime photochemical processing might also increase the number of ammonium nitrate particles, the increasing temperature tends to push particulate ammonium nitrate back to the gas phase.

Primary particulate emissions from local industrial sources most likely have no intrinsic meteorological correlation, as the particles are produced whenever the industrial process occurs, which may or may not be at regular intervals. However, the decrease in mixing

layer height in the nighttime may lead to an increase in the concentrations of these particles. It is found that particle classes associated with local industrial emissions all have characteristic increases in concentration in the early morning, late evening or both. The classes which fit this profile are sodium (Figure 3-6), iron with cerium/lanthanum (Figure 3-9), lead (Figure 3-10), zinc (Figure 3-11), zinc with lead (Figure 3-12), lithium (3- 14), vanadium (Figure 3-15), and other metals (Figure 3-17). The common time dependence signature could indicate enhanced emission activity at the beginning and/or end of the normal working day.

3.1.5. Source Sampling

Nine separate sites were identified by AQMS as PM emitters to be sampled directly with RSMS-3, and 12 separate experiments were performed. These source samples were collected to help identify specific particle classes that could be used as an identifier for the source. The source sampling methodology is described in Section 2.4. Table 3.4 shows the sources sampled, their relative direction from the measurement site, and whether bag samples was taken downwind from the site ("indirect" sample) or directly from an emission stack ("direct sample"). Each indirect measurement typically involved the analysis of two separate bag samples. Note that CitiSteel was indirectly sampled on two different dates.

Table 3-4. PM emission sites sampled directly by RSMS-3 during E-DATAS, their direction relative to the MLK measurement site, and whether the sample was taken downwind (indirect) or directly from the emission stack.

Location	Direction from Site	Indirect Sample	Direct Sample
Bus Exhaust –DART Yard	270º	X	
Wastewater Treatment Plant	100º	X	
American Minerals	145º	X	
International Petroleum	180º	X	
CitiSteel	60º	X X	X
IndustriaPlate	170º	X	
Amtrak Maintenance	75º	X	
Landfill	100º	X	X
Delmarva Edgemoor	90º		X

Before source sampling was performed, control experiments were performed by sampling ambient aerosol outside the MLK trailer into a bag and comparing the results to a simultaneous direct measurement of the ambient aerosol with RSMS-3. It was found that when the ambient temperature was different than the temperature inside the trailer, the relative loading of ammonium nitrate class particles did not agree between the bag and ambient measurements. This result is not surprising since ammonium nitrate is semivolatile and can cycle on and off particles as the temperature changes. Because of this artifact, ammonium nitrate particles were excluded from the comparison between the bag and ambient measurements. Once the nitrate particles were eliminated from the analysis, the relative loading of the remaining particle classes were compared by calculating the fraction of total particle hits corresponding to each class. In the control experiments, the bag and ambient loadings generally agreed to within $\pm$ 2%, which was taken as the uncertainty in subsequent field bag sampling experiments.

Unfortunately, all of the indirect source sampling failed to produce a bag aerosol sample that was statistically different than the ambient aerosol at the MLK site. While the bag samples were collected downwind from the emission site, it is quite possible that the particles emitted would require a longer distance to settle down to the bag sampling height (6 ft.) since the emission stacks extend high above the ground. While the "indirect" bag samples did not provide any useful source signature information, they did provide insight into how ambient aerosol varies over different locations in Wilmington. The lack of a difference between the indirect samples and MLK measurements suggest that the MLK measurements are a good representation of the *relative* mass loadings of particle classes at other locations in the city. This result is not surprising as almost 90% of the ambient aerosol is due to secondary components or primary emissions from diffuse sources (biomass burning, traffic).

Three samples were taken directly from emission stacks at three of the identified sources. The first sample was taken from a treatment pipe at a local landfill. The aerosol was sampled before it was treated and showed 100% of the particles to be oxidized and reduced sulfur. While this sample was interesting, the fact that the sample was taken before treatment does not represent the types of particles that are characteristically emitted from the site. The second and third samples were from emission stacks at CitiSteel (a steel processing facility) and Delmarva Edgemoor (a coal-fired power generation facility).

The stack sample from CitiSteel showed two particle classes: organic carbon and a mixed metal composition of potassium, zinc, and lead (Figure 3-20). The mixed metal particles are consistent with particle types that are generally attributed to steel manufacturing facilities and are very similar to the zinc with lead class (Figure 3-12). Note that CitiSteel is located approximately 60º from the measurement site, and this direction corresponds to an elevated number of particle hits from zinc with lead class. Thus, the bag sample confirms the source signature indicated in the ambient measurements.

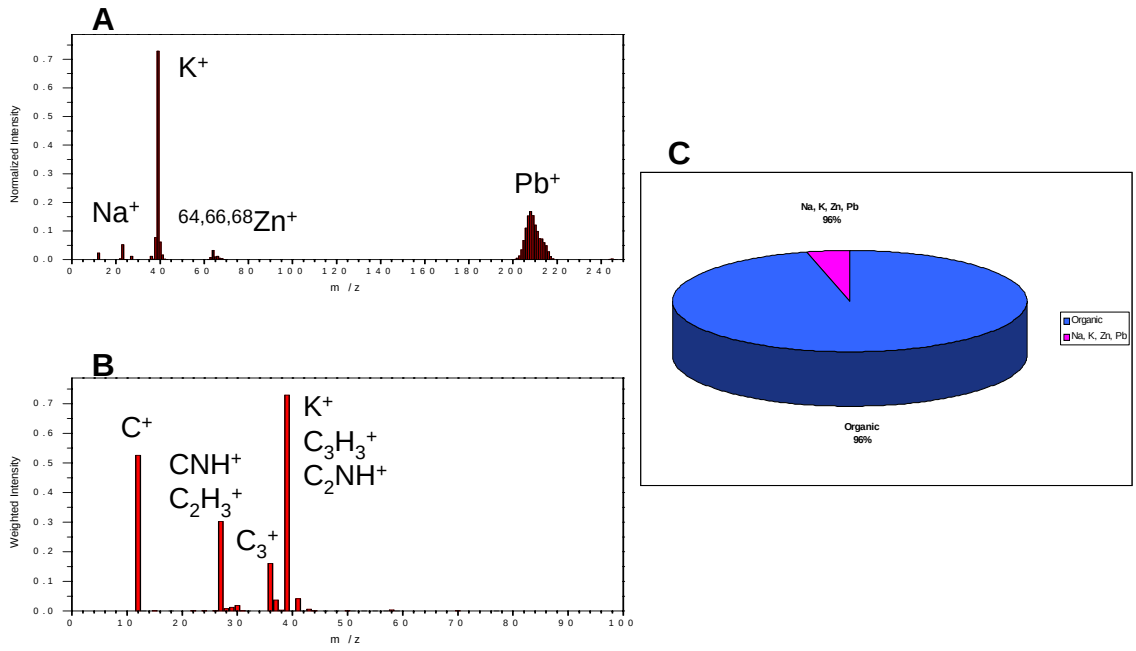

Figure 3-20. Two particle classes found in the bag sample taken from the CitiSteel emission stack, A) mixed metal, B) organic, and C) the relative amounts of each.

The Delmarva Edgemoor facility stack sample showed five classes of particles: EOC, OCANS, sodium with potassium, iron, and particles containing iron, cerium/lanthanum, and cerium/lanthanum oxide. The sodium with potassium (Figure 3-6), iron (Figure 3-8), and iron with cerium/lanthanum (Figure 3-9) all show clear preference for detection from the direction of the facility (90^{o}). The similarity of the ambient and bag particle classes is illustrated in Figure 3-21, where the iron with cerium/lanthanum particle class from the bag sample is shown. Other classes that appear to be emitted from the direction of the Edgemoor facility include amine (Figure 3-5) lithium (Figure 3-14) and vanadium (Figure 3-16). The lithium and vanadium particles may not have been detected in the bag sample because of their low aerosol loadings, while the amine particles may have not been detected because they are formed outside the stack. It is also possible that these classes are instead emitted from nearby facilities, for example DuPont Edgemoor.

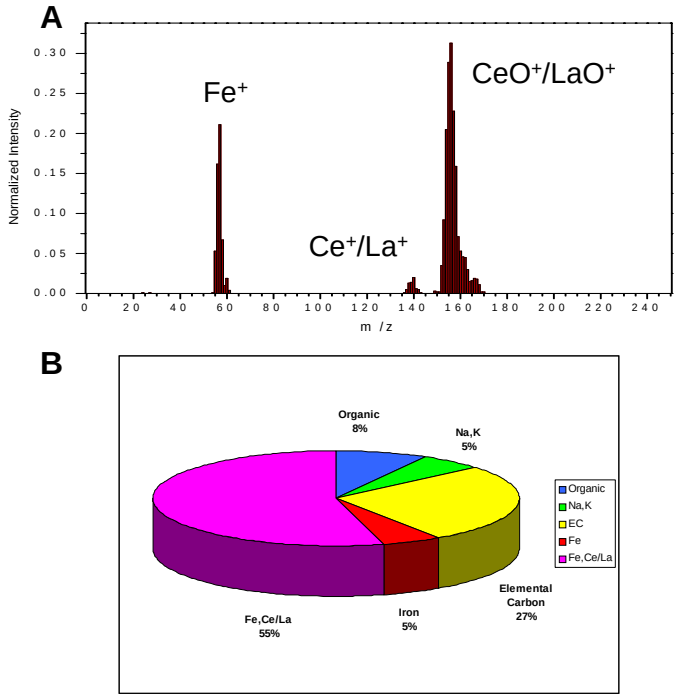

Figure 3-21. A) Averaged mass spectrum of the iron with cerium/lanthanum particle class found n the bag sample taken from the emission stack at Delmarva, Edgemoor, and B) the relative amounts of other particle classes found in the bag sample.

While several particle classes appear to be signatures for the Delmarva Edgemoor facility, they are not unique. For example, many iron with cerium/lanthanum particles measured at the MLK site (Figure 3-9) seem to be coming from the southwest of the site (210°), which corresponds to a petroleum refining facility in Delaware City, DE. These data show how wind direction measurements must be coupled with chemical composition measurements to isolate emissions from a particular source. Other particle classes that may be a signature for the Delaware City refinery are sodium (Figure 3-6), potassium with sodium (Figure 3-7), and zinc (Figure 3-11).

3.1.6. Significant findings

RSMS-3 measurements have allowed 16 particle classes to be identified on the basis of chemical composition. The size distributions, wind directionalities and time of day dependences of these classes permit characterization of the corresponding sources. From this data, the relative contribution of each class to the total number and mass concentrations of Wilmington aerosol can be determined. The mass concentrations can be regarded as a measure of the relative contributions to PM_1. Because of the many assumptions built into these calculations, the results should be treated as **estimates** only.

With this caveat, the following conclusions can be made regarding Wilmington aerosol. Refer to Figure 3-19 for further details.

1. Secondary aerosol of regional origin (given by the combination of OCANS and nitrate class masses $\geq$ 220 nm) constitutes about 39% of PM_1.
2. Secondary aerosol of local origin (given by the combination of OCANS and nitrate class masses $\leq$ 110 nm) constitutes about 28% of PM_1.
3. Biomass burning (potassium class) contributes about 13% of PM_1.
4. Primary particulate emissions from vehicular traffic (EOC class) contribute about 7% of PM_1.
5. Primary particulate emissions from local industrial sources (sum of metals and amine classes) contribute about 13% of PM_1. Of this, classes containing heavy and/or transition metals contribute about 2% of PM_1.
6. Potential signatures for primary particulate emissions from several PM sources have been identified from "direct" bag sampling of emission stacks.
7. "Indirect" bag sampling of ambient aerosol downwind of the targeted emission sites failed to identify potential signatures. However, the indirect sampling data showed that the *relative* loadings of particle composition classes were the same for the sampled locations and the MLK site.

3.2. Mobile Cr(III), Cr(VI), HCHO, O3, SMPS analysis

During the study, a very large dataset was collected for each of the measured species. 61,776 aerosol size distributions were collected, 42,426 data points for formaldehyde and 26,843 for chromium. We report here the results of the initial analysis of the data, showing the main findings and the potential areas for future research and analysis.

3.2.1. Sub-grid variability of the data

Because of the spatial inhomogeneity of sources of pollutants within a city, a single monitoring station may not provide accurate information for estimating the exposure of population to different pollutants. For example, traffic is a major emission source of particles especially in urban areas. Because of variations in vehicular intensity and building infrastructure (open or connected, high or low), the spatial distribution of pollutants within a city is highly inhomogeneous [*Weijers, et al.*, 2004]. Formaldehyde is also emitted by the traffic, which may contribute significantly to the photochemically produced formaldehyde. Likewise, most sources of hexavalent chromium are localized, originating from such activities as metal plating, dye and pigment manufacturing, cleaning of various metal parts in automobile and aircraft industry, and industrial processes such as welding [*Carlton*, 2003; *Paustenbach, et al.*, 1991; *Wang, et al.*, 1999].

It is thus possible that there are regions of elevated concentrations ("hotspots") caused by the proximity of such activities.

The existing monitoring networks provide information on prevailing average concentration near the monitoring site. Areas with unusually high concentrations ("hot-spots") will not be detected by the few stationary monitoring sites. The direct daily personal exposure to the pollutants is therefore difficult to assess based on the available data from the monitoring networks. Such "hotspots" of pollutants can be identified and characterized by means of mobile sampling during which a high-time resolution instrument is placed on a vehicle and spatial distribution assessed by measurements while driving through a city [*Bukowiecki, et al.*, 2002; *Weijers, et al.*, 2004; *Westerdahl, et al.*, 2005]. This approach was adopted in this study. The general approach to the study and the driving route are described in Section 2.2.

Using this mobile monitoring approach, we generated spatially and temporally resolved surfaces of pollutant concentrations in the study area. Examples of spatial distributions of 3-hr average concentrations of formaldehyde and ozone are shown in Figure 3-22 and 3-23, respectively. The concentrations are shown as a function of the location on the track. These graphs demonstrate the capability of the mobile platform to resolve concentrations on a very fine scale (in this case, 100 m resolution).

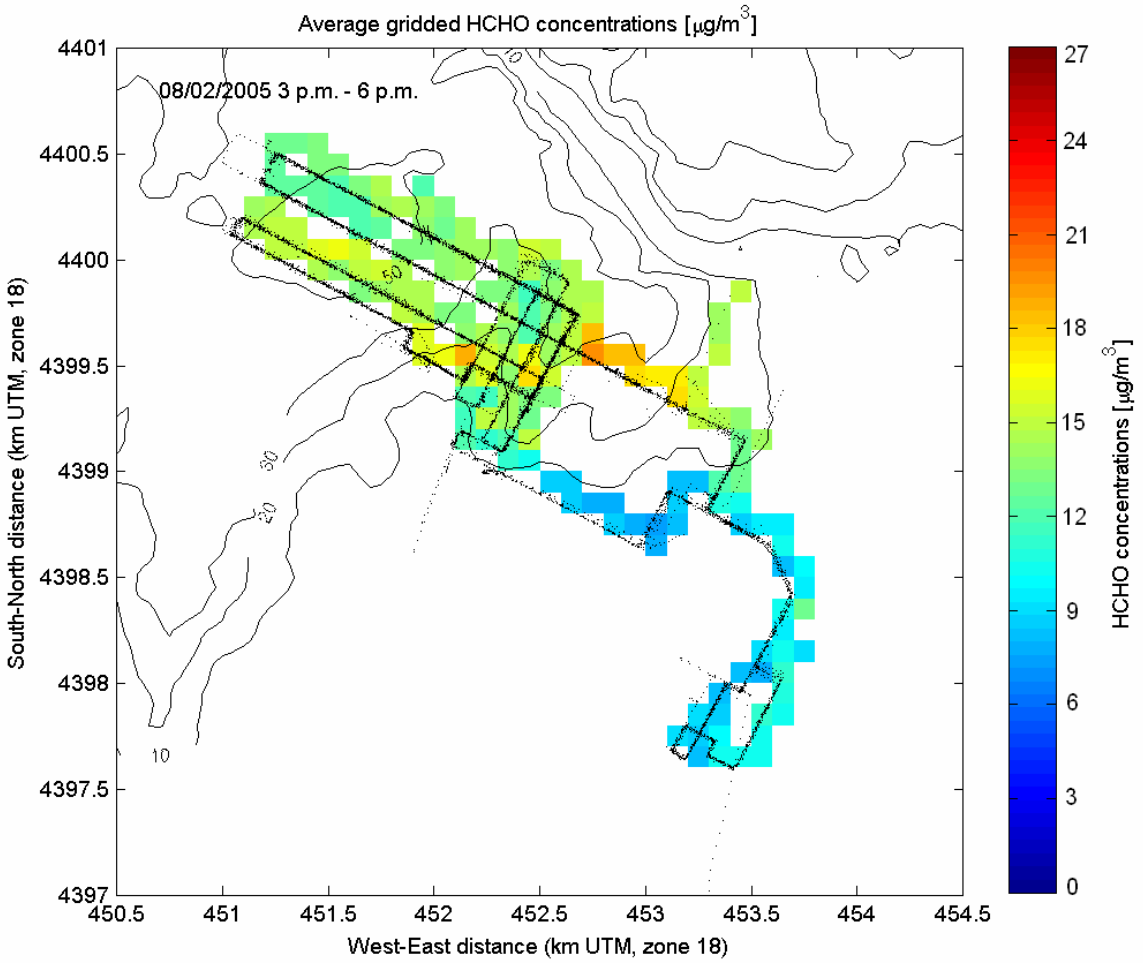

Figure 3-22. An example of the spatial distribution data for formaldehyde collected with the mobile platform during the afternoon of August 2, 2005.

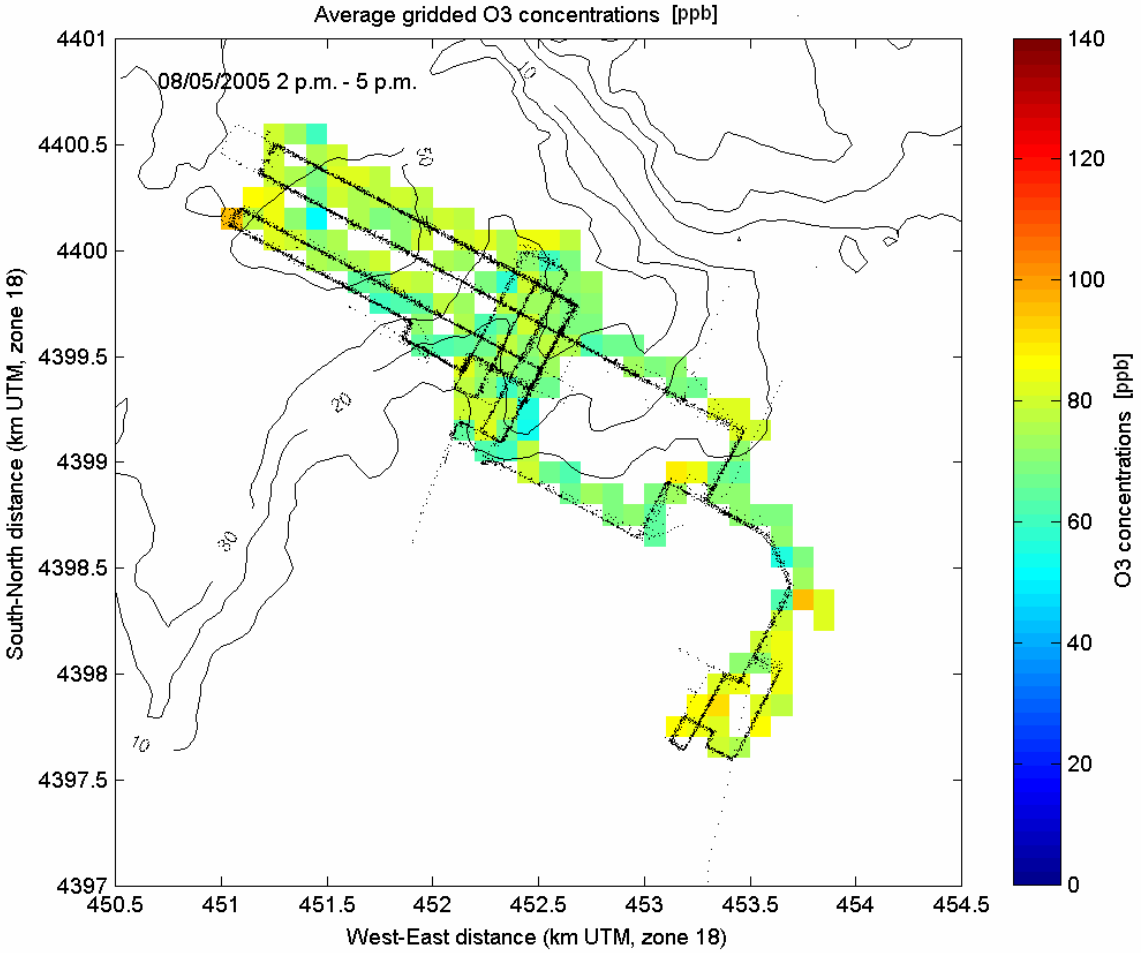

Figure 3-23. An example of the spatial distribution data for ozone collected with the mobile platform during the afternoon on August 5, 2005.

To characterize the temporal and spatial variability of pollutants in an urban environment on a neighborhood scale, and to provide detailed fine-scale data for model evaluation with 1 km grid resolution we have divided the area covered by the mobile route into 15 grids of 1 km x 1 km (Figure 3-24). The left panel of Figure 3-24 shows the map of Wilmington, DE, while the right panel shows 1 km grids corresponding to the CMAQ model grid. The mobile data were attributed to the corresponding 1 km grids according to the location measured with the GPS and sub-grid variability distributions were calculated for each grid.

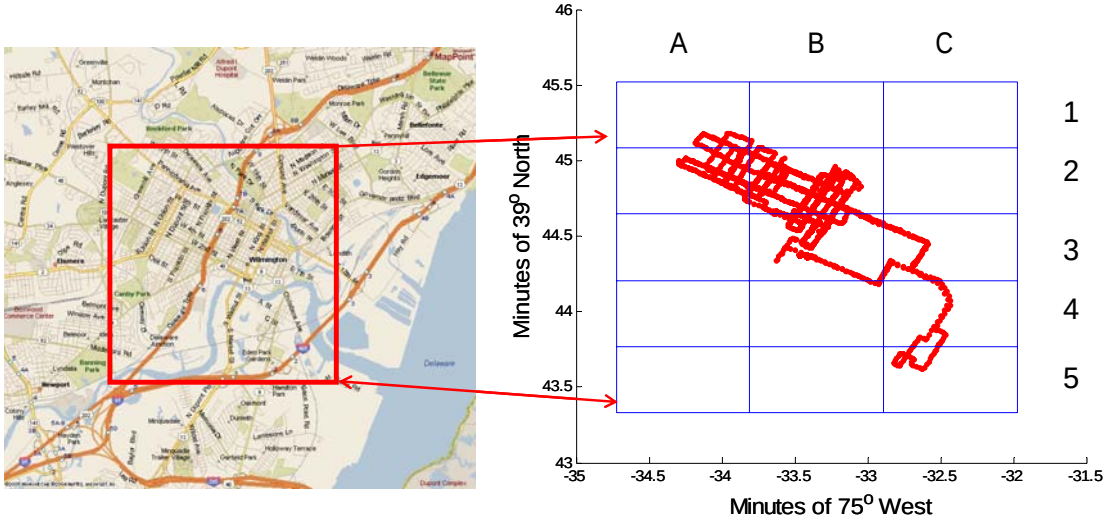

Figure 3-24. The map of Wilmington, DE and the gris assignments corresponding to the CMAQ 1km x 1km grid.

Figures 3-25 to 3-27 show the sub-grid variability distributions measured during the summer campaign of E-DATAS. The grids correspond to those shown in Figure 3-24. The plots for each grid represent histograms showing the number of observations as a function of the observed concentration.

Statistically significant differences were observed between different grids. There are also differences in the shape of sub-grid distributions. For the summer period the largest differences in average concentrations between the grids were observed for the aerosol number concentration. Vehicular traffic is known to emit large quantities of ultrafine particles contributing strongly to the aerosol number concentration. Variability in the traffic intensity and speed is the most probable reason for the observed differences in the number concentration between the grids. Lower variability was observed for formaldehyde and ozone. A large source of formaldehyde is the photochemical production in the atmosphere that apparently has a masking effect on the variability due to the differences in primary emissions. Ozone is entirely produced by photochemical reactions and the only source of difference between the grids could be its titration with NO emitted by the traffic. These findings demonstrate the presence of spatial variability within a city and its dependence on the nature of the pollutant. A more detailed analysis of the data is required to identify the sources of the variability observed in this study.

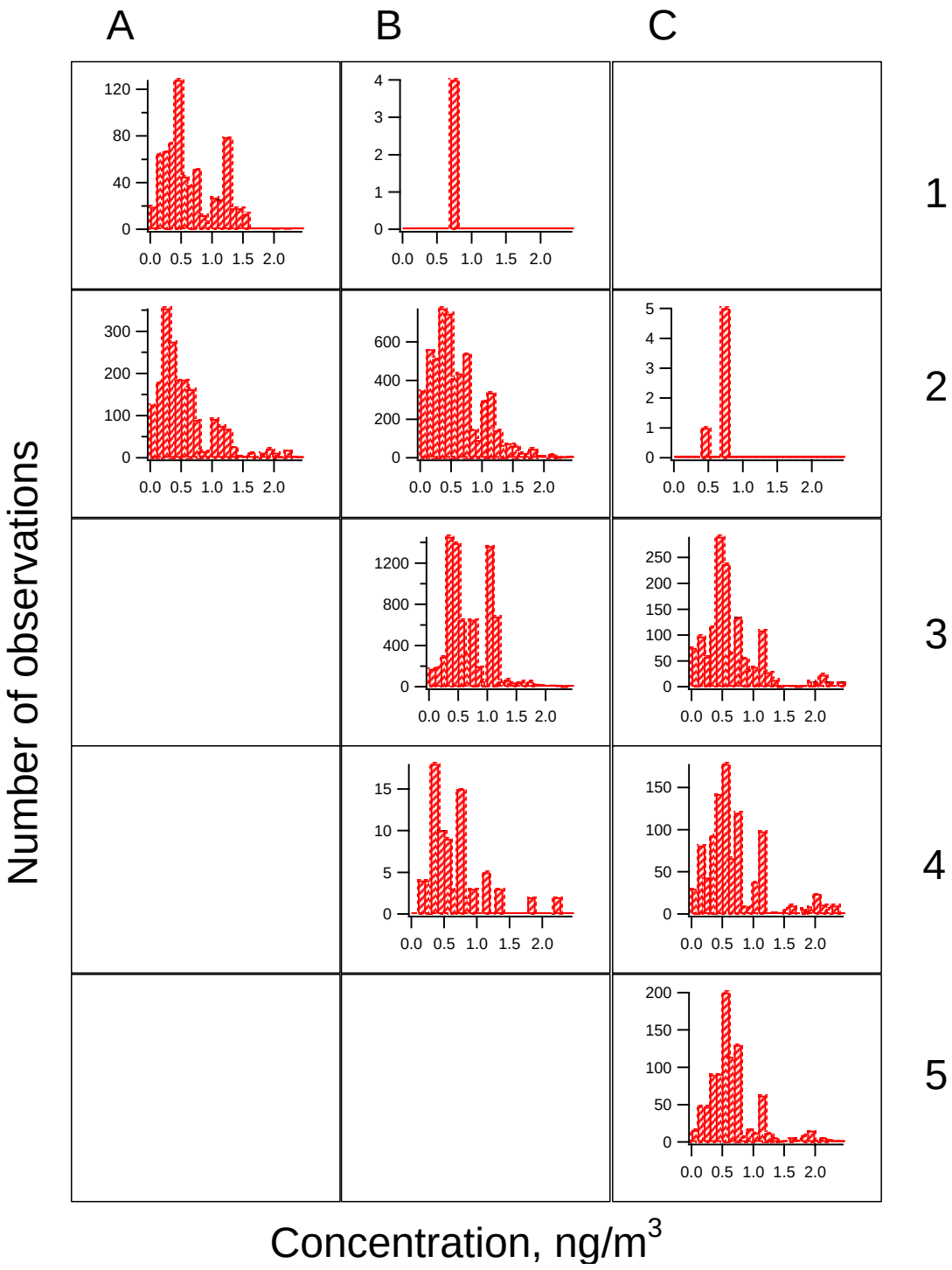

Figure 3-25. Subgrid variability distributions of Cr(VI) for the summer 2005 campaign. The X-axis shows the concentration of Cr(VI) in ng/m^3, the Y-axis shows the number of observations. The grids correspond to the ones given in Figure 3-24.

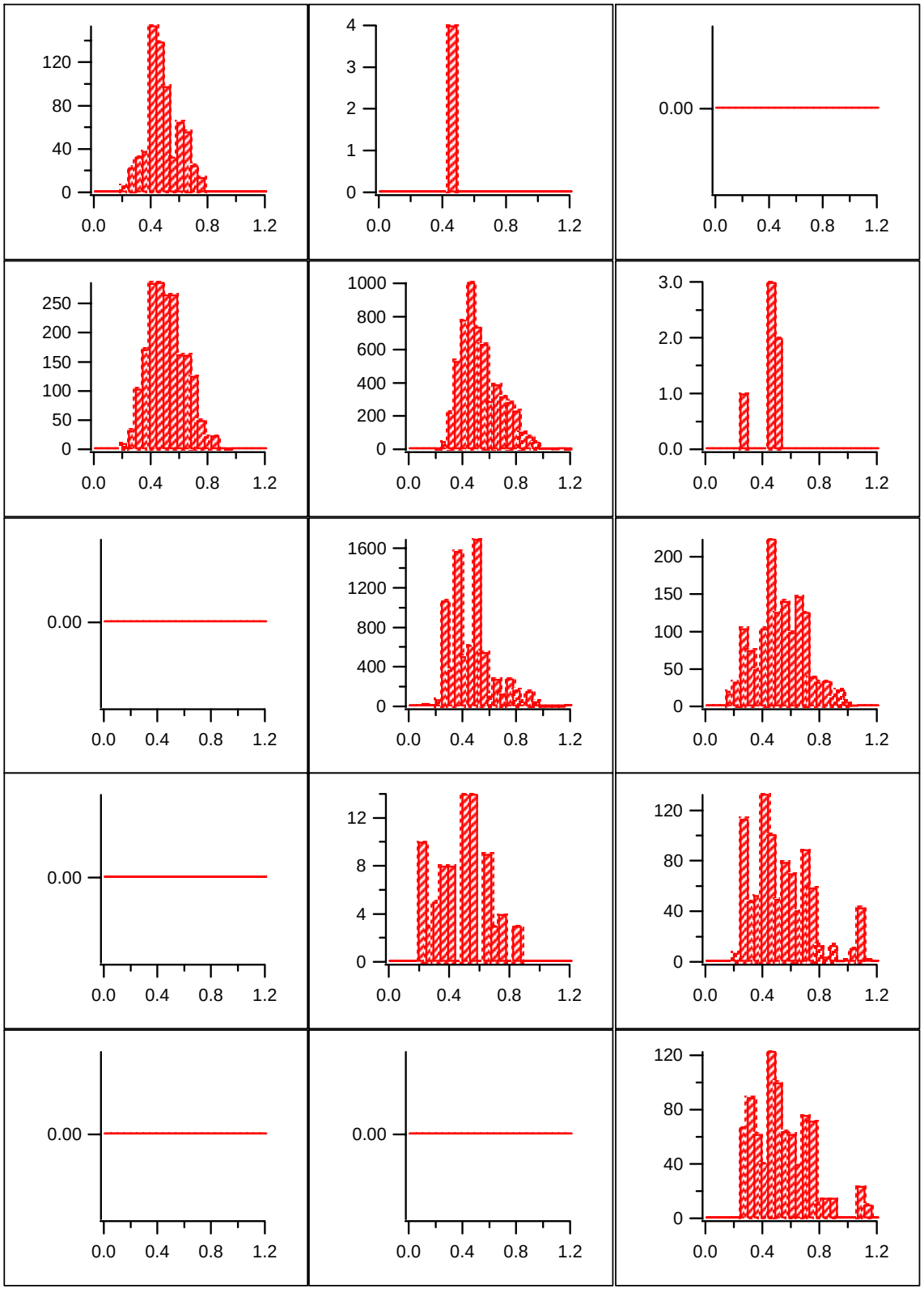

Figure 3-26. Subgrid variability of the HCHO for the summer 2005 campaign. The X-axis shows the concentration of HCHO in µmol/m^3, the Y-axis shows the number of observations. The grids correspond to the ones given in Figure 3-24.

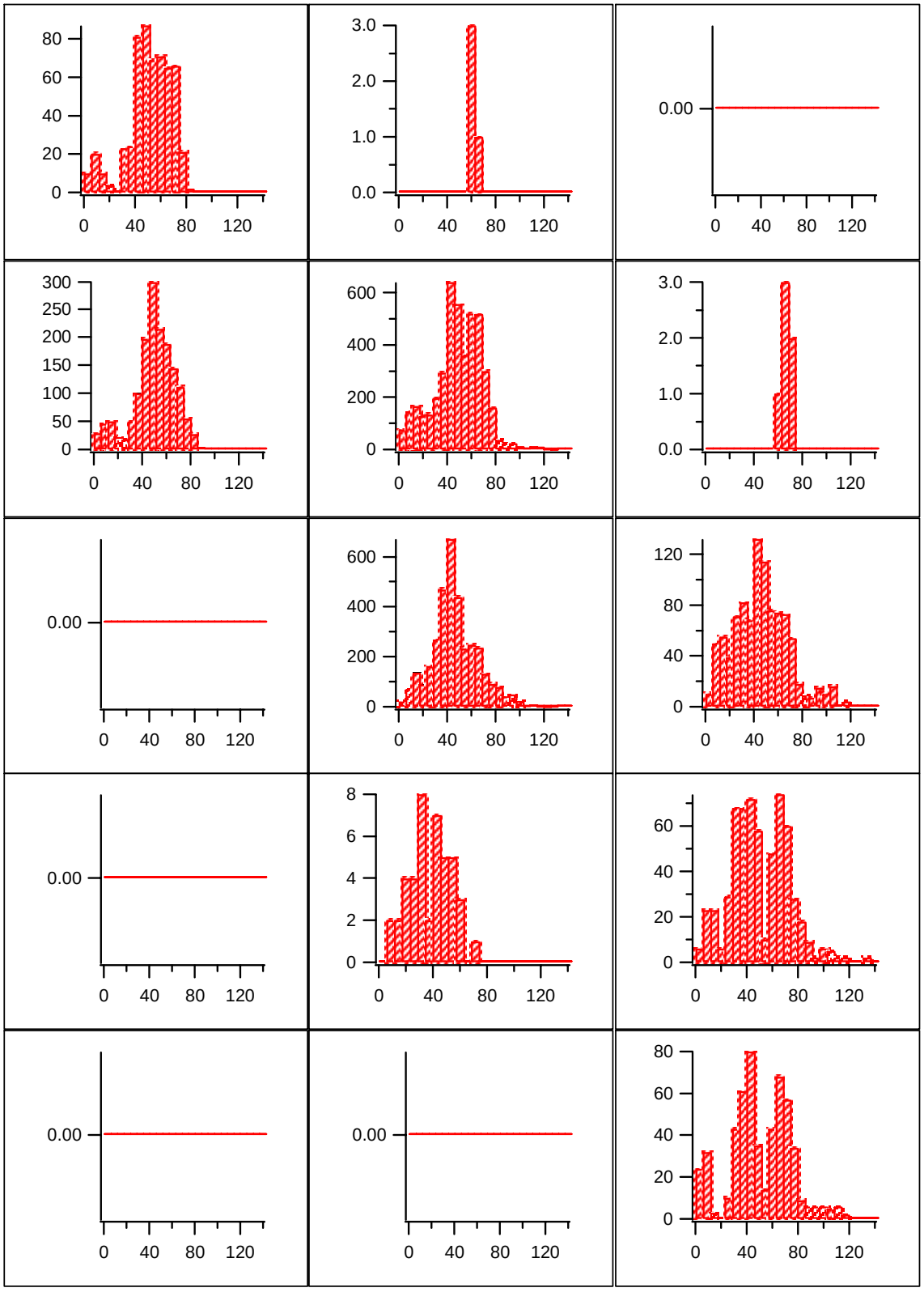

Figure 3-27. Subgrid variability distributions of O_3 for the summer 2005 campaign. The X-axis shows the concentration of O_3 in ppb, the Y-axis shows the number of observations. The grids correspond to the ones given in Figure 3-24.

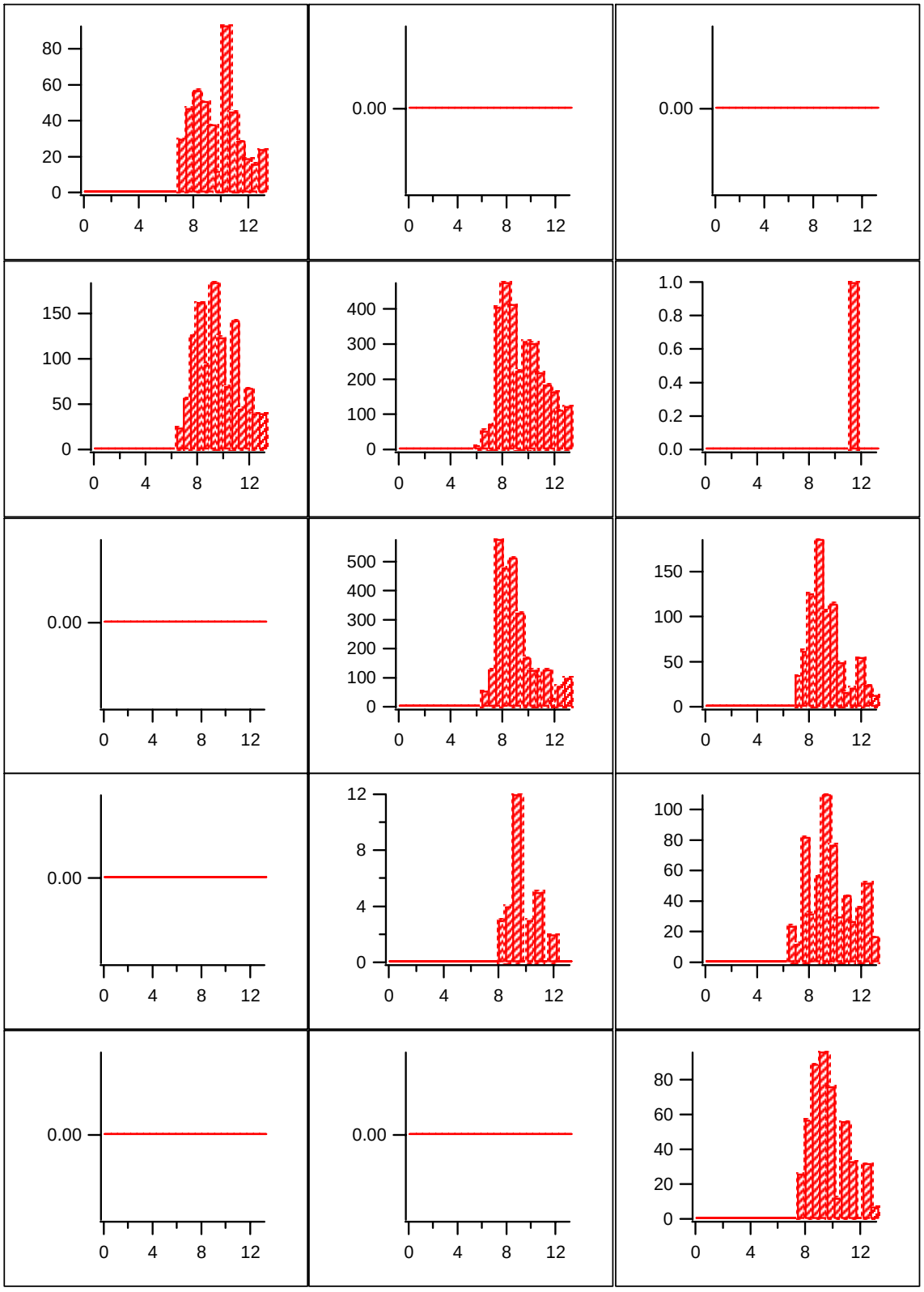

Figure 3-28. Subgrid variability distributions of $PM_{0.27}$ for the summer 2005 campaign. The X-axis shows the number concentration in µg/m^3, the Y-axis shows the number of observations. The grids correspond to the ones given in Figure 3-24.

3.2.2. Descriptive statistics for data

A summary of the statistical characteristics for each day of the measurements is given in Tables 3-5 to 3-8. The data show a very strong variability, both within one day and from campaign to campaign. The averages and standard deviations of the measured concentrations for each campaign are given in Table 3-8. One should keep in mind that the data collected with the mobile platform do not provide seasonally representative data, because of the limited duration of the measurements. However, some insight can be gained by observing the differences between the campaigns.

Only formaldehyde shows a seasonal trend with concentrations being highest during the spring and summer, while the winter campaign had the lowest concentrations. This trend is explained by the strong influence of photochemical activity on formaldehyde concentration, which is strongest during the warm period of the year. The other components (Cr(VI), aerosol number concentration and $PM_{0.27}$) exhibit a strong variability of the data. $PM_{0.27}$ shows a seasonal trend similar to that of formaldehyde, suggesting an effect of photochemically produced secondary aerosol on the aerosol mass. However, this trend is largely obscured by the strong variability in the data, indicating the importance of other sources that are variable in time and space.

Table 3-5. Statistical parameters of daily distributions of observed HCHO [μg/m^3] concentrations.

month	day	min	2.5%	5%	25%	50%	75%	95%	97.5%	max	# obs
4	25	13.64	14.6	14.92	15.79	16.47	17.06	18.34	18.76	19.69	1939
4	26	21.1	21.1	21.21	21.54	21.93	22.5	26.5	26.71	26.71	88
4	27	12.77	13.39	13.65	14.68	15.53	18.01	20.66	22.03	23.45	3068
4	28	1.52	2.1	2.43	5.96	9.71	14.62	15.81	15.97	16.91	3675
4	29	0.85	1.25	1.56	3.93	4.88	5.35	6.11	7.37	11.26	1540
5	1										
7	31	3.34	6.14	7.31	9.49	10.89	12.51	13.57	13.85	15.94	2618
8	1	4.75	6.99	7.7	11.49	13.12	15	19.51	19.91	22.23	2604
8	2	5.48	7.88	8.84	12.58	14.89	16.18	18.29	18.8	21.01	2728
8	3	7.66	10.05	10.91	13.27	16.66	20.26	24.3	25.68	35.06	2414
8	4	14.27	15.25	15.65	19.17	22.2	25.17	31.94	32.97	36.14	2231
8	5	8.9	9.83	10.68	14.12	16.87	21	22.79	23.2	24.34	2019
8	6										
11	10										
11	11	3.71	5.66	6.12	7.98	9.38	10.46	14.5	16.28	19.66	2670
11	12	2.98	4.23	4.86	7.35	9.13	10.78	13	14.03	16.15	1869
11	13	2.89	3.26	3.61	4.6	6.03	8.24	11.76	12.94	13.64	1373
11	14	2.87	3.24	3.41	4.32	5.17	6.28	7.48	7.71	9.81	959
2	23	0.8	0.9	0.96	1.27	1.46	1.61	1.82	1.87	2	1907
2	24	4.51	4.64	4.74	5.15	5.65	6.1	6.6	6.66	7.1	2011
2	25	1.35	1.39	1.4	1.46	1.51	1.55	2.07	2.4	2.51	3325
2	26	2.05	2.22	2.26	3.47	3.77	3.92	4.19	4.24	4.36	3388

Table 3-6. Statistical parameters of daily distributions of observed $PM_{0.27}$ [$\mu g/m^3$] concentrations.

month	day	min	2.5%	5%	25%	50%	75%	95%	97.5%	max	# obs
4	25	5.99	6.36	6.62	8.55	9.45	11.88	24.9	32.81	51.31	1939
4	26	12.59	13.7	14.02	15.23	16.21	25.09	37.44	40.17	63.07	2825
4	27	11.56	13.02	13.89	18.41	20.76	23.73	35.79	49.55	76.65	3547
4	28	5.05	5.32	5.52	7.21	10.17	12.36	19.82	25.74	44.82	3995
4	29	5.69	5.85	5.96	7.96	11.13	13.59	18.08	19.8	29.92	3088
5	1	6.48	6.74	6.81	7.4	8.77	10.86	12.63	13.39	14.07	1207
7	31	10.71	11.04	11.21	11.88	12.58	13.37	15.62	18.83	24.08	3078
8	1	13.32	13.61	13.96	15.52	18.86	21.46	27.91	32.85	90.69	2708
8	2	16.29	21.16	22.86	25.42	30.3	34.74	59.72	87.77	143.22	2299
8	3	10.67	11.31	11.91	13.65	15.75	18.33	23.8	27	98.15	2746
8	4	31.05	32.55	33.05	35.3	39.63	45.99	54.7	81.97	136.77	1308
8	5	9.2	9.96	10.44	14.5	20.12	23.67	32.38	35.97	99.89	2587
8	6	9.84	10.12	10.63	11.56	12.39	13.53	16.46	17.76	21.48	1596
11	10	1.23	1.33	1.41	1.78	2.18	2.79	6.01	6.52	14.13	2270
11	11	3.3	3.77	3.86	4.62	5.34	6.38	8.78	9.85	28.24	2570
11	12	8.89	9.21	9.36	10.38	11.65	13.1	15.97	18.53	47.36	3185
11	13	13.85	14.42	14.57	15.54	16.59	17.33	18.86	19.35	35.07	3439
11	14	2.91	3.5	3.63	5.11	6.76	9.29	14.69	20.93	68.87	3046
2	23	9.81	10.45	10.84	12.37	15.31	18.16	24.59	30.52	36.19	3049
2	24	1.83	1.96	2	2.42	2.8	3.33	5.26	6.37	21.01	3253
2	25	3.25	4	4.29	4.96	5.8	7.02	9.6	11.23	17.8	3746
2	26	1.83	2.07	2.13	2.4	2.73	3.49	5.55	7.09	20	4295

Table 3-7. Statistical parameters of daily distributions of observed CrVI [ng/m^3] concentrations.

month	day	min	2.5%	5%	25%	50%	75%	95%	97.5%	max	# obs
4	25	0.148	0.151	0.167	0.277	0.337	0.509	0.71	0.724	0.732	115
4	26	0.044	0.989	1.187	1.881	5.076	5.812	6.141	6.224	6.446	2325
4	27	0.001	0.061	0.125	0.496	0.848	1.485	1.833	1.943	2.184	2124
4	28										
4	29	0.004	0.017	0.042	0.154	0.292	0.435	0.554	0.592	0.704	1061
5	1	0.002	0.01	0.016	0.103	0.167	0.292	0.845	1.169	1.459	887
7	31	0.131	0.32	0.36	0.448	0.506	0.633	0.874	0.962	1.484	1986
8	1	0.007	0.037	0.065	0.178	0.237	0.304	0.437	0.537	0.855	1851
8	2	0.011	0.141	0.23	0.384	0.461	0.529	0.659	0.687	0.748	1285
8	3	0.013	0.139	0.174	0.486	0.687	0.829	1.041	1.12	1.297	1173
8	4	0.037	0.116	0.156	0.312	0.43	0.545	0.779	0.825	1.186	2480
8	5	0.001	0.006	0.009	0.042	0.09	0.201	0.436	0.508	0.662	1224
8	6	0.402	0.757	0.881	1.247	1.499	1.847	2.206	2.263	2.462	1517
11	10										
11	11										
11	12										
11	13	0.201	0.236	0.271	0.477	0.651	0.883	1.174	1.268	1.631	2179
11	14	0.2	0.213	0.224	0.344	0.554	1.205	1.7	1.73	1.815	1663
2	23	0.191	0.204	0.23	0.376	0.662	0.922	1.136	1.19	1.286	777
2	24	0.194	0.22	0.234	0.47	0.685	1.001	1.539	1.663	2.033	1346
2	25	0.228	0.893	0.983	1.167	1.496	1.725	1.912	1.954	2.128	727
2	26										

Table 3-8. Averages and standard deviations for the each of measurement campaign.

		Cr(VI) (ng/m^3)			HCHO (μg/m^3)			$PM_{0.27}$ (μg/m^3)		
month	day	mean	std	# obs	mean	std	# obs	mean	std	# obs
Spring										
4	25	0.382	0.149	115	16.46	1.00	1939	11.49	6.4	1939
4	26	3.931	1.958	2325	22.67	1.74	88	20.25	8.51	2825
4	27	0.970	0.562	2124	16.36	2.32	3068	22.19	8.12	3547
4	28	–	–	–	10.06	4.52	3675	10.83	5.04	3995
4	29	0.301	0.171	1061	4.55	1.58	1540	11.26	3.91	3088
5	1	0.256	0.272	887	–	–	–	9.19	1.95	1207
Summer										
7	31	0.556	0.174	1986	10.77	2.11	2618	12.93	1.86	3078
8	1	0.245	0.119	1851	13.33	3.32	2604	19.61	6.97	2708
8	2	0.451	0.126	1285	14.31	2.78	2728	33.78	16.89	2299
8	3	0.651	0.26	1173	17.02	4.57	2414	17.01	7.54	2746
8	4	0.441	0.187	2480	22.46	4.47	2231	42.64	12.95	1308
8	5	0.14	0.134	1224	17.23	4.04	2019	20.24	8.47	2587
8	6	1.529	0.41	1517	–	–	–	12.82	1.87	1596
Fall										
11	10	–	–	–	–	–	–	2.65	1.57	2270
11	11	–	–	–	9.49	2.4	2670	5.88	2.67	2570
11	12	–	–	–	9.01	2.48	1869	12.18	3.38	3185
11	13	0.682	0.277	2179	6.67	2.54	1373	16.64	1.88	3439
11	14	0.764	0.497	1663	5.32	1.27	959	8.11	6.28	3046
Winter										
2	23	0.667	0.299	777	1.43	0.25	1907	16.04	4.82	3049
2	24	0.764	0.386	1346	5.67	0.58	2011	3.21	1.8	3253
2	25	1.445	0.333	727	1.55	0.2	3325	6.23	1.87	3746
2	26	–	–	–	3.6	0.53	3388	3.28	1.59	4295

3.2.3. Comparison of mobile and fixed-site measurements

The results of the mobile measurements were compared to some of the parameters and concentrations measured at the central site of E-DATAS to gain insight into the effect of some meteorological parameters, as well as to compare the average concentrations over the city with the concentrations of traffic-related pollutants measured at the central site. For each day, the data collected at the monitoring site were averaged over the period corresponding to the time of the mobile measurements. These "daily" averages are then compared with the average concentrations measured with the mobile platform during the corresponding days.

Figure 3-29 shows a comparison of mobile measurements of HCHO, $PM_{0.27}$, and Cr(VI) concentrations with ambient temperature at the central monitoring site. Formaldehyde and $PM_{0.27}$ exhibit a positive correlation with the temperature, suggesting again an effect

of the photochemical activity. In contrast, there is no correlation between the temperature and Cr(VI) concentrations.

Figures 3-30 and 3-31 show comparisons with CO and NOx concentrations measured at the central site. Carbon monoxide is a general combustion tracer and, like NOx can be used to assess the effect of traffic emissions. No appreciable correlations with HCHO, $PM_{0.27}$, or Cr(VI) are observed. This suggests that concentrations of these traffic-related compounds at the central site are decoupled from the concentrations of the compounds measured throughout the city with the mobile laboratory.

Figures 3-32 and 3-33 show a comparison of the mobile measurements with PM_{10} and $PM_{2.5}$ concentrations measured at the central site. Both PM_{10} and $PM_{2.5}$ have local and long-range sources. Long-range sources are due to advection of the aerosol from outside the city. Aerosol from such sources is usually rich in secondary compounds, which are due to photochemical reactions in the atmosphere. Local sources of PM are usually associated with combustion sources and traffic in particular. It is interesting to note in this respect that both formaldehyde and $PM_{0.27}$ correlate well with the PM_{10} and $PM_{2.5}$ measured at the central site. This, in combination with the fact that these compounds did not correlate with other traffic-related compounds (CO and NOx, see Figures 3-30 and 3-31) at the central site, suggests that formaldehyde and $PM_{0.27}$ are influenced by long-range sources.

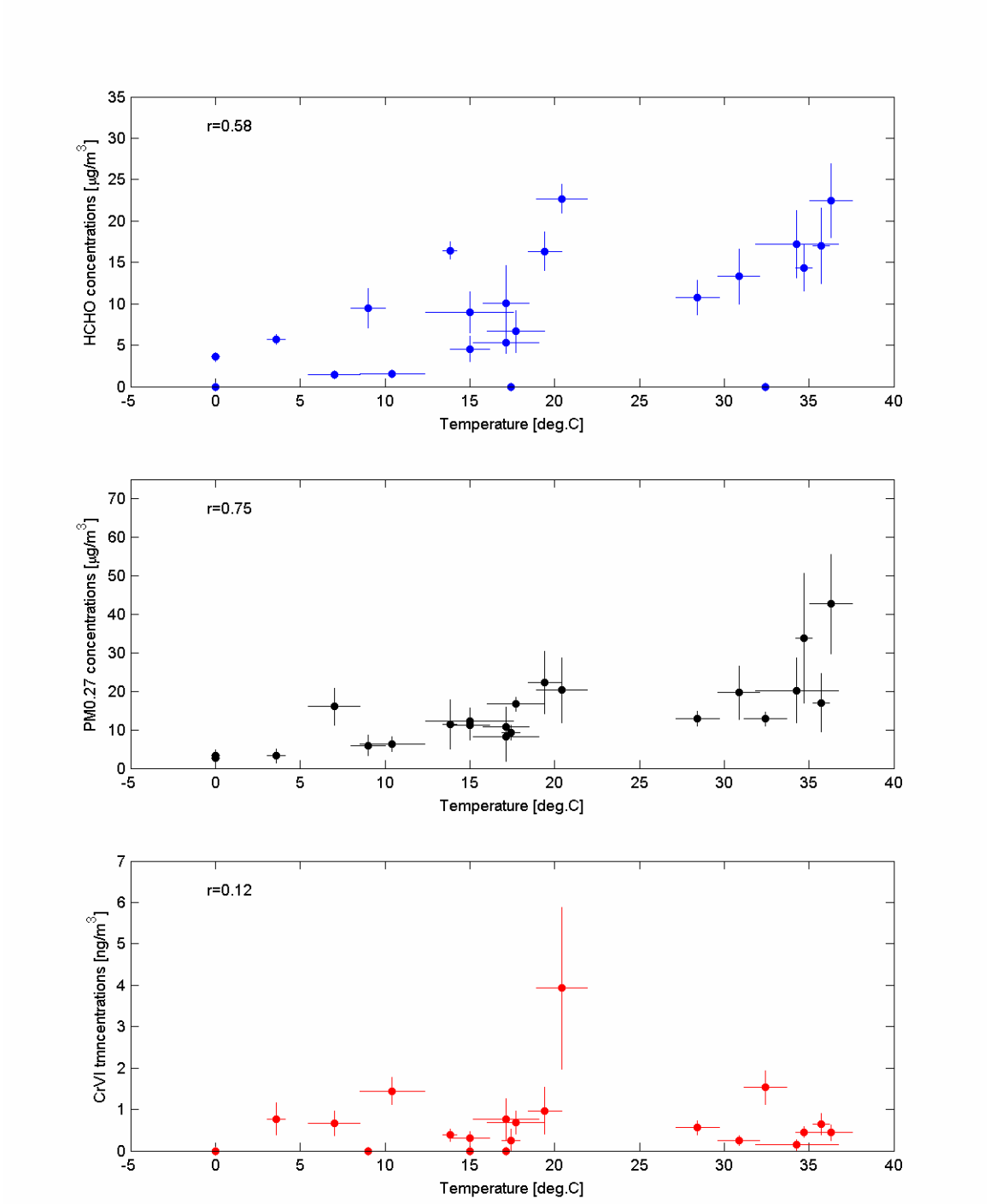

Figure 3-29. Comparison of mobile measurements of HCHO, $PM_{0.27}$, and Cr(VI) concentrations with ambient temperature measured at the central monitoring site.

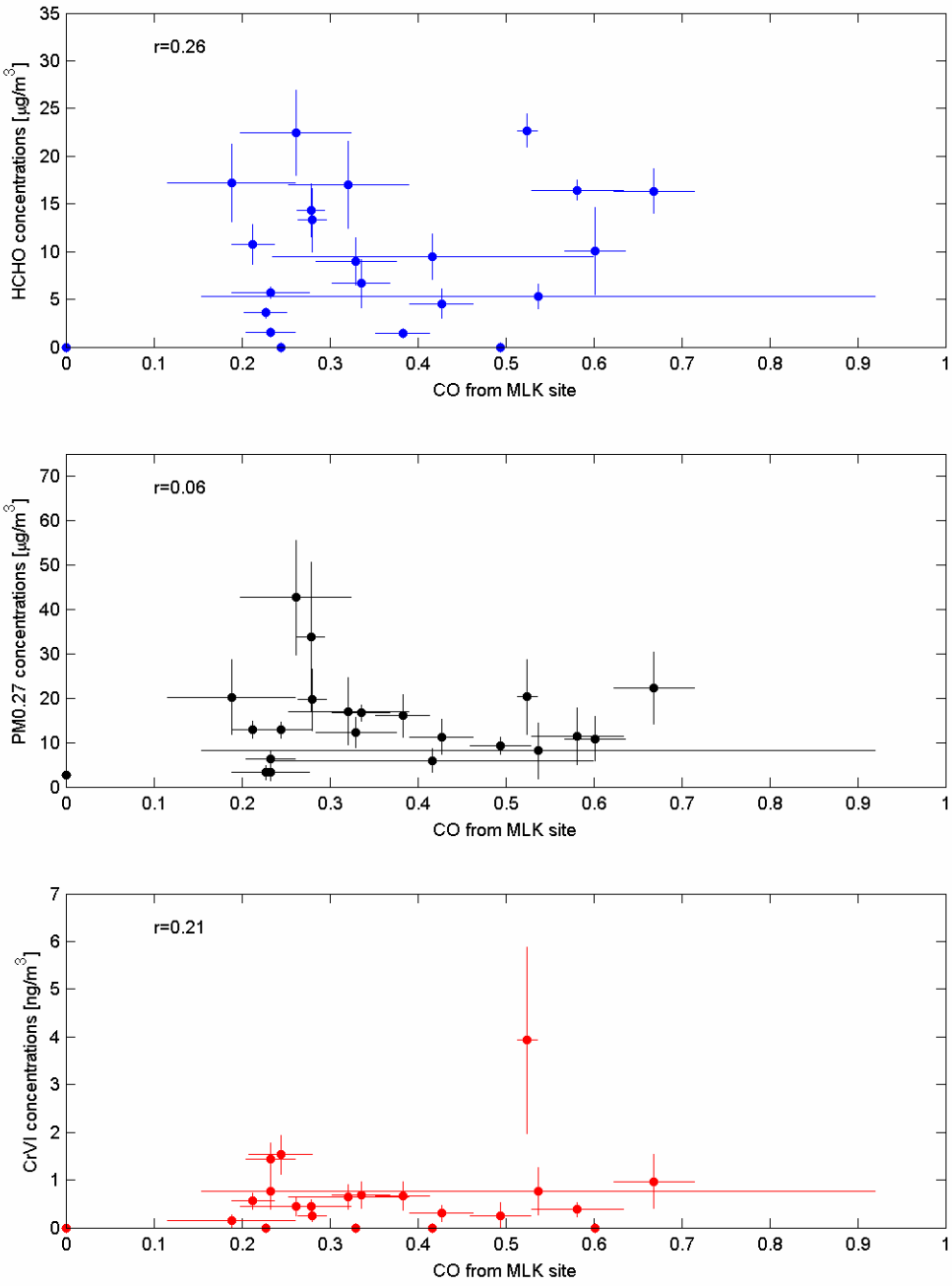

Figure 3-30. Comparison of mobile measurements of HCHO, $PM_{0.27}$, and Cr(VI) concentrations with CO concentrations measured at the central monitoring site.

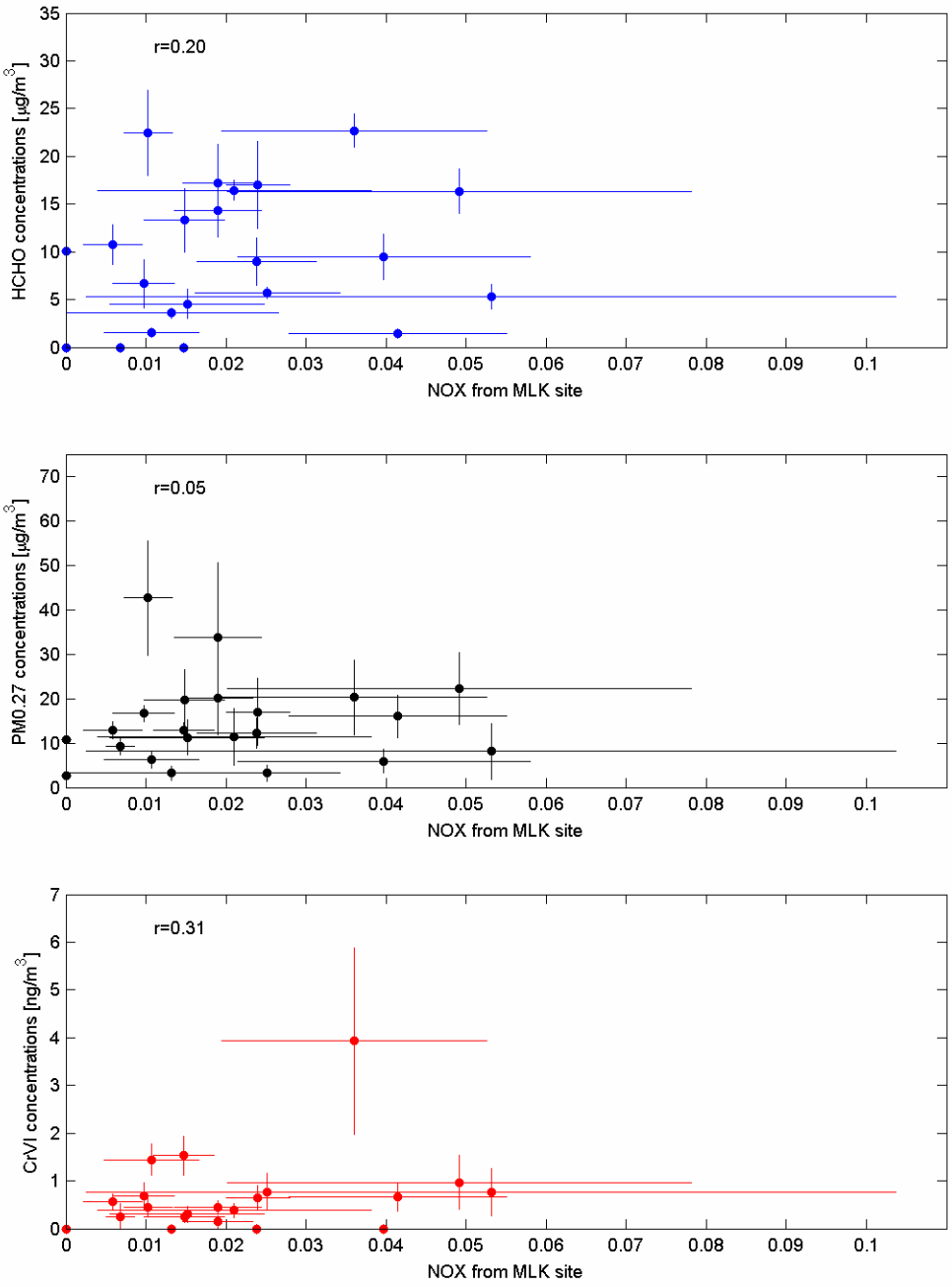

Figure 3-31. Comparison of mobile measurements of HCHO, $PM_{0.27}$, and Cr(VI) concentrations with NOx concentrations measured at the central monitoring site.

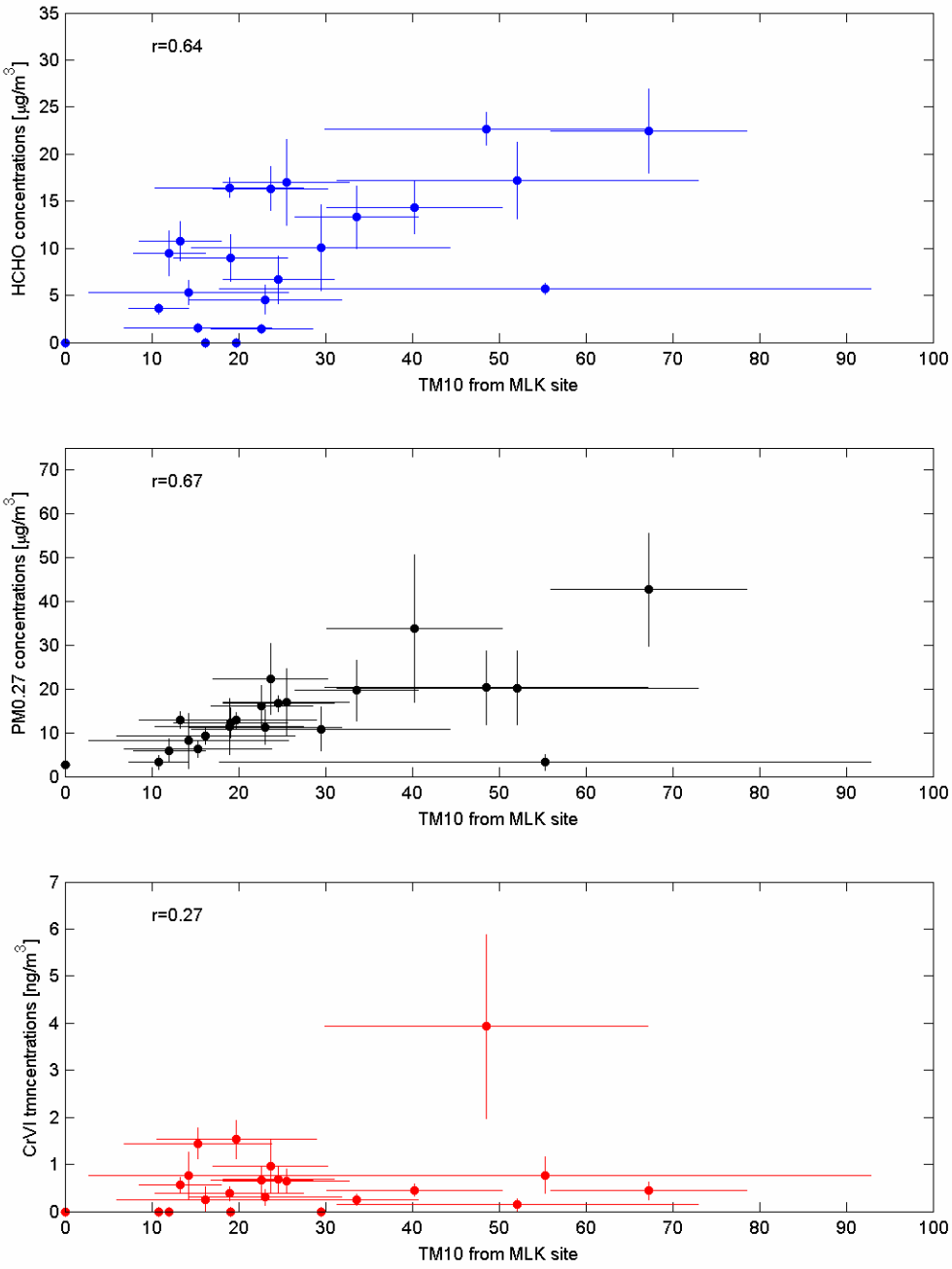

Figure 3-32. Comparison of mobile measurements of HCHO, $PM_{0.27}$, and Cr(VI) concentrations with PM_{10} concentrations measured with the TEOM at the central monitoring site.

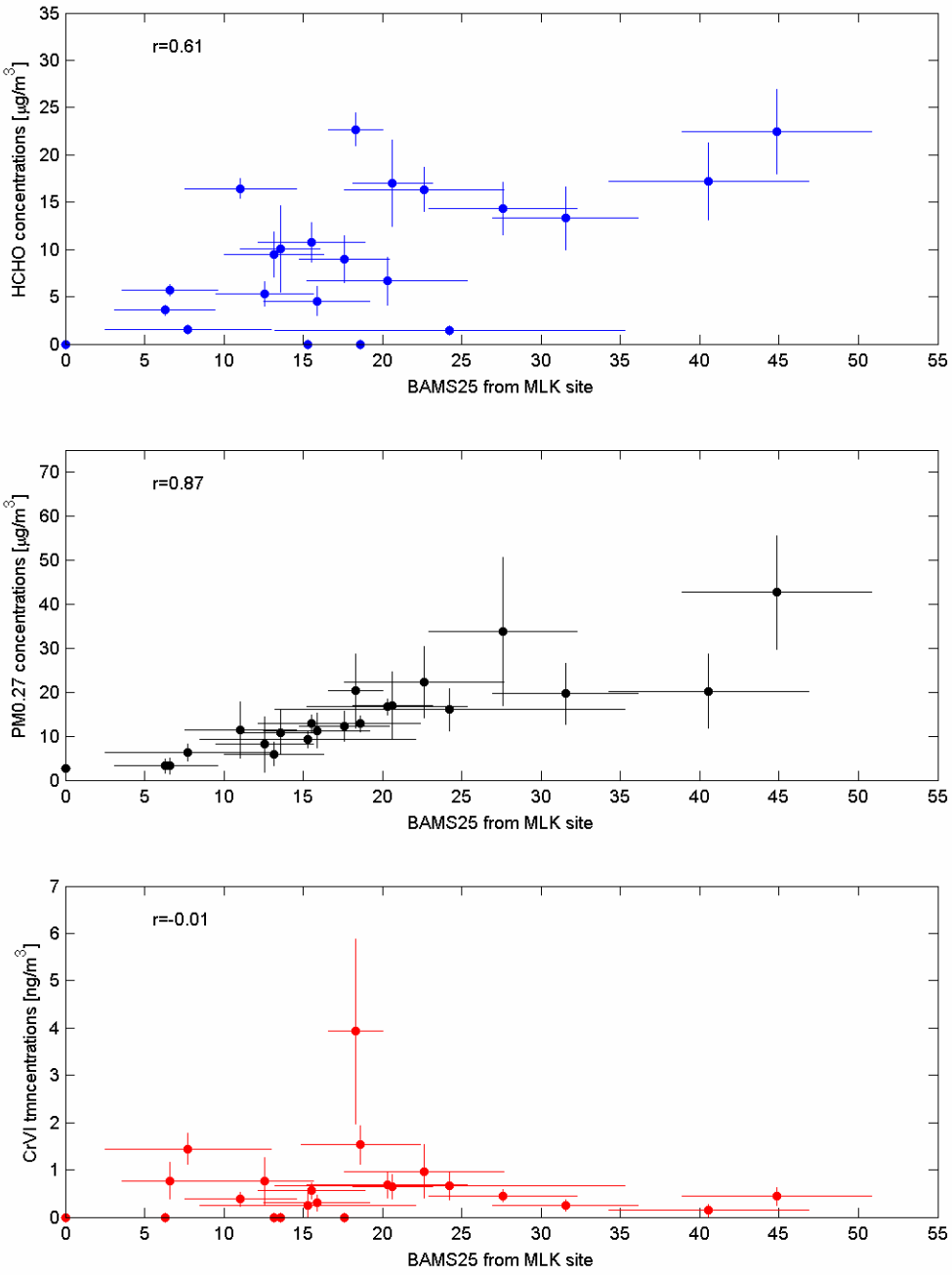

Figure 3-33. Comparison of mobile measurements of HCHO, $PM_{0.27}$, and Cr(VI) concentrations with $PM_{2.5}$ concentrations measured with BAMS at the central monitoring site.

4.0 Conclusions/Recommendations

4.1. Summary and Conclusions

Through funding opportunities provided by the National Air Toxics Monitoring Program – Community Assessments, the AQMS's Air Quality Management Section (AQMS) was able to expand the initial monitoring work that was performed during the 2003 DATAS effort.

During the development, implementation, and conclusion of this enhanced study, AQMS strived to better understand the suite of pollutant sources that are impacting the air quality at the Martin Luther King Station (MLK), located in Wilmington, Delaware.

Through collaborative partnerships with University of Delaware and Duke University research teams, an ambient air monitoring study, defined as the Enhanced Delaware Air Toxics Study (E-DATAS) was conducted at the MLK. The study began in April 2005 and continued through February 2006.

Specifically, E-DATAS was designed to:

- Characterize the seasonal ambient variability of ambient aerosols of aerodynamic diameters of 50, 110, 220, 440, and 770 nm at the MLK site. Real-time measurements were performed during four, one-month intensive efforts using the Real-time Single-particle Mass Spectrometer, version 3 (RSMS-3).
- Implement an approach in which selected industry within a 10-km radius of the MLK site could be characterized according to their ambient aerosol contribution. Data obtained during this effort was vital to better identifying a source's contribution to the ambient air composition at the MLK site.
- Study the spatial and seasonal variability of target ambient compounds (formaldehyde, chromium species, particulate matter, and ozone) using both research-specific and commercially available technology to perform mobile, real-time ambient measurements within the Wilmington area. These measurements were performed during four, one-week intensive efforts that were coordinated with the aerosol measurements.
- Utilize and integrate into E-DATAS many of the federal- and state-run ambient measurements being performed at the MLK site. For this study, particulate, carbon monoxide, nitric oxide, and wind measurements were incorporated into E-DATAS.
- Develop efficient, effective, and long-term partnerships with the research community, which will provide value-added data to enhance AQMS' and the public's understanding of the state of Delaware's air quality. E-DATAS clearly signifies the importance of developing these partnerships, as this field application would not have been performed otherwise.

4.1.1. Project Conclusions

At the conclusion of the E-DATAS field monitoring efforts an enormous dataset was established for ambient aerosol characterization at the MLK site with over 500,000 ambient aerosol particles being analyzed with the RSMS-3. Additionally, over 61,000 aerosol size distributions were collected via the mobile monitoring effort with 42,426 data points being collected for formaldehyde, and 26,843 data points collected for chromium.

The project conclusions that are summarized below are organized by monitoring activity, (fixed-site aerosol monitoring vs. mobile monitoring)

4.1.2. Mobile Monitoring

Through implementation of the Duke University Mobile Laboratory, over 130,000 data points were measured during the E-DATAS to characterize the spatial, temporal and seasonal variability of water-soluble hexavalent and trivalent chromium, formaldehyde, ozone, and particulate matter.

The analyses of these data indicate the following significant conclusions:

- Aerosol number concentration, chromium VI, and $PM_{0.27}$ varied significantly by location.
- The variability in formaldehyde and ozone concentrations during the summer 2005 campaign was lower in comparison to the aerosol concentration. Since both formaldehyde and ozone are either partially or fully produced by photochemistry, this result is expected.
- Only formaldehyde showed a seasonal trend with concentrations being highest during the spring and summer, while the winter campaign had the lowest concentration.
- $PM_{0.27}$ shows a seasonal trend similar to that of formaldehyde, but the trend is largely obscured by the strong variability in the data.
- Comparison of the mobile data to the federal- / state-run network indicates:
    - Comparisons with CO and NOx concentrations measured at the central site do not correlate well with the mobile results for formaldehyde, $PM_{0.27}$, or chromium VI.
    - Both formaldehyde and $PM_{0.27}$ correlate well with the PM_{10} and $PM_{2.5}$ measured at the central site. This suggests that $PM_{0.27}$ and formaldehyde are influenced by long-range sources.
    - Formaldehyde and $PM_{0.27}$ show a positive correlation with temperature, suggesting the photochemical activity.

4.1.3. Fixed-Site Aerosol Monitoring

With over 500,000 ambient aerosol particles, data had to be analyzed in clusters of 40,000 particles. Data collected from each of the four monitoring intensives was kept separate from other intensives. For the MLK site, data were separated into 16 chemical composition classes: OCANS, ammonium nitrate, potassium, EOC, amine, sodium, potassium with sodium, iron, iron with cerium/lanthanum, lead, zinc, zinc with lead, tin/antimony, lithium, vanadium, and other metals.

From the analysis of this dataset, AQMS has the following understanding of the source contributions at the MLK site.

- Air quality at the MLK site has both local and regional characteristics.
- The MLK site is impacted by wood and biomass burning. There is a slight bias toward wind directions for the northwest where the greatest nearby residential population exits. There is also a slight bias toward the nighttime, consistent with residential wood burning.
- The MLK site is impacted by diesel vehicle exhaust, as indicated by the EOC measurements. The slight enhancement of EOC when the wind is from the east may indicate a contribution from industrial combustion sources. Also, diesel emissions from the nearby DART depot impact the MLK site.
- The MLK site measurements have signatures from stack emissions where aliphatic amines have been added during the scrubbing process used to remove SO2 from the effluent.
- Multiple local industrial combustion processes to the east and southwest contribute to the MLK site signature.
- Particle composition signatures associated with emissions from the Delaware City Refinery, CitiSteel, and the Delmarva Edgemoor Power Plant were detected in the ambient air sampled at the MLK site. Bag sampling at the CitiSteel site confirmed this source signature and association.
- Emissions from local industrial combustion impact the MLK site. Particle classes associated with local industrial emissions all have characteristic increases in concentration in the early morning, late evening or both.
- Signatures from particles thought to be emitted from large ships were measured at the MLK site. Wind dependence (110°) indicates that the Port of Wilmington is a possible source for the MLK site ambient measurements.
- In broad estimates, the Wilmington aerosol is characterized as follows:
    - Secondary aerosol of regional origin constitutes about 38% of PM_1.
    - Secondary aerosol of local origin constitutes about 27% of PM_1.
    - Biomass burning contributes about 14% of PM_1.

- Primary particulate emissions from vehicular traffic contribute about 8% of $PM_{1.}$
- Primary particulate emissions from local industrial sources contribute about 13% of $PM_{1.}$

4.2. Potential Applications for the Use of Datasets

Conventional data collected from fixed sites (MLK in this case) provide a time series at a stationary point, and may not yield useful information away from the monitoring station. On the other hand, data collected with mobile measurements provide high spatially and temporally resolved data. The combined datasets can provide information on the dispersion and transformation of pollutants in the atmosphere. Section 4.2.1 provides some applications of this approach.

Sub-grid scale variability (SGV) is within-the-grid variability, and is an inherent property of the regional-scale modeling approach. The SGV is usually resolved by modeling at fine-scales and/or by modeling at local-scales. Mobile measurements provide a means of checking the SGV derived from the modeling. The SGV-based approach is presented in Section 4.2.2.

SGV is also useful in the regulatory applications – as a means of weight-of-evidence analysis should the traditional modeled attainment demonstration fail. Such an application is presented in Section 4.2.3.

Sources of ultra fine particles are often considered to be primary. However, a considerable portion of these particles are formed due to photochemical secondary reactions (see Table 3-3). A study is proposed in Section 4.2.4 to assess the mechanisms and sources responsible for these particles.

The use of particle number and size information is growing in the characterization of fine particles including diesel PM. Health driven concerns are increasing for ultra fine particles (< 100 nm) and nano particles (< 50 nm). The greatest number of particles tends to be in ultra fine range (3-100 nm), whereas the greatest mass of the particles will be in the accumulation mode (100-300 nm). Section 4.2.5 proposes a study to make use of the mobile van and RSMS-3 measurements to assess the performance of local-scale modeling for diesel PM.

Section 4.2.6 proposes a positive matrix factorization (PMF) technique to identify sources contributing to $PM_{2.5}$.

4.2.1. Use of Stationary and Mobile Measurements

Data collected at the conventional monitoring stations cannot provide information away from the monitoring sites. However, the mobile measurements can be supplemented with the conventional data to study the dispersion and transformation of pollutants in the atmosphere.

Data collected at MLK site are limited to temperature, wind speed, wind direction, NOx (NO, NO2, NOx), CO, $PM_{2.5}$ and PM_{10}. These data can be combined with the mobile measurements to study the following.

- Temporal and spatial distributions of pollutants from the mobile transects are likely to inform whether the pollutants follow Gaussian or lognormal distributions, and whether any large-scale transport is influencing the transects
- Particle size distribution data can be analyzed to identify if the particles are generated from primary sources (such as motor vehicle emissions) or if secondary formation is important.
- High resolution particle size distribution data obtained by the mobile measurements can identify if in-cloud processes exist
- The combined datasets can explain why the correlation in ozone and HCHO mobile measurements is poor.

4.2.2. Corroboration of Sub-Grid scale Variability (SGV) in Regional-scale modeling

Characterization of spatial variability of pollutants in urban areas is critical for improved air toxics exposure assessments, model evaluation studies, and air quality regulatory applications. Advanced air quality models, such as the Community Multi-scale Air Quality (CMAQ) model, provide hourly values of simulated pollutants for each grid cell for the period of simulation. They are limited to coarse grid resolutions and provide volume averaged concentrations for each grid cell. Even though the grid size can be refined through nested grid modeling approach, computational and physical constraints limit the spatial refinement to 1 km grid size. The inherent property of the grid modeling is the existence of the sub-grid scale variability (SGV) within the grid. This SGV is generally resolved with local-scale models (e.g., AERMOD), which is integrated with the regional-scale modeling results. Such an hybrid approach provides a structure to the volume averaged concentrations estimated by the regional-scale models. The SGV thus derived from the local-scale modeling can be corroborated with the spatial and temporal variability derived from the mobile measurements. Such an SGV based parameterization will ultimately provide the modeling community the benefit of modeling with CMAQ at coarse-scales instead of modeling at fine-scales. The integrated CMAQ/AERMOD modeling approach for deriving the SGV and corroborating with the SGV based on the mobile measurements is in progress for HCHO.

In Wilmington, particles in ultra fine range (100 nm) are mainly from mobile source vehicle exhaust, biomass burning, and photochemical secondary reactions (see Table 3-3). Particles in the fine range (0.3-0.5 μm) are mainly due to long-range transport. Therefore, the spatial and temporal variability in an urban area is mostly caused by the vehicle exhaust, which displays a strong a diurnal pattern. In the absence of other direct emissions in an urban area, mobile source emissions will be the main source for spatial

and temporal variability in $PM_{2.5}$. For such a case, spatial and temporal variability can be derived from the ultra PM fine measurements. This study will be undertaken after the conclusion of the HCHO study.

4.2.3. Sub-Grid scale Variability (SGV) in Regulatory Applications

Modeled attainment demonstration is one of the requirements of the State Implementation Plans (SIP) for demonstrating attainment of the ozone and $PM_{2.5}$ National Ambient Air Quality Standards (NAAQS). Such a demonstration is accomplished with regional-scale modeling at coarse scales (12-/4-km grid size). Should states fail to demonstrate such a modeled attainment and are within a close proximity of the ozone/$PM_{2.5}$ NAAQS, states have the option of demonstrating attainment through a weight-of-evidence analyses. Traditionally state SIPs accepted their volume averaged concentrations on the face value, and did not question the inherent SGV that exists in the modeling grid cells. States can utilize the inherent SGV that exists in the modeling grid cells as a weight-of-evidence analysis in demonstrating attainment of the ozone and $PM_{2.5}$ NAAQS.

4.2.4. Sources of Ultra Fine Particles in Wilmington

Information on the size and chemical composition of ultra fine particles is essential in understanding their formation mechanisms in urban and rural areas. Mobile sources, biomass burning, and power plants are considered the main sources of the ultra fine particles. While the sources of these ultra fine particles are considered primary, a good fraction of these particles could be formed by photochemical reactions in spring and summer months. A study will be undertaken to determine if mechanisms other than direct emissions play a significant role in the formation of ultra fine particles in Wilmington area.

4.2.5. Diesel PM Source Assessment

The use of particle number and size information is growing in the characterization of fine particles including diesel PM. Health driven concerns are increasing for ultra fine particles (< 100 nm) and nanoparticles (< 50 nm). Soot particles emitted from diesel engines are in the size range of 40-500 nm. These chain agglomerates are generated from small particles (10-30 nm) by coagulation inside the diesel engine combustion chamber. The greatest number of particles tend to be in ultra fine range (3-100 nm), which contains soot particles larger than 30 nm and volatile nuclei mode particles smaller 30 nm. On the other hand, the greatest mass of the particles will be in the accumulation mode (100-300 nm). The mobile van and RSMS-3 measurements will be utilized to assess the performance of local-scale modeling for diesel PM.

4.2.6. $PM_{2.5}$ Source Identification

A positive matrix factorization (PMF) technique will be utilized for the analysis of size distributions measured by SMPS/RSMS. Sources can be identified by using the number and volume distributions, time frequency properties of contribution of each source and correlations of contribution values with the gas-phase and $PM_{2.5}$ composition. Use of continuous size distribution measurements and PMF can provide valuable information about the contribution of local traffic and nucleation to the aerosol number and mass concentrations.

5.0 References

Allen, T. L. (1958), Microdetermination of Chromium with 1,5-Diphenylcarbohydrazide, *Analytical Chemistry*, *30*, 447-450

Altkorn, R., et al. (1997), Low-loss liquid-core optical fiber for low-refractive-index liquids: fabrication, characterization, and application in Raman spectroscopy, *Applied Optics*, *36*, 8992-8998

Antony Chen, L.-W., B.G. Doddridge, R.R. Dickerson, J.C. Chow, and R.C. Henry, 2002. Origins of fine aerosol mass in the Baltimore-Washington corridor: implications from observation, factor analysis, and ensemble air parcel back trajectories, *Atmospheric Environment*, *36* (28), 4541-4554.

Bein, K.J., Zhao, Y., Wexler, A.S., Johnston, M.V., *Speciation of Size-Resolved Individual Ultrafine Particles in Pittsburgh, Pennsylvania*. Journal of Geophysical Research, Atmospheres, 2005. **110**(D7): D07S05.

Bein, K.J., Zhao, Y., Wexler, A.S., Johnston, M.V., *Identification of Sources of Atmospheric PM at the Pittsburgh Supersite. Part II: Quantitative Comparisons of Single Particle, Particle Number, and Particle Mass Measurements.* Atmospheric Environment, 2006. In Press.

Brouwer, D.H., J.H.J. Gijsbers, M.W.M. Lurvink, 2004. Personal Exposure to Ultrafine Particles in the Workplace: Exploring Sampling Techniques and Strategies, *Ann. Occup. Hyg.,* 48 (5), 439-453.

Bukowiecki, N., et al. (2002), A mobile pollutant measurement laboratory-measuring gas phase and aerosol ambient concentrations with high spatial and temporal resolution, *Atmospheric Environment*, *36*, 5569-5579.

Carlton, G. N. (2003), Hexavalent chromium exposures during full-aircraft corrosion control, *Aiha Journal*, *64*, 668-672.

DeCarlo, P.F., Slowik, J.G., Worsnop, D.R., Davidovits, P. and Jimenez, J.L., *Particle Morphology and Density Characterization by Combined Mobility and Aerodynamic Diameter Measurements. Part 1. Theory.* Aerosol Science and Technology, 2004. **38**: p. 1185-1205

Fan, Q., and P. K. Dasgupta (1994), Continuous Automated-Determination of Atmospheric Formaldehyde at the Parts-Per-Trillion Level, *Analytical Chemistry*, *66*, 551-556.

Geller, M.D., Biswas, S., Fine, P.M., Sioutas, C., *A new compact aerosol concentrator for use in conjunction with low flow-rate continuous aerosol instrumentation*, Journal of Aerosol Science, 2005. **36**: p. 1006-1022.

Johnston, M.V., 2000. Sampling and analysis of individual particles by aerosol mass spectrometry, *Journal of Mass Spectrometry*, *35*, 585-595.

Johnston, M.V., and A.S. Wexler, 1995. MS of Individual Aerosol Particles., *Analytical Chemistry*, *67*, 721A-726A.

Kane, D.B., Johnston, M.V., *Size and Composition Biases on the Detection of Individual Ultrafine Particles by Aerosol Mass Spectrometry*. Environmental Science and Technology, 2000. **34**: p. 4887-4893.

Khlystov, A., et al. (2004), An algorithm for combining electrical mobility and aerodynamic size distributions data when measuring ambient aerosol, *Aerosol Science and Technology*, *38*, 229-238.

Khlystov, A., et al. (1995), The Steam-Jet Aerosol Collector, *Atmospheric Environment*, *29*, 2229-2234.

Lake, D.L., Tolocka, M.P., Wexler, A.S. and Johnston, M.V., *Mass Spectrometry of Individual Particles Between 50 and 750 nm in Diameter at the Baltimore Supersite.* Environmental Science and Technology, 2003. **37**(15): p. 3268-3274.

Lei, W., et al. (1983), Determination Of Phosphorus In Natural-Waters By Long-Capillary-Cell Absorption Spectrometry, *Analytical Chemistry*, *55*, 951-955.

Li, Q. Y., et al. (2003), Portable flow-injection analyzer with liquid-core waveguide based fluorescence, luminescence, and long path length absorbance detector, *Analytica Chimica Acta*, *479*, 151-165.

McElroy, M.W., Carr, R.C., Ensor, D.S., Markowski, G.R., *Size Distribution of Fine Particles from Coal Combustion*. Science, 1982. **215**: p. 13-19.

Noble, C.A., and K.A. Prather, 2000. Real-Time Single Particle Mass Spectrometry: A Historical Review of a Quarter Century of the Chemical Analysis of Aerosols, *Mass Spectrometry Reviews*, *19*, 248-274.

Ondov, J.M., Wexler, A.S., *Where Do Particulate Toxins Reside/ An Improved Paradigm for the Structure and Dynamics of the Urban mid-Atlantic Aerosol.* Environmental Science and Technology, 1998. **32**: p. 2547-2555.

Paustenbach, D. J., et al. (1991), The Health-Hazards Posed By Chromium-Contaminated Soils In Residential And Industrial-Areas - Conclusions Of An Expert Panel, *Regulatory Toxicology And Pharmacology*, *13*, 195-222.

Phares, D.J., Rhoads, K.P., Wexler, A.S., Johnston, M.V., *Application of the ART-2a Algorithm to Laser Ablation Aerosol Mass Spectrometry of Particle Standards*. Analytical Chemistry, 2001. **73**: p. 2338-2344.

Phares, D.J., Rhoads, K.P., Wexler, A.S., *Performance of a Single Ultrafine Particle Mass Spectrometer*. Aerosol Science and Technology, 2002. **36**: p. 583-592.

Pitz, M., Cyrys, J., Karg, E., Wiedensohler, A., Wichmann, H.-E., Heinrich, J., *Variability of Apparent Particle Density of an urban Aerosol*. Environmental Science and Technology, 2003, **37**: p. 4336-4342.

Rhoads, K.P., Phares, D.J., Wexler, A.S., Johnston, M.V., *Size-Resolved Ultrafine Particle Composition Analysis, Part 1: Atlanta*. Journal of Geophysical Research, Atmospheres, 2003. **108**(D7): 8418.

Seinfeld, J. H., and S. N. Pandis (1998), *Atmospheric chemistry and physics: From air pollution to climate change.*, John Wiley & Sons Inc., New York.

Simon, P. K., et al. (1991), Wet Effluent Denuder Coupled Liquid Ion Chromatography Systems, *Analytical Chemistry*, *63*, 1237-1242.

Slowik, J.G., Stainken, K., Davidovits, P., Williams, L.R., Jayne, J.T., Kolb, C.E., Worsnop, D.R., Rudich, Y., DeCarlo, P.F. and Jimenez, J.L., *Particle Morphology and Density Characterization by Combined Mobility and Aerodynamic Diameter Measurements. Part 2: Application to Combustion-Generated Soot Aerosols as a Function of Fuel Equivalence Ratio.* Aerosol Science and Technology, 2004. **38**: p. 1206-1222.

Tolocka, M.P., Lake, D.A., Johnston, M.V., Wexler, A.S., *Size-Resolved Fine and Ultrafine Particle Composition in Baltimore, Maryland*. Journal of Geophysical Research, Atmospheres, 2005. **110**(D7): D07S04.

Tolocka, M.P., Reinard, M.S., Lake, D.A., Ondov, J.M., Wexler, A.S., Johnston, M.V., *Characterization of Short-term Particulate Matter Events by Real-Time Single Particle Mass Spectrometry*. Aerosol Science and Technology, 2006. **40**: p. 873-882.

Wang, J., et al. (1999), Field method for the determination of hexavalent chromium by ultrasonication and strong anion exchange solid phase extraction, *Analytical Chemistry*, *71*, 1027-1032.

Wang, S. C., and R. C. Flagan (1989), Scanning Electrical Mobility Spectrometer, *Journal of Aerosol Science*, *20*, 1485-1488.

Weijers, E. P., et al. (2004), Variability of particulate matter concentrations along roads and motorways determined by a moving measurement unit, *Atmospheric Environment*, *38*, 2993-3002.

Westerdahl, D., et al. (2005), Mobile platform measurements of ultrafine particles and associated pollutant concentrations on freeways and residential streets in Los Angeles, *Atmospheric Environment*, *39*, 3597-3610.

Yao, W. S., and R. H. Byrne (1999), Determination of trace chromium(VI) and molybdenum(VI) in natural and bottled mineral waters using long pathlength absorbance spectroscopy (LPAS), *Talanta*, *48*, 277-282.

Appendices

Disclaimer: This work was funded by the U.S. EPA but was not subjected to internal review and no endorsement by the U.S. EPA should be inferred.